Structural conversion of layered titanates for enhancing the photocatalytic performance

Mohamed Mohamed Esmat Mohamed Mohamed

February 2022

Structural conversion of layered titanates for enhancing the photocatalytic performance

Mohamed Mohamed Esmat Mohamed Mohamed

Doctoral Program in Materials Science and Engineering

Submitted to the Graduate School of

Pure and Applied Sciences

in Partial Fulfillment of the Requirements

for the Degree of Doctor of Philosophy in

Engineering

at the

University of Tsukuba

ABSTRACT

This thesis aims to investigate the photocatalytic performance enhancement of TiO_2-based photocatalytic materials. The photocatalysts developed in our work have been used in various photocatalytic applications, including solar hydrogen production and environmental remediation.

The first chapter describes the basic principles of photocatalysis, an overview of semiconducting photocatalytic materials, and the concept of photocatalytic reactions along with selected photocatalytic applications.

In the second chapter, we investigated the topochemical conversion of layered protonated titanates to anatase TiO_2 with both nitrogen dopant and oxygen vacancy (Vo) for the application in photocatalytic hydrogen production from water. This structural transformation was performed via a new, readily achieved, and facile solvothermal strategy. During the synthesis, a spherical assembly of layered titanate nanosheets, containing N source in the structure, is topochemically converted to N-doped anatase TiO_2 with concomitant oxygen vacancies. The photocatalyst showed state-of-the-art-level co-catalyst-free solar photocatalytic activity for hydrogen evolution via water splitting, which is significantly higher than that of typical co-catalyst-free defective TiO_2 materials. Improving the photocatalytic activity was explained by its Vo-induced high charge separation efficiency.

The third chapter describes the synthesis of the 1D nanowire structure of a layered titanate, $K_xTi_{2-x/3}Li_{x/3}O_4$ (named KTLO), via the one-pot solvothermal treatment of KTLO. Cation exchange ability and charge separation efficiency of layered titanates were both improved because of this structural transformation. The obtained KTLO nanowire exhibited efficient and ultrafast adsorption/immobilization (photoreduction) of toxic metal cations, like Cd^{2+}, from water under sunlight irradiation, whereas the pristine KTLO and a benchmark TiO_2 photocatalyst showed no performance.

Layered titanates have a high potential for cation exchange, leading to an opportunity to create hybrid heterostructures with new and tunable structures which may have a better interface. Thus, the fourth chapter deals with the structural conversion of Cu-titanate into photoactive $CuO-TiO_2$ for H_2 generation from ammonia borane under visible light. We additionally investigated the structural evolution of the photocatalyst once it is being treated with the ammonia borane. The results showed that the CuO nanostructures converted to metallic Cu, photocatalyzing the reaction through its *in-situ*-obtained plasmonic features and enhancing the photocatalytic activity in the visible light range. Finally, the fifth chapter summarizes all parts of the thesis.

Table of Contents

List of Figures

List of Tables

Chapter 1:
Introduction

1.1   Background

Nowadays, the growth in resource extraction and processing to fulfill human consumption has been triggered by lifestyle. This has resulted in increased industrial growth, as well as negative environmental consequences. With the industrial revolution, the energy demand has increased significantly. The global energy demand is, at most, met by fossil fuels since more than 80% of current primary energy consumption is provided by fossil fuels [1]. Excessive use of fossil fuels strongly induces air pollution crisis since it produces large quantities of carbon dioxide (CO_2), which is the major reason for climate change and global warming [2–5]. How does CO_2 warm the earth? When the sunlight reaches the earth, some energy is reflected into space, and some are absorbed and re-radiated as heat. Most of this heat is absorbed by greenhouse gases, like CO_2, and then radiated in all directions, warming the earth. **Figure 1.1** shows the annual observance of CO_2 concentration from 1960 till 2021, and it is steadily increasing with time. Therefore, our current living conditions have been dramatically affected by using fossil fuels, and new energy sources that can provide a large-scale, sustainable energy supply must be developed.
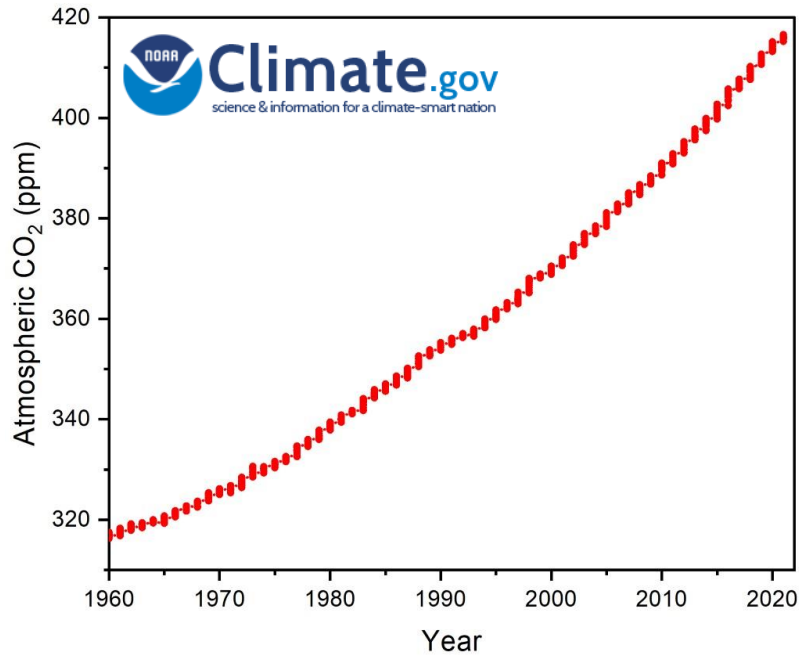
Figure 1.1. *The latest observation of CO_2 concentrations from Mauna Loa Observatory (MLO). This chart is plotted using data from the MLO in Hawaii, which has Earth's longest continuous record of direct measurements of atmospheric CO_2.*

Over and above, water pollution issues have become more prevalent because of the rapid population and industrial growth. In addition to other demands, water consumption has expanded dramatically in the agricultural, industrial, and home sectors, consuming large amounts of the available freshwater, allowing various pollutants to get into the water [6,7]. The presence of these pollutants in water threatens both humans and the environment. Thus, the removal of these pollutants from water is an urgent requirement for providing good life.

Accordingly, finding the technology that provides energy and treats polluted water in a reliable, cost-effective, and environmentally friendly manner should be our mission. Both objectives are among the most pressing issues confronting scientists today. Of many possible technologies currently being investigated to counter the energy and environmental issues, photocatalysis stands out as an appealing option for solving energy and environmental problems.

1.2   Principles of Photocatalysis

1.2.1   Definition

The development of photocatalysis was indeed inspired by natural photosynthesis in which sunlight is captured by plants to convert CO_2 and H_2O to O_2 and energy in the form of sugar. Thus, the use of light to accelerate the chemical reaction in the presence of a catalyst is termed photocatalysis. Photocatalysts are usually solid semiconductors that must meet the following criteria: i) excellent UV and/or visible light absorber, ii) chemically and biologically inert and photostable, iii) low cost, and iv) nontoxic [8].

1.2.2   Photocatalytic process

Figure 1.2 shows the main steps happening during the photocatalytic process on semiconductor photocatalyst. As presented in **Figure 1.2**, when a semiconductor is exposed to light with an energy equal to or greater than the semiconductor's bandgap energy ($h\nu \geq Eg$) (**step 1**), electrons can be excited from the valence band (VB) to the conduction band (CB), resulting in the generation of electron-hole pairs (**step 2**). This can be expressed as follows:

$$\text{Semiconductor photocatalyst} + h\nu \rightarrow e^- \text{(CB)} + h^+ \text{(VB)}$$
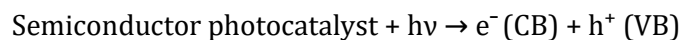
These photogenerated charge carriers are then engaged in one of the following three paths [9,10]:

1. migration to the semiconductor' surface.

2. be captured by surface or bulk defect sites.

3. recombination, which releases the energy as heat.

Only photogenerated charges that get to the semiconductor's surface will be beneficial for photocatalytic reactions (**step 3**). In the case of the other two paths (2, 3), the photogenerated electrons and holes do not participate in the photocatalytic reaction and thus are viewed as deactivation processes [11]. Fundamentally, a photocatalytic process composes of two-half reactions, oxidation-reduction reactions. The oxidation reaction is begun by holes in the valence band (VB), while electrons in the conduction band (CB) initiate the reduction reaction (**Figure 1.2**).
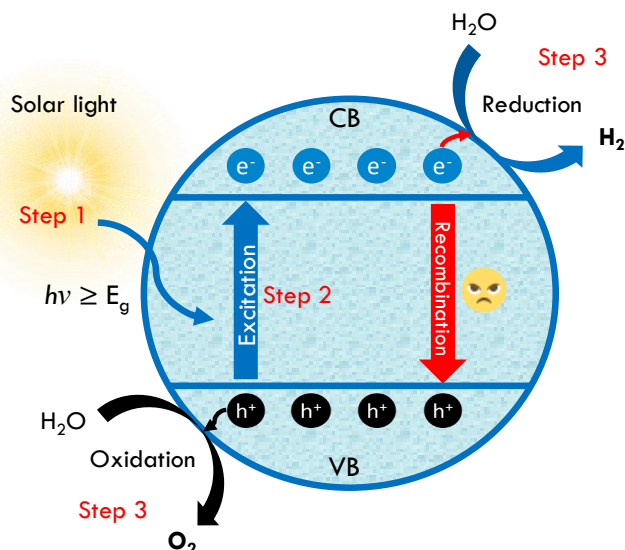
Figure 1.2. *Schematic representation for the steps of photocatalytic reactions on semiconductor photocatalyst. CB=Conduction band, VB=Valence band, E_g=bandgap.*

By looking at **Figure 1.2**, it has been noticed that the three key factors that control the performance of the semiconductor photocatalyst include i) light-harvesting (light absorption capacity), ii) separation of photogenerated charge carriers, and iii) redox (reduction-oxidation) reactions.

1.2.3   *Semiconducting photocatalytic materials*

Semiconductor photocatalysis is currently one of the most active research areas, which has been widely investigated in many fields such as catalysis, photochemistry, electrochemistry, and environmental chemistry [12]. Because of a good combination of their electronic structure, light absorption, and charge transport characteristics, binary semiconductors such as TiO_2, Cu_2O, ZnO, CdS, and Fe_2O_3 have mostly been utilized as photocatalysts. Other advantages like stability in the aqueous phase, efficient recovery, and reasonable recyclability make them favorable in environmental applications [7]. Importantly, the band structure, including the bandgap and positions of VB and CB, is one of the main characteristics of the semiconductor since it determines the light-harvesting as well as the redox abilities of the semiconductor photocatalyst. The reduction and oxidation capabilities of the photocatalyst are determined by the positions of CB and VB, respectively. For instance, in the water-splitting reaction, the position of CB must be more negative than the redox potential of H^+/H_2 (-0.414 V vs NHE, pH = 7), while the energy level of VB must be more positive than the redox potential of O_2/H_2O (0.815 V vs NHE, pH =

14

7). As presented in **Figure 1.3**, the appropriate semiconductor photocatalyst can be employed for a specific photocatalytic application after comparing its band edge positions with the chemical potential of the redox species. In summation, the strategy is to discover photocatalytic surfaces that possess the potential to absorb light and produce electron–hole pairs. These charge carriers can then proceed in the redox reactions.
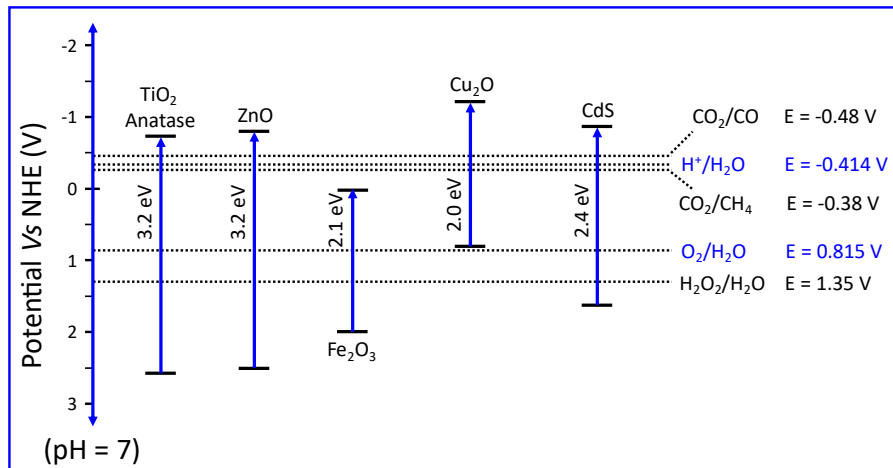
Figure 1.3. Band edge positions of common semiconductors compared with the chemical potential of different redox reactions.

1.2.4   Titanium oxide (TiO₂) photocatalysts

Of many possible semiconductors, TiO_2 quickly attracted numerous research interests in the photocatalysis field due to its high reactivity, excellent stability, nontoxicity, low cost, and, more importantly, suitable electronic band structure for many photocatalytic reactions [13–18]. TiO_2 was the first semiconductor to be reported as a photocatalyst back in 1972 [15], and it has been well investigated and applied in many research fields. Therefore, we thought that TiO_2-based materials are very promising potentials for application in photocatalytic hydrogen generation and environmental pollution control.

1.2.4.1   Phase structures of TiO₂

The phase structure of TiO_2 is one of the key elements ruling its photocatalytic performance. Mainly, TiO_2 exists in three crystallographic forms: anatase (tetragonal), rutile (tetragonal), and brookite (orthorhombic). **Figure 1.4** presents the schematic crystal structure of the three common TiO_2

polymorphs using TiO_6 octahedrons as the basic building block. Edges/corners' sharing and distortion of the octahedron units occur differently in each TiO_2 phase with maintaining TiO_2 as the overall stoichiometry. For instance, in rutile, every two opposite edges of the TiO_6 octahedron are shared, making a linear chain along the (001) direction. Chains are then connected by sharing corner oxygen atoms [19]. In anatase, octahedra share four edges forming zigzag chains along the (221) direction [19]. While, in brookite, both corners and edges are connected [20]. As a result, mass density and electronic bandstructure varied in different TiO_2 phases [11]. Thermodynamically, rutile is the most stable phase between TiO_2 phases, while the anatase and brookite are metastable phases. The anatase phase is commonly obtained but always formed in solution-based or low-temperature preparation systems. High-temperature or annealing treatments would usually convert anatase to rutile [21–23]. Brookite phase is less common and typically formed in solution-based growth systems. On the other hand, anatase and rutile polymorphs of TiO_2 are frequently utilized as photocatalysts in various applications of the environment and energy [24,25]. The differences in the crystal structure of anatase and rutile lead to variation in optical and electronic properties in terms of energy bandgaps (3.2 eV corresponding to 384 nm and 3.02 eV corresponding to 410 nm for anatase and rutile, respectively). Therefore, the redox driving force of anatase is a bit higher than that of rutile, although the light-harvesting by anatase is slightly less. Compared to rutile, anatase exhibits higher surface area and lower crystallinity, providing more active sites and facilitating the generation of defect species (such as oxygen vacancies) [11]. These properties lead to efficient charge separation in anatase and hence high photocatalytic performance. Thus, photocatalytically, anatase is considered the most active TiO_2 phase.

Anatase

Photocatalytically most active phase

Rutile

Thermodynamically most stable phase

Brookite
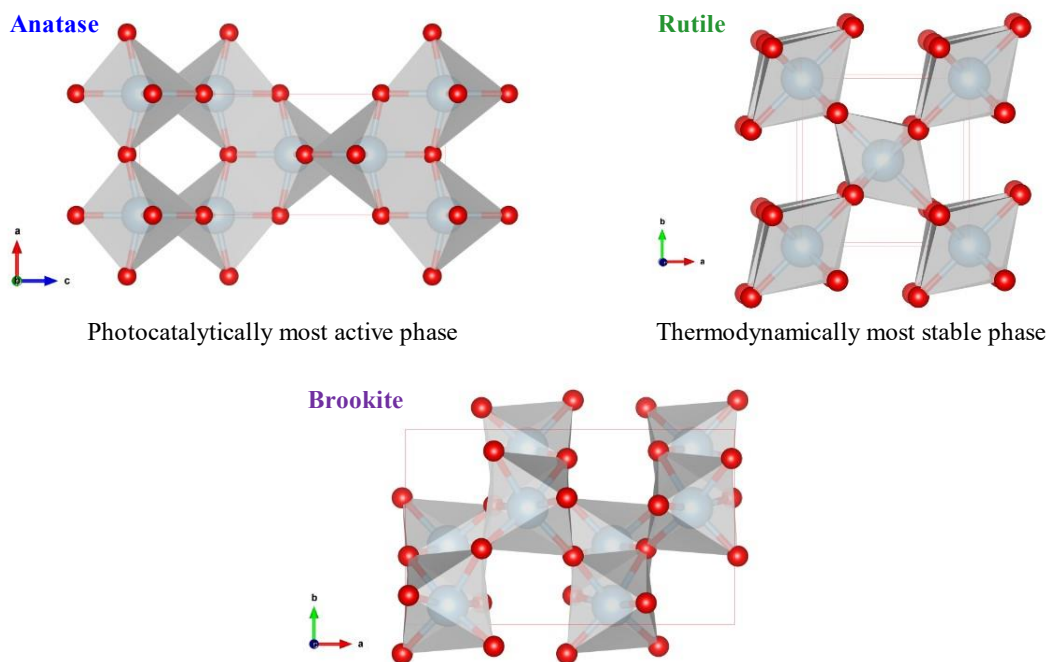
Figure 1.4. The schematic unit cell structure of common TiO₂ polymorphs. Ti (Blue); Oxygen (red); TiO₆ octahedra blocks (grey).

Additionally, there is another exotic phase of pure TiO_2, called TiO_2 (B) (monoclinic). It has a relatively open crystal structure (**Figure 1.5**) and is closer to titanate (to be discussed later) than other TiO_2 phases. It can be assumed as a titanate sheet with a structural entity made up of merely two TiO_6 octahedra, connected through edge-sharing between adjacent sheets [26]. In addition to the synthesis of TiO_2 (B) from solution, it can be formed in the calcination of titanate by the transformation sequence of protonated titanate → TiO_2 (B) → anatase TiO_2 [27].
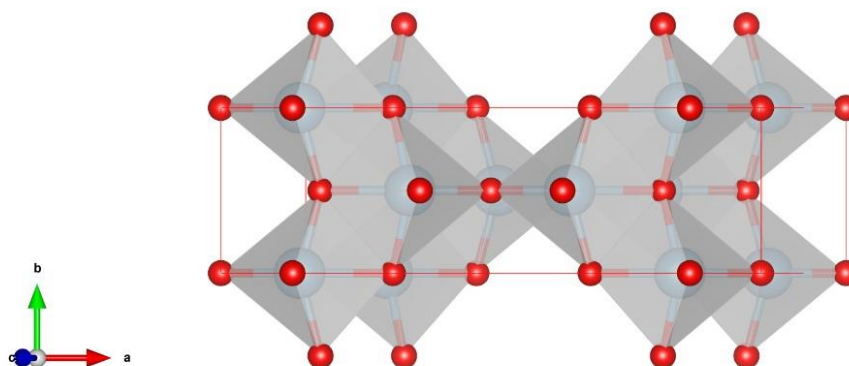
Figure 1.5. The schematic unit cell structure of TiO₂ (B). Ti (Blue); Oxygen (red); TiO₆ octahedra blocks (grey).

17

1.2.4.2 Layered Titanates

Other forms of TiO_2-based materials exist. They are a class of layered inorganic solids composed of nanometer-thick layers connected naturally in a layer-by-layer manner, providing an interlayer space to accommodate guest species, called layered titanates [28–32]. The general chemical formula of layered titanates is $M_xTi_yO_{x/2+y/2}.zH_2O$ (M, an interlayer cation (Na^+ or K^+)). Therefore, layered titanates are best considered to be salts of polytitanic acids, for example, $Na_2Ti_3O_7$ as sodium trititanate (**Figure 1.6 a**), $K_2Ti_4O_9$ as potassium pentatitanate (**Figure 1.6 b**), and $K_2Ti_2O_5$ as potassium dititanate (**Figure 1.6 c**). These structures are all monoclinic with stepped layered structures. $Na_2Ti_3O_7$ and $K_2Ti_4O_9$ consist of edge- and corner-sharing of TiO_6 octahedra with being stepped every three or four TiO_6 octahedrons, respectively, while $K_2Ti_2O_5$ is composed of a pair of TiO_5 trigonal bipyramids [33–35]. Another structural possibility is closely related to lepidocrocite structure with the formula of $A_xTi_{2-y}M_yO_4$ (A, an interlayer cation; M, metal, or vacancy), called lepidocrocite-type layered titanate (**Figure 1.6 d**). x and y values are related to each other depending on the valency of M (y = x/4 for a vacancy, y = x/3 for M^+, y = x/2 for M^{2+}, and y = x for M^{3+}). Lepidocrocite-type layered titanates usually crystallize in an orthorhombic structure and consist of edge-shared TiO_6 octahedrons [36–38].

Layered titanates have remarkable physicochemical properties due to their open crystal structure, which allows them to accommodate a wide range of cations and neutral molecules in the interlayer spaces. Additionally, the titanate sheet's negative charge allows it to effectively adsorb positively charged molecular species. Therefore, the cation exchange capacity of layered titanates is found to be outstanding [39–41]. Besides, layered titanates have been used as photocatalysts, fillers, and functional nanosheets [42–44], which make them of great technological interest. Thus, layered titanates nanostructures, composed of negatively charged titanates nanosheets and the interlayer cations, are one of the most widely studied cation exchangers [45]. For instance, layered titanates nanowires (NWs) have been recognized as ultrafast cation exchangers because they have extremely small dimensions for ion diffusion [46–48]. On the other hand, layered titanates have the potential to photocatalytically reduce metal ions in water to immobilize metals on the surface.

Interestingly, layered titanates are unique in the structure and reactivity to reach out to a set of new nanoarchitectures and sometimes to a specific type of heterostructure [49]. These versatile layered

titanates in interconversion to a new structure can sometimes lead to serendipity in finding a new structure of titania which usually has either a rutile or anatase structure [50,51]. In such cases, the obtained new structure can adopt defect, vacancy, doped species, and a heterostructure or a pure crystal phase (e.g., anatase or rutile) but a new nano shape. The interconversion can simply occur by changing the media's pH by adding an acid or an alkaline species (*e.g.*, quaternary alkylammonium hydroxide solutions) at room temperature or under solvothermal conditions [52,53].
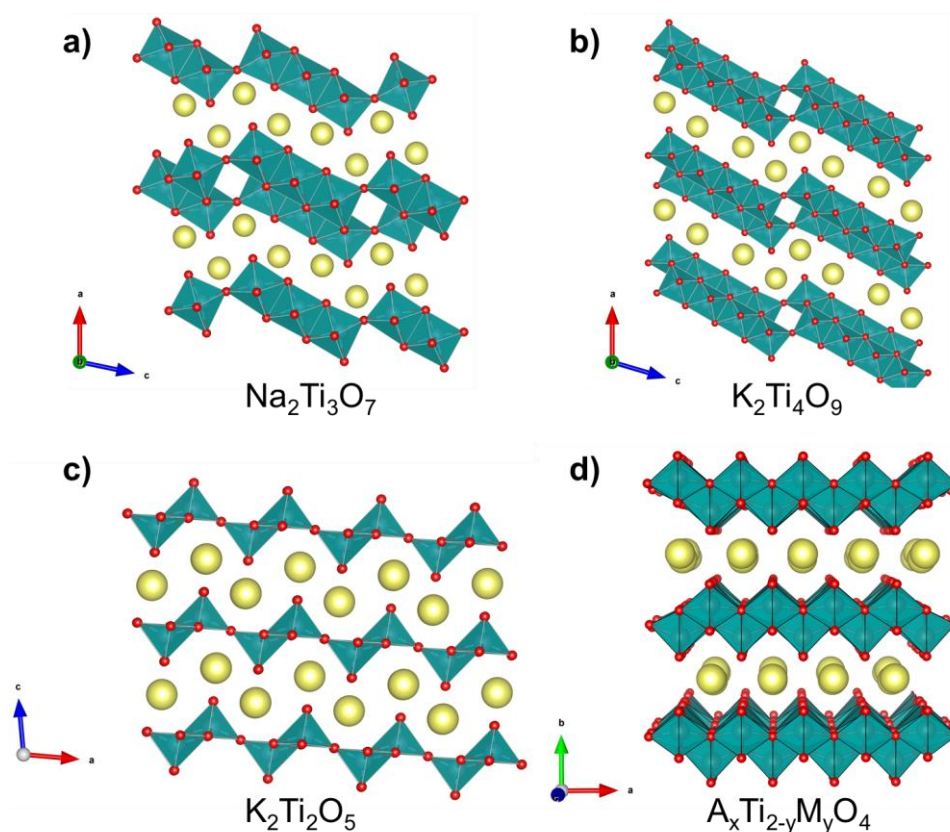
Figure 1.6. *Crystal structures of a) $Na_2Ti_3O_7$, b) $K_2Ti_4O_9$, c) $K_2Ti_2O_5$, and d) lepidocrocite-type layered titanate ($A_xTi_{2-y}M_yO_4$). Ti (grey); Oxygen (red); TiO_6 octahedra and TiO_5 trigonal blocks (green); intercalated metal cation (yellow).*

1.2.4.3   Drawbacks of TiO$_2$ photocatalysts

Since the first report of the TiO_2 photoelectrode by Fujishima and Honda in 1972 [15], none of the developed photocatalysts have fully satisfied all practical demands. The optimal photocatalyst must meet several criteria [54–56], including:

(i)   photogenerated charges with extended lifetimes,

(ii)   a suitable bandgap,

(iii)   a wide range of solar light utilization, and

(iv)   low cost, high efficiency, and stability.

Although TiO_2 fulfills some of these criteria (as mentioned earlier in this section), its efficiency has been obstructed by its 3.2 eV wide bandgap that confines light absorption to the UV region of the solar light (represents ~4% of the total solar irradiation). Additionally, TiO_2 shows high recombination of photogenerated electron-hole pairs.

1.2.4.4 *Modification strategies of TiO_2*

To overcome the drawbacks of TiO_2, various attempts have been introduced. Among them, doping with metal and non-metal was proposed to extend the optical absorption to the visible light region. Moreover, creating heterojunctions with other semiconductors, deposition of noble metals, and formation of defects in TiO_2 lattice were also proposed strategies to enhance charge transfer and separation in TiO_2.

i. *Metal and non-metal doping*

Limited light absorption has been addressed by doping TiO_2 with foreign atoms, which alter the optical properties of TiO_2 through the introduction of suitable intragap electronic states. Transition metals (e.g., V, Cr, Mn, Fe, and Cu) were added as substitutional atoms inside the TiO_2 lattice to form 3d electronic states below the CB, enhancing visible light absorption and photocatalytic activity (**Figure 1.7**). Nevertheless, in some cases, metal doping results in the creation of deep electronic states, which typically results in increased charge recombination, showing an unsatisfactory compromise between light absorption and photocatalytic activity [57,58]. Therefore, worthy enhancements are only possible at a low ratio of metal dopant and/or using precise synthesis methods to diminish lattice distortion [59].
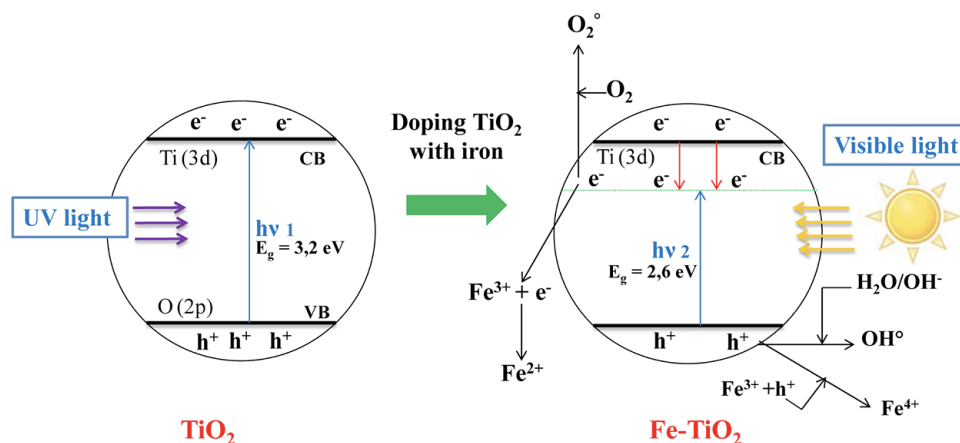
Figure 1.7. *Schematic representation of metal (Fe) doped TiO₂. Reprinted with permission from {Ind. Eng. Chem. Res. 2013, 52, 3581–3599}. Copyright {2013} American Chemical Society.*

Nonmetal (e.g., N, C, and S) doping, on the other hand, has shown great promise in offering efficient visible light active TiO₂ photocatalysts, owing to inducing 2p electronic states above the VB able to efficiently transfer electrons to the 3d CB of TiO₂ and therefore providing high photocatalytic activity [58]. N-doping, for example, has been shown to produce yellow TiO₂ powders with a redshift of the optical absorption onset of up to 500 nm [60]. However, non-metal species sometimes induce only a surface modification of TiO₂ rather than bulk doping [61].
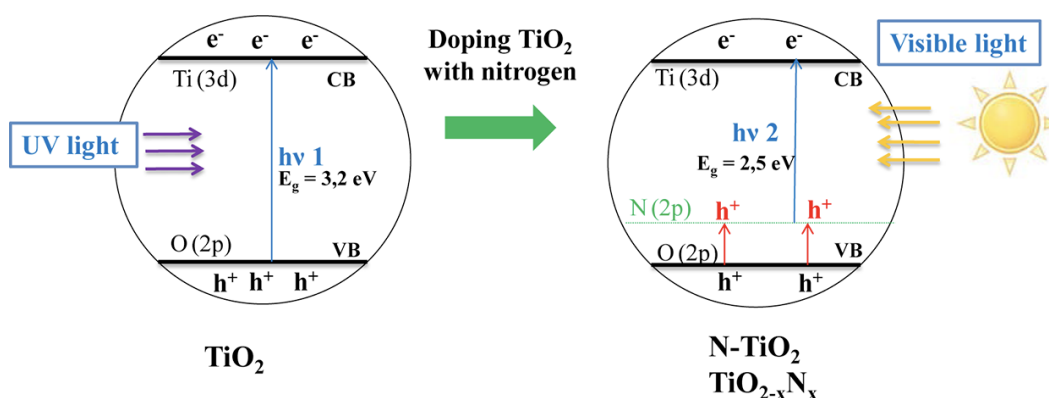
Figure 1.8. *Schematic representation of non-metal (N) doped TiO₂. Reprinted with permission from {Ind. Eng. Chem. Res. 2013, 52, 3581–3599}. Copyright {2013} American Chemical Society.*

When compared to metal doping, non-metal doping is expected to be more favorable since it minimizes the creation of charge carrier recombination sites [62]. N was employed as a non-metal dopant in the most recent research to improve TiO₂'s water-splitting efficiency [63,64]. The formation

of gap states by the interaction of N 2p and O 2p states narrows the bandgap energy of TiO_2 [60]. The mixing of orbitals uplifts the VB level of TiO_2 but does not affect the CB. The photoreduction capacity of TiO_2 has therefore remained unchangeable, but its oxidation ability has reduced.

ii.   TiO₂-Semiconductor heterojunction

Another interesting approach that has gained a lot of interest is coupling TiO_2 with another semiconductor with a different band structure. If the band structure of both semiconductors is adequate, electrons and holes become physically separated, and thus the recombination rate is considerably mitigated, improving the photocatalytic activity [10,65,66]. Various types of heterojunction semiconductors have been developed to address the previously mentioned issues. Among them, Type II and direct Z-scheme heterojunctions. In Type II heterojunction, after generating electron and hole pairs in both photocatalysts (semiconductor I and semiconductor II, hereafter SC I and SC II), photogenerated electrons transfer from SC I to SC II, whereas photogenerated holes transfer in the opposite direction (**Figure 1.9**). Consequently, photocatalytic reduction and oxidation reactions proceed via the accumulation of electrons and holes on SC II and SC I, respectively. Therefore, the photogenerated charge carriers are spatially separated [67,68].
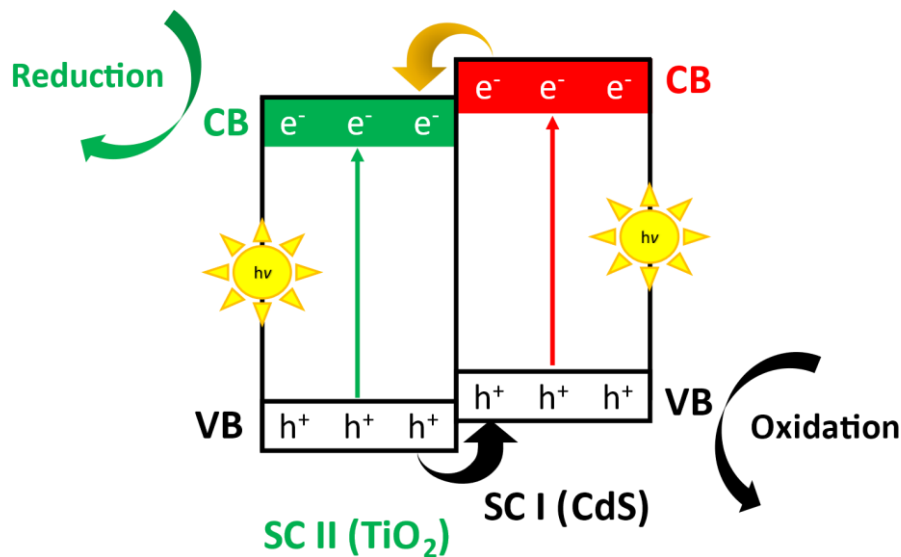
Figure 1.9. Type II heterojunction. For example, TiO₂/CdS system.

Although type-II charge transfer appears to be ideal due to superb charge separation, it has some disadvantages. As shown in **Figure 1.9**, photogenerated electrons gather on the CB of SC II with a

weak reduction potential, whereas photogenerated holes accumulate on the VB of SC I with a weak oxidation potential. Therefore, the improved charge separation comes at the expense of diminished redox ability, which is undesirable for the photocatalytic reaction from a thermodynamic standpoint. From a dynamic viewpoint, electrostatic repulsive forces between holes or electrons are great to hold their transfer in type-II heterojunction. Thus, achieving the expected charge transfer in a type-II heterojunction is difficult. To sum up, the proven charge-transfer process in type-II heterojunction is debatable [69].

To enhance charge separation efficiency and maintain the strong redox ability of the system, direct Z-scheme heterojunction was proposed [70]. In this process, photogenerated holes in the VB of SC I (with lower oxidation ability) recombine with electrons in the CB of SC II (with lower reduction ability). Then, photogenerated electrons in the CB of SC I and holes in the VB of SC II participate in the reduction and oxidation reactions, respectively (**Figure 1.10**). Such a charge transfer process can provide this system with strong redox ability, together with spatially separated redox reaction sites [71].
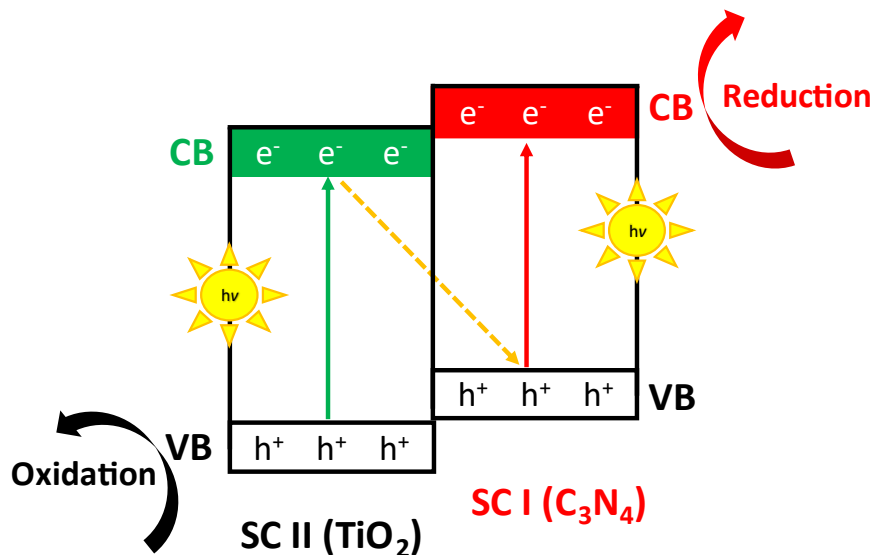
Figure 1.10. *Direct Z-scheme heterojunction. For example, TiO_2/C_3N_4 system.*

iii. *Noble metal deposition*

Incorporating noble metals with semiconductor photocatalysts was proposed to improve the photocatalytic performance due to their different Fermi levels, distinguished by the metals' work function and semiconductors' band structure. Upon combination, a Schottky barrier can be created between metal and semiconductor, resulting in a significant charge carrier transfer and separation comparable to that in coupled semiconductors (**Figure 1.11**) [72–74]. Although this strategy has achieved satisfactory results in the field of photocatalysis, it lacks the advantage of its practical application due to the high cost of noble metals. Therefore, most of the researchers now tend to eliminate the use of co-catalysts with TiO_2 during the photocatalytic process to reduce the cost of the process and realize the photocatalyst simplicity.
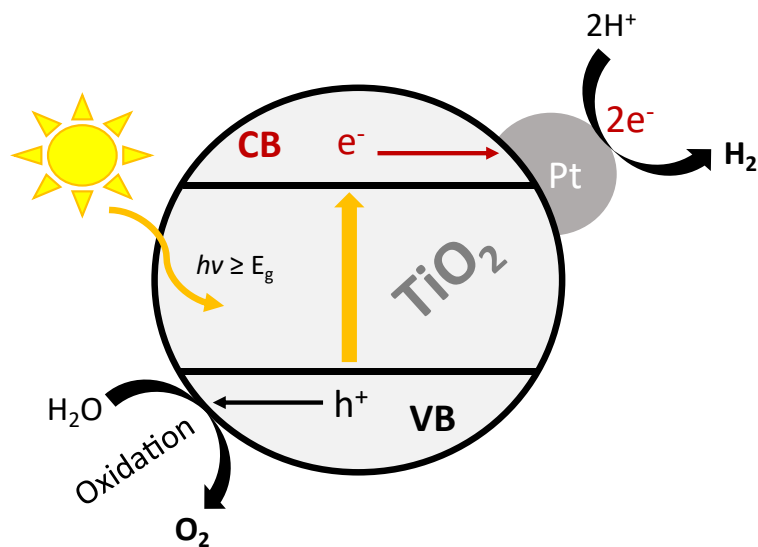
Figure 1.11. Noble metal/TiO_2 photocatalytic system.

iv. *Defective (colored) TiO_2*

Defective (reduced or colored) TiO_2 is originally formed by intrinsic doping, namely by introducing oxygen vacancies (Vo) and/or Ti^{3+} defect species into the lattice. These materials are typically synthesized by high-temperature treatment of TiO_2 in various reducing atmospheres (e.g., vacuum, Ar, Ar/H_2, or H_2) [75,76]. Defective TiO_2 can be grey, blue, brown, or black depending on the conditions used. The resultant color is attributed to the creation of differing amounts of defects (Vo and Ti^{3+}). Increasing the level of reduction results in a larger concentration of defects and, as a result, darker TiO_2

24

powders. Defective TiO_2 has been demonstrated to be an efficient photocatalyst for hydrogen generation from water under visible-light irradiation, and research has persisted since the first report by Chen *et al.* in 2011 [77].

Recently, defective TiO_2 has gained great interest, especially for its unique co-catalyst-free photocatalytic activity towards hydrogen generation [78]. Synthesis of such materials features intrinsic cocatalytic active centers that have the same cocatalytic effect obtained by noble metals decoration. When evaluating the solar H_2 production activity, most reports using defective TiO_2 have employed noble metal cocatalysts. Despite the apparent link between the two effects (visible light absorption versus intrinsic cocatalytic activation), it remains unclear if the photocatalytic activity in cocatalyst-free hydrogen production is mechanistically linked to the increased visible light absorption.

1.3   Applications of TiO_2 photocatalysis

Photocatalysis has received a lot of attention in recent years, with photocatalysis being used in a wide range of applications, particularly in energy and environment-related fields [79–81]. Since the first report of Fujishima and Honda's hydrogen production discovery in 1972 [15], interesting photocatalytic properties of TiO_2 have been exploited to produce valuable solar fuels (i.e., solar energy conversion) and to remove pollutants, including organic, inorganic, and biological species, from water and air [14,81–83].

Overall, the state-of-the-art strategies that have improved the photocatalytic activity were detailed in two aspects: energy conversion and environmental remediation (**Figure 1.12**). Among them, we focused on photocatalytic hydrogen evolution and removal of toxic metal ions from water and will be detailed later.
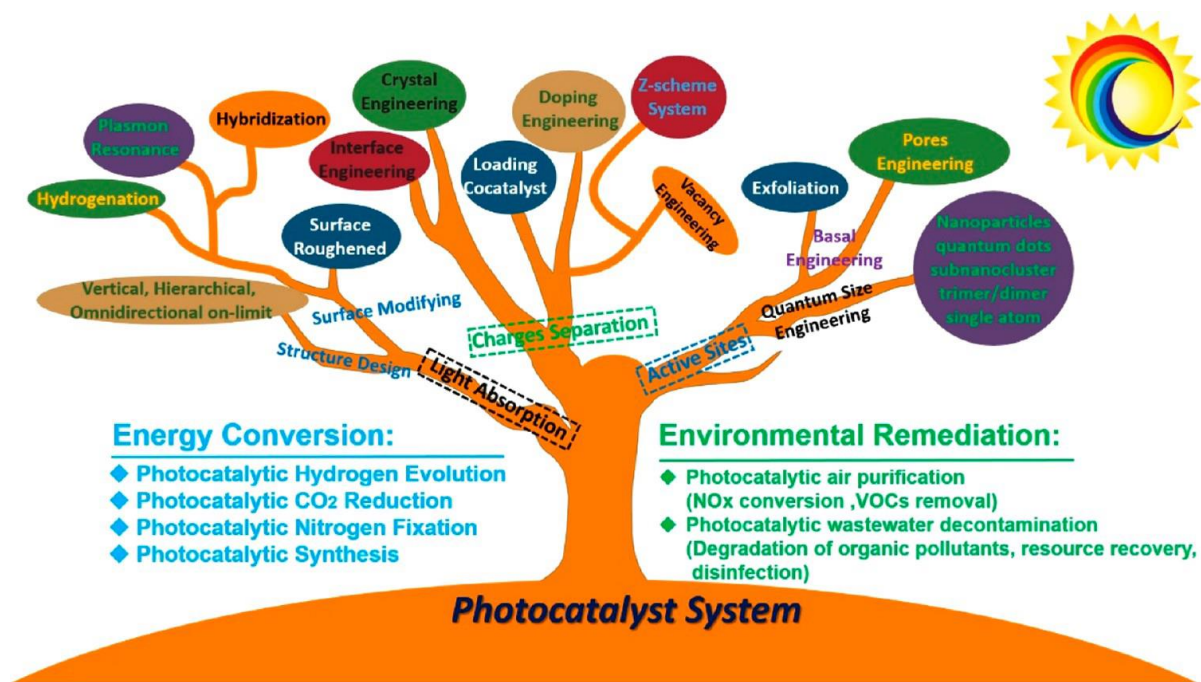
Figure 1.12. State-of-the-art strategies for enhanced photocatalytic energy conversion and environmental remediation. Reprinted with permission from {ACS Nano 2019, 13, 9811–9840}. Copyright {2019} American Chemical Society.

1.4   Photocatalytic hydrogen generation

For achieving a low-carbon economy, H_2 is an ideal energy carrier. It has a high calorific value per mass unit, which is three times more than gasoline and four times higher than natural gas. Furthermore, during the combustion of H_2, no greenhouse gases are generated [11]. As a result, solar energy storage in the form of H_2 is recommended as one of the most suitable prospective pathways for generating clean and sustainable energy. On the other hand, hydrogen is the most plentiful element that can be released from a wide variety of materials. More importantly, in the chemical sector, H_2 is an essential chemical reagent. Since the initial discovery of the photoelectrochemical water splitting process on TiO_2 electrode by Fujishima and Honda in 1972 [15], significant research has been conducted on photocatalytic or photoelectrochemical (PEC) splitting of water into H_2 and O_2.

Although H_2 is a clean and extremely effective energy carrier, the main drawback for hydrogen application lies in the safe transport and storage of hydrogen on a large scale [84]. Chemical hydrogen storage materials with high hydrogen contents are very attractive for practical application. Another significant reaction for H_2 generation is the dehydrogenation of ammonia borane ($NH_3 \cdot BH_3$; AB), which

has been emerged as a promising candidate due to its non-toxicity, low molecular weight (30.87 g.mol^{-1}), high stability in solid-state and solution under ambient conditions, and high hydrogen content (19.6 wt%). Therefore, H$_2$ generation using hydrogen storage materials, like AB, is regarded as a practical, cost-effective, and efficient method for addressing energy and environmental concerns.

1.5   Photocatalytic removal of toxic metal ions

Of many water pollutants, heavy metals are one of the most serious pollution problems due to their nonbiodegradability and bioaccumulation in living tissues, and therefore have been considered by many researchers around the world. Heavy metals can be released into water bodies through many sources including wastewater, industrial activities (e.g., pigments and paints, extraction and mining, electroplating, glass production, and battery manufacturing plants), and domestic effluents. Natural sources (i.e., weathering, erosion from rock and soil, and rainwater) can also be another source of heavy metals pollution.

Traditional methods for treating heavy metals pollution involve various methods such as precipitation, ion exchange, reverse osmosis, adsorption, and biological processes [85]. Using such methods can only help in capturing heavy metal ions and transforming them from one phase to another without changing their toxic behavior [86]. Consequently, it is necessary to develop a process where heavy metal ions can be reduced to their zero-valent state, which is nontoxic.

To meet the above objectives, the photocatalytic process is thought to be a promising technique. In recent decades, photocatalysis has gained a lot of interest as a viable option for treating wastewater including organic substances as well as certain heavy metals. Heavy metal removal is mostly accomplished by a reduction process that results in metal ions with a reduced oxidation state. Only arsenic occurs in anionic form and must be converted to a non-toxic higher oxidation state by an oxidation process. Heterogeneous photocatalysis, unlike other advanced oxidation systems, can perform both oxidation and reduction reactions. It is a well-known technique in which light energy is used to stimulate the semiconductor material, resulting in the formation of electron-hole pairs. Metal ions utilize the photogenerated electrons in the conduction band and get reduced to their non-toxic

state. For a variety of heavy metals, including chromium, nickel, platinum, zinc, cadmium, and mercury, photoreduction has been widely investigated [87].

1.6   Motivation and aim of doctoral research

At present, the process of hydrogen production involves CO_2 evolution in huge amounts, increasing the Earth's temperatures. Therefore, finding viable alternatives excluding the generation of any greenhouse gases is the key element. Hydrogen production from water, as a clean and renewable energy process, is introduced as a promising approach to mitigating climate change caused by CO_2 emissions.

On the other hand, one of the serious environmental problems is heavy metal pollution in water, which causes many risky effects on humans and animals. Therefore, the efficient elimination of these toxic elements from the environment is becoming a crucial need.

This thesis, therefore, aimed to develop advanced and efficient materials for solving energy and environmental-related problems. Photocatalysis, as sustainable, efficient, and cheap technology, was the main component to reach the desired goals. As an ideal and powerful photocatalyst, TiO_2 was the material we rely on in our research.

1.7   References:

[1]   J. Yoon, Y. Sun, J.A. Rogers, Flexible Solar Cells Made of Nanowires/Microwires, Elsevier Ltd., 2010.

[2]   Y. Ma, X. Wang, Y. Jia, X. Chen, H. Han, C. Li, Titanium dioxide-based nanomaterials for photocatalytic fuel generations, Chemical Reviews. 114 (2014) 9987–10043.

[3]   P. Poizot, F. Dolhem, Clean energy new deal for a sustainable world: From non-CO2 generating energy sources to greener electrochemical storage devices, Energy and Environmental Science. 4 (2011) 2003–2019.

[4]   E.A. Quadrelli, G. Centi, J. L. Duplan, S. Perathoner, Carbon Dioxide Recycling: Emerging Large-Scale Technologies with Industrial Potential, ChemSusChem. 4 (2011) 1194–1215.

[5]   M.I. Hoffert, K. Caldeira, G. Benford, D.R. Criswell, C. Green, H. Herzog, A.K. Jain, H.S. Kheshgi, K.S. Lackner, J.S. Lewis, H.D. Lightfoot, W. Manheimer, J.C. Mankins, M.E. Mauel, L.J. Perkins, M.E. Schlesinger, T. Volk, T.M.L. Wigley, Engineering: Advanced technology paths to global climate stability: Energy for a greenhouse planet, Science. 298 (2002) 981–987.

[6]   C. Santhosh, V. Velmurugan, G. Jacob, S.K. Jeong, A.N. Grace, A. Bhatnagar, Role of nanomaterials in water treatment applications: A review, Chemical Engineering Journal. 306 (2016) 1116–1137.

[7]   M.R. Hoffmann, S.T. Martin, W. Choi, D.W. Bahnemann, Environmental Applications of Semiconductor Photocatalysis, Chemical Reviews. 95 (2002) 69–96.

[8]   A. Kubacka, M. Fernández-García, G. Colón, Advanced nanoarchitectures for solar photocatalytic applications, Chemical Reviews. 112 (2012) 1555–1614.

[9]   S.T. Martin, H. Herrmann, W. Choi, M.R. Hoffmann, Time-resolved microwave conductivity. Part 1. TiO_2 photoreactivity and size quantization, Journal of the Chemical Society, Faraday Transactions. 90 (1994) 3315–3322.

[10]   A.L. Linsebigler, G. Lu, J.T. Yates, Photocatalysis on TiO_2 Surfaces: Principles, Mechanisms, and Selected Results, Chem. Rev. 95 (1995) 735–758.

[11]   Y. Ma, X. Wang, Y. Jia, X. Chen, H. Han, C. Li, Titanium dioxide-based nanomaterials for photocatalytic fuel generations, Chemical Reviews. 114 (2014) 9987–10043.

[12]   J. Luo, S. Zhang, M. Sun, L. Yang, S. Luo, J.C. Crittenden, A Critical Review on Energy Conversion and Environmental Remediation of Photocatalysts with Remodeling Crystal Lattice, Surface, and Interface, ACS Nano. (2019).

[13]   Xiaobo Chen, S.S. Mao, Titanium Dioxide Nanomaterials: Synthesis, Properties, Modifications, and Applications, Chemical Reviews. 107 (2007) 2891–2959.

[14]   X. Chen, S. Shen, L. Guo, S.S. Mao, Semiconductor-based Photocatalytic Hydrogen Generation, Chemical Reviews. 110 (2010) 6503–6570.

[15]   A. FUJISHIMA, K. HONDA, Electrochemical Photolysis of Water at a Semiconductor Electrode, Nature 1972 238:5358. 238 (1972) 37–38.

[16]   Quanjun Xiang, Jiaguo Yu, Mietek Jaroniec, Graphene -based semiconductor photocatalysts, Chemical Society Reviews. 41 (2012) 782–796.

[17]   X. Wang, Z. Li, J. Shi, Y. Yu, One-Dimensional Titanium Dioxide Nanomaterials: Nanowires, Nanorods, and Nanobelts, Chemical Reviews. 114 (2014) 9346–9384.

[18]   A. Fujishima, T.N. Rao, D.A. Tryk, Titanium dioxide photocatalysis, Journal of Photochemistry and Photobiology C: Photochemistry Reviews. 1 (2000) 1–21.

[19]   M. Gopal, W.J.M. Chan, L.C. de Jonghe, Room temperature synthesis of crystalline metal oxides, JOURNAL OF MATE RIALS SCIENCE. 32 (1997) 6001–6008.

[20]   O. Carp, C.L. Huisman, A. Reller, Photoinduced reactivity of titanium dioxide, Progress in Solid State Chemistry. 32 (2004) 33–177.

[21]   Jianying Shi, Jun Chen, Zhaochi Feng, Tao Chen, Yuxiang Lian, and Xiuli Wang, C. Li, Photoluminescence Characteristics of TiO_2 and Their Relationship to the Photoassisted Reaction of Water/Methanol Mixture, Journal of Physical Chemistry C. 111 (2006) 693–699.

[22]   W. Su, J. Zhang, Z. Feng, T. Chen, P. Ying, C. Li, Surface Phases of TiO_2 Nanoparticles Studied by UV Raman Spectroscopy and FT-IR Spectroscopy, Journal of Physical Chemistry C. 112 (2008) 7710–7716.

[23]   Jing Zhang, Meijun Li, Zhaochi Feng, and Jun Chen, C. Li, UV Raman Spectroscopic Study on TiO_2. I. Phase Transformation at the Surface and in the Bulk, Journal of Physical Chemistry B. 110 (2005) 927–935.

[24]   M. Ge, C. Cao, J. Huang, S. Li, Z. Chen, K.-Q. Zhang, S.S. Al-Deyab, Y. Lai, A review of one-dimensional TiO_2 nanostructured materials for environmental and energy applications, Journal of Materials Chemistry A. 4 (2016) 6772–6801.

[25]   Y. Zhang, Z. Jiang, J. Huang, L.Y. Lim, W. Li, J. Deng, D. Gong, Y. Tang, Y. Lai, Z. Chen, Titanate and titania nanostructured materials for environmental and energy applications: a review, RSC Advances. 5 (2015) 79479–79510.

[26]   R. Marchand, L. Brohan, M. Tournoux, TiO2(B) a new form of titanium dioxide and the potassium octatitanate $K_2Ti_8O_{17}$, Materials Research Bulletin. 15 (1980) 1129–1133.

[27]   D. v. Bavykin, M. Carravetta, A.N. Kulak, F.C. Walsh, Application of Magic-Angle Spinning NMR to Examine the Nature of Protons in Titanate Nanotubes, Chemistry of Materials. 22 (2010) 2458–2465.

[28]   S.K. and M.K. H. Izawa, Ion Exchange and Dehydration of Layered Titanates, $Na_2Ti_3O_7$ and $K_2Ti_4O_9$, J. Phys. Chem. 86 (1982) 5023–5026.

[29]   Y.K. and Y.F. Takayoshi Sasaki, Protonated Pentatitanate: Preparation, Characterizations, and Cation Intercalation, Chem. Mater. 4 (1992) 894–899.

[30]   T. Sasaki, M. Watanabe, Y. Michiue, Y. Komatsu, F. Izumi, S. Takenouchi, Preparation and Acid-Base Properties of a Protonated Titanate with the Lepidocrocite-like Layer Structure, Chem. Mater. 7 (1995) 1001–1007.

[31]   T. Sasaki, F. Izumi, M. Watanabe, Intercalation of Pyridine in Layered Titanates, Chem. Mater. 8 (1996) 777–782.

[32]   S. Nakano, T. Sasaki, K. Takemura, M. Watanabe, Pressure-Induced Intercalation of Alcohol Molecules into a Layered Titanate, Chem. Mater. 10 (1998) 2044–2046.

[33]   S. Andersson, A.D. Wadsley, The Crystal Structure of $Na_2Ti_3O_7$, Acta Cryst. 14 (1961) 1245–1249.

[34]   STEN ANDERSSON, A. D. WADSLEY, Five Co-ordinated Titanium in $K_2Ti_2O_5$, Nature. 187 (1960) 499–500.

[35]   I. Yusuke, S. Masahiro, S. Tsuneji, O. Makoto, Functionalization of layered titanates, Journal of Nanoscience and Nanotechnology. 14 (2014) 2135–2147.

[36]   M. Shirpour, J. Cabana, M. Doeff, Lepidocrocite-type Layered Titanate Structures: New Lithium and Sodium Ion Intercalation Anode Materials, (2014).

[37]   A. F. REID, W. G. MUMME, A. D. WADSLEY, A New Class of Compound $M_x^+A_x^{3+}Ti_{2-x}O_4$. (0.60 < x < 0.80) Typified by $Rb_xMn_xTi_{2-x}O4$, Acta Cryst. 24 (1968) 1228–1233.

[38]   R. Ma, Y. Bando, T. Sasaki, Nanotubes of lepidocrocite titanates, Chemical Physics Letters. 380 (2003) 577–582.

[39]   Y. Ide, W. Shirae, T. Takei, D. Mani, J. Henzie, Merging Cation Exchange and Photocatalytic Charge Separation Efficiency in an Anatase/$K_2Ti_4O_9$ Nanobelt Heterostructure for Metal Ions Fixation, Inorganic Chemistry. 57 (2018) 6045–6050.

[40]   T. (Tip) Sirinakorn, S. Bureekaew, M. Ogawa, Layered Titanates ($Na_2Ti_3O_7$ and $Cs_2Ti_5O_{11}$) as Very High Capacity Adsorbents of Cadmium(II), 92 (2018) 1–6.

[41]   T.K. Saothayanun, T.T. Sirinakorn, M. Ogawa, Ion Exchange of Layered Alkali Titanates ($Na_2Ti_3O_7$, $K_2Ti_4O_9$, and $Cs_2Ti_5O_{11}$) with Alkali Halides by the Solid-State Reactions at Room Temperature, Inorganic Chemistry. 59 (2020) 4024–4029.

[42]   Akihiko Kudo, Takeshi Kondo, Photoluminescent and photocatalytic properties of layered caesium titanates, $Cs_2Ti_nO_{2n+1}$ (n=2, 5, 6), Journal of Materials Chemistry. 7 (1997) 777–780.

[43]   M. Osada, Y. Ebina, H. Funakubo, S. Yokoyama, T. Kiguchi, K. Takada, T. Sasaki, High-κ Dielectric Nanofilms Fabricated from Titania Nanosheets, Advanced Materials. 18 (2006) 1023–1027.

[44]   Yasufumi Fuse, Yusuke Ide, Makoto Ogawa, Hybridization of epoxy resin with a layered titanate and UV light durability and controlled refractive index of the resulting nanocomposite, Polymer Chemistry. 1 (2010) 849–853.

[45]   Y. Komatsu, Y. Fujiki, Adsorption of Cesium from Aqueous Solutions Using a Crystalline Hydrous Titanium Dioxide Fibers, Chemistry Letters. 9 (1980) 1525–1528.

[46]   W. Zhou, X. Liu, Y. Sang, Z. Zhao, K. Zhou, H. Liu, S. Chen, Enhanced performance of layered titanate nanowire-based supercapacitor electrodes by nickel ion exchange, ACS Applied Materials and Interfaces. 6 (2014) 4578–4586.

[47]   Y. Ishikawa, S. Tsukimoto, K.S. Nakayama, N. Asao, Ultrafine sodium titanate nanowires with extraordinary Sr ion-exchange properties, Nano Letters. 15 (2015) 2980–2984.

[48]   Q. Zhang, Y. Guo, K. Guo, T. Zhai, H. Li, Ultrafine potassium titanate nanowires: a new Ti-based anode for sodium ion batteries, Chemical Communications. 52 (2016) 6229–6232.

[49]   T. (Tip) Sirinakorn, S. Bureekaew, M. Ogawa, Layered Titanates ($Na_2Ti_3O_7$ and $Cs_2Ti_5O_{11}$) as Very High Capacity Adsorbents of Cadmium(II), Bulletin of the Chemical Society of Japan. 92 (2018) 1–6.

[50]   H. Yuan, R. Besselink, Z. Liao, J.E. ten Elshof, The swelling transition of lepidocrocite-type protonated layered titanates into anatase under hydrothermal treatment, Scientific Reports 4 (2014) 1–6.

[51]   D. Mani, R. Tahawy, E. Doustkhah, M. Shanmugam, M. Arivanandhan, R. Jayavel, Y. Ide, A rutile TiO_2 nanobundle as a precursor of an efficient visible-light photocatalyst embedded with Fe_2O_3, Inorganic Chemistry Frontiers. 8 (2021) 4423–4430.

[52]   M. Ogawa, T. Yoshinao, Intercalation of Alkylammonium Cations into a Layered Titanate in the Presence of Macrocyclic Compounds, Chemistry of Materials. 11 (1998) 30–32.

[53]   F. Kishimoto, Y. Takamura, S. Nakagawa, Y. Wada, Manipulation of the Magnetic Properties of Co- and Fe-Doped Layered Titanates by Alkyl Ammonium Intercalation, Advanced Materials Interfaces. 3 (2016) 1600509.

[54]   Huanli Wang, Lisha Zhang, Zhigang Chen, Junqing Hu, Shijie Li, Zhaohui Wang, Jianshe Liu, Xinchen Wang, Semiconductor heterojunction photocatalysts: design, construction, and photocatalytic performances, Chemical Society Reviews. 43 (2014) 5234–5244.

[55]   W. Q. Wu, H. L. Feng, H. S. Rao, Y. F. Xu, D. B. Kuang, C. Y. Su, Maximizing omnidirectional light harvesting in metal oxide hyperbranched array architectures, Nature Communications 5 (2014) 1–9.

[56]   Q. Wang, T. Hisatomi, Q. Jia, H. Tokudome, M. Zhong, C. Wang, Z. Pan, T. Takata, M. Nakabayashi, N. Shibata, Y. Li, I.D. Sharp, A. Kudo, T. Yamada, K. Domen, Scalable water splitting on particulate photocatalyst sheets with a solar-to-hydrogen energy conversion efficiency exceeding 1%, Nature Materials 15 (2016) 611–615.

[57]   X.C. and, S.S. Mao†, Titanium Dioxide Nanomaterials: Synthesis, Properties, Modifications, and Applications, Chemical Reviews. 107 (2007) 2891–2959.

[58]   R. Daghrir, P. Drogui, D. Robert, Modified TiO_2 For Environmental Photocatalytic Applications: A Review, Industrial and Engineering Chemistry Research. 52 (2013) 3581–3599.

[59]   C. Adán, A. Bahamonde, M. Fernández-García, A. Martínez-Arias, Structure and activity of nanosized iron-doped anatase TiO_2 catalysts for phenol photocatalytic degradation, Applied Catalysis B: Environmental. 72 (2007) 11–17.

[60]   R. Asahi, T. Morikawa, T. Ohwaki, K. Aoki, Y. Taga, Visible-light photocatalysis in nitrogen-doped titanium oxides, Science. 293 (2001) 269–271.

[61]   A.B. Murphy, Does carbon doping of TiO_2 allow water splitting in visible light? Comments on "Nanotube enhanced photoresponse of carbon modified (CM)-n-TiO_2 for efficient water splitting," Solar Energy Materials and Solar Cells. 92 (2008) 363–367.

[62]   S. Martha, P.C. Sahoo, K.M. Parida, An overview on visible light responsive metal oxide based photocatalysts for hydrogen energy production, RSC Advances. 5 (2015) 61535–61553.

[63]   M.P. Kumar, R. Jagannathan, S. Ravichandran, Photoelectrochemical System for Unassisted High-Efficiency Water-Splitting Reactions Using N-Doped TiO_2 Nanotubes, Energy & Fuels. 34 (2020) 9030–9036.

[64]   R. Shi, Z. Li, H. Yu, L. Shang, C. Zhou, G.I.N. Waterhouse, L. Z. Wu, T. Zhang, Effect of Nitrogen Doping Level on the Performance of N-Doped Carbon Quantum Dot/TiO_2 Composites for Photocatalytic Hydrogen Evolution, ChemSusChem. 10 (2017) 4650–4656.

[65]   M. D. Hernández-Alonso, Fernando Fresno, Silvia Suárez, J. M. Coronado, Development of alternative photocatalysts to TiO_2 : Challenges and opportunities, Energy & Environmental Science. 2 (2009) 1231–1257.

[66]   Huanjun Zhang, Guohua Chen, D. W. Bahnemann, Photoelectrocatalytic materials for environmental applications, Journal of Materials Chemistry. 19 (2009) 5089–5121.

[67]   S. Bai, J. Jiang, Q. Zhang, Y. Xiong, Steering charge kinetics in photocatalysis: intersection of materials syntheses, characterization techniques and theoretical simulations, Chemical Society Reviews. 44 (2015) 2893–2939.

[68]   N. Serpone, P. Maruthamuthu, P. Pichat, E. Pelizzetti, H. Hidaka, Exploiting the interparticle electron transfer process in the photocatalysed oxidation of phenol, 2-chlorophenol and pentachlorophenol: chemical evidence for electron and hole transfer between coupled semiconductors, Journal of Photochemistry and Photobiology A: Chemistry. 85 (1995) 247–255.

[69]   J. Low, J. Yu, M. Jaroniec, S. Wageh, A.A. Al-Ghamdi, Heterojunction Photocatalysts, Advanced Materials. 29 (2017) 1601694.

[70]   J. Yu, S. Wang, J. Low, W. Xiao, Enhanced photocatalytic performance of direct Z-scheme g-C_3N_4–TiO_2 photocatalysts for the decomposition of formaldehyde in air, Physical Chemistry Chemical Physics. 15 (2013) 16883–16890.

[71]   J. Low, C. Jiang, B. Cheng, S. Wageh, A.A. Al-Ghamdi, J. Yu, A Review of Direct Z-Scheme Photocatalysts, Small Methods. 1 (2017).

[72]   V. Subramanian, E.E. Wolf, P. v Kamat, Catalysis with TiO_2 /Gold Nanocomposites. Effect of Metal Particle Size on the Fermi Level Equilibration, (2004).

[73]   Y.M. Gao, W. Lee, R. Trehan, R. Kershaw, K. Dwight, A. Wold, Improvement of photocatalytic activity of titanium (IV) oxide by dispersion of Au on TiO_2, Materials Research Bulletin. 26 (1991) 1247–1254.

[74]   K.D. Schierbaum, U.K. Kirner, J.F. Geiger, W. Göpel, Schottky-barrier and conductivity gas sensors based upon Pd/SnO_2 and Pt/TiO_2, Sensors and Actuators B: Chemical. 4 (1991) 87–94.

[75]   D.C. Cronemeyer, Infrared Absorption of Reduced Rutile TiO_2 single Crystals, Physical Review. 113 (1959) 1222.

[76]   X. Chen, L. Liu, F. Huang, Black titanium dioxide (TiO_2) nanomaterials, Chemical Society Reviews. 44 (2015) 1861–1885.

[77]   X. Chen, L. Liu, P.Y. Yu, S.S. Mao, Increasing solar absorption for photocatalysis with black hydrogenated titanium dioxide nanocrystals, Science. 331 (2011) 746–750.

[78]   A. Naldoni, M. Altomare, G. Zoppellaro, N. Liu, Š. Kment, R. Zbořil, P. Schmuki, Photocatalysis with Reduced TiO_2: From Black TiO_2 to Cocatalyst-Free Hydrogen Production, ACS Catalysis. 9 (2018) 345–364.

[79]   K. Hashimoto, H. Irie, A. Fujishima, TiO_2 Photocatalysis: A Historical Overview and Future Prospects, Japanese Journal of Applied Physics. 44 (2005) 8269.

[80]   A. Fujishima, X. Zhang, D.A. Tryk, TiO_2 photocatalysis and related surface phenomena, Surface Science Reports. 63 (2008) 515–582.

[81]   K. Nakata, A. Fujishima, TiO_2 photocatalysis: Design and applications, Journal of Photochemistry and Photobiology C: Photochemistry Reviews. 13 (2012) 169–189.

[82]   C. McCullagh, J.M.C. Robertson, D.W. Bahnemann, P.K.J. Robertson, The application of TiO_2 photocatalysis for disinfection of water contaminated with pathogenic micro-organisms: a review, Research on Chemical Intermediates 2007 33:3. 33 (2007) 359–375.

[83]   J. Low, B. Cheng, J. Yu, Surface modification and enhanced photocatalytic CO_2 reduction performance of TiO_2: a review, Applied Surface Science. 392 (2017) 658–686.

[84]   Jun Yang, Andrea Sudik, Christopher Wolverton, D. J. Siegel, High capacity hydrogen storage materials: attributes for automotive applications and techniques for materials discovery, Chemical Society Reviews. 39 (2010) 656–675.

[85]   V.N.H. Nguyen, R. Amal, D. Beydoun, Effect of formate and methanol on photoreduction/removal of toxic cadmium ions using TiO_2 semiconductor as photocatalyst, Chemical Engineering Science. 58 (2003).

[86]   M. Litter, Heterogeneous photocatalysis Transition metal ions in photocatalytic systems, Applied Catalysis B: Environmental. 23 (1999).

[87]   P. Chowdhury, A. Elkamel, A.K. Ray, CHAPTER 2. Photocatalytic Processes for the Removal of Toxic Metal Ions, Heavy Metals In Water, presence, removal and safety 16 (2014) 25-43.

Chapter 2:

Co-catalyst-free solar hydrogen production from water over defective TiO$_2$ nanosheets

2.1   Introduction

H$_2$ generation from water, as a clean and renewable energy operation, affords a promising way for alleviating climate change provoked by CO$_2$ emissions due to surplus consumption of fossil fuels [1–3]. Thus, it is recognized as one of the most significant solutions for a sustainable future [4,5].

Offering effective and sustainable photocatalysts to generate H$_2$ from water utilizing solar energy, which is the unlimited energy source, shows developing possibility. Different semiconducting materials (e.g., sulfides, nitrides, and oxides) have been investigated for photocatalytic hydrogen generation. Among them, TiO$_2$ is considered as an ideal and powerful material, thanks to its nontoxicity, low cost, and outstanding stability [6–8]. Nevertheless, the photocatalytic performance of TiO$_2$ has been restricted by its ~3.2 eV bandgap, which limits its optical absorption to the UV part of the solar light (~4% of the total solar spectrum). TiO$_2$ also has the drawback of fast charge carrier recombination [9–12], and thus the photocatalytic hydrogen generation rate is quite slow if no noble-metal co-catalyst such as Pt, Pd, or Au is being used [13–15]. Such a co-catalyst boosts the separation of photogenerated charge carriers and thus enhances the hydrogen generation efficiency. This strategy is unfortunately limited in the large-scale hydrogen production industry by the high cost of noble metals. Consequently, finding a way to get rid of using the expensive noble metals is of prime value in achieving the photocatalyst simplicity and low cost of the process and thus is crucially important for practical applications [5,16].

A more recent attractive finding is that hydrogen can be produced from water by co-catalyst free-based TiO$_2$ photocatalysts, allowing the manufacture of such photocatalytic materials on large scale to fulfill economic and commercial goals [16–18]. The co-catalytic effect attained by noble-metal decoration can be also achieved by introducing intrinsic co-catalytic active centers (e.g., oxygen vacancy

37

(Vo), Ti^{3+}) into TiO_2 [18–24], which is called defective (colored or reduced) TiO_2. Introducing such intrinsic active centers can facilitate the electron transfer and consequently boost the photocatalytic efficiency [19,20]. A specific kind of reduced TiO_2 shows photocatalytic hydrogen generation efficiency relative to that of Pt-based TiO_2 [16]. The preparation of the defective TiO_2 materials generally includes treating TiO_2 by reductive conditions in addition to operating at high-pressure/high temperature conditions [19,21–24]. Other types can be prepared using less harsh conditions (*e.g.*, solvothermal processes), but dangerous or costly chemicals are still required [16,25,26]. The method used to form defects in TiO_2 requires to be more cost-effective and environmentally friendly.

Nitrogen (N) doping, a well-known strategy for activating TiO_2 under visible light by reducing its bandgap, can concurrently create Vo in the structure [27–32]. Although N-doping in TiO_2 can be achieved under milder and safer conditions than those utilized to make defective TiO_2 [29], the resulting Vo in N-doped TiO_2 (and sole Vo in TiO_2) is thought to act as recombination centers for photogenerated charge carriers, reducing its solar (UV light-induced) photocatalytic efficiency [31,32]. Some reports, on the other side, claim that a specific type of Vo in TiO_2 can enhance charge separation and photocatalytic performance [33–36]. If properly designed, TiO_2 with both N-doping and Vo appears to be a promising platform for promoting the solar hydrogen generation process.

2.2   Chapter scope

In this chapter, we describe the synthesis of nitrogen-doped TiO_2 photocatalyst with concomitant oxygen vacancies by calcination of a spherical assembly of layered titanate nanosheets containing an organic N source, *N,N*-dimethylformamide (DMF), as the synthesis solvent. This method drives the topochemical transformation of the layered titanate precursor into spherically assembled nanosheets made up of anatase TiO_2 having both nitrogen dopant and oxygen vacancies (Vo). The developed photocatalyst demonstrates cutting-edge co-catalyst-free solar hydrogen generation activity from water, which can be attributed to high charge separation efficiency caused by Vo and possibly hierarchically mesoporous nature [37–40].
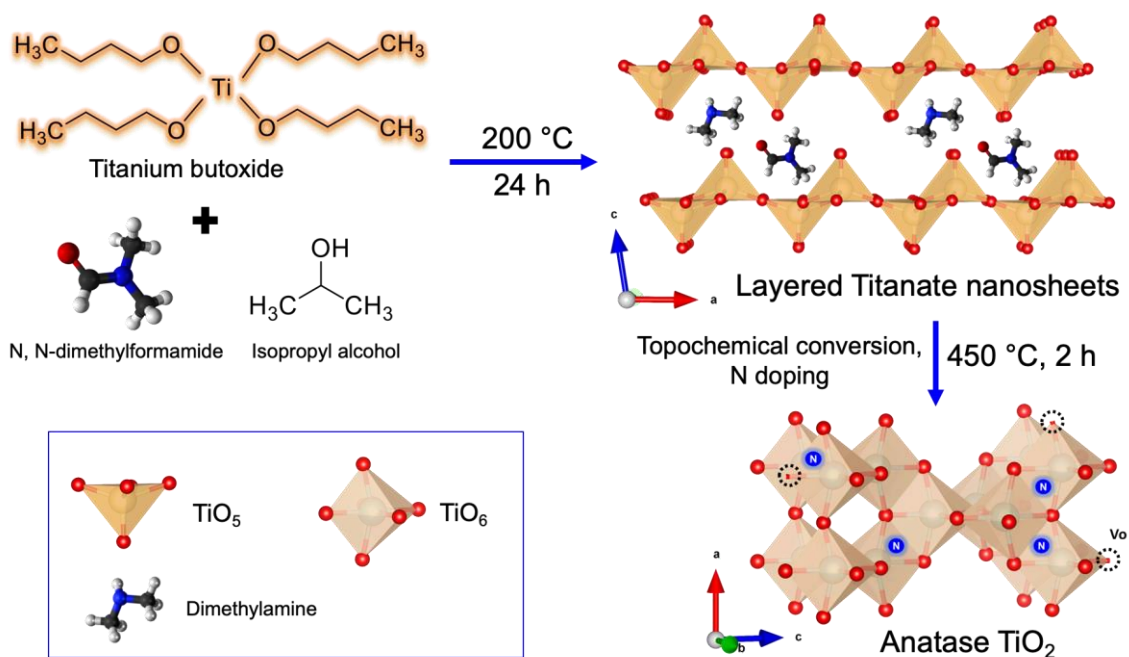
Figure 2.1. *Graphical representation for the preparation of layered titanate precursor ($H_2Ti_2O_5 \cdot nH_2O$) and the transformation of layered titanate nanosheets into anatase TiO_2 having N dopant and Vo. Reprinted with permission from {Applied Catalysis B: Environmental 285 (2021): 119755} Copyright {2020} Elsevier B.V.*

2.3   Experimental Details

2.3.1   Materials

All chemicals were utilized as recieved. N,N-dimethylformamide (99.8%), titanium (IV) butoxide (97%), and P25 were purchased from Sigma-Aldrich. Isopropyl alcohol (99.8%) was purchased from Chameleon.

2.3.2   Preparation of layered titanate precursor

The solvothermal procedure reported by Lou's group [41] was modified to produce the layered protonated titanate (LPT) precursor. After mixing 25 ml of isopropyl alcohol (IPA) with 8.3 ml of N,N-dimethylformamide (DMF) for several minutes, titanium (IV) butoxide was added (TBOT, 0.83 ml). The solution was then transferred to a stainless-steel autoclave lined with Teflon and held at 200°C for 24 hours. The precipitate was recovered by centrifugation at 3500 rpm for 10 minutes after the autoclave had cooled, washed with ethanol multiple times, and dried at 60°C to obtain LPT.

2.3.3 Synthesis of the catalyst

TiO_2 mesoporous spheres was obtained by the calcination of LPT precursor in an alumina crucible at 450°C for 2 hours at a heating rate of 2°C min^{-1}. LPT-450 was the name given to the calcined product. LPT was also calcined at temperatures of 550, 650, and 750°C to produce LPT-550, LPT-650, and LPT-750, respectively. Similarly, Solv-P25-450, a control sample, was made with P25, DMF, and IPA.

2.3.4 Characterization

A Rigaku SmartLab diffractometer was used to collect powder X-ray diffraction (XRD) data, with Cu K radiation at 40 kV and 30 mA at a scan rate of 1 min^{-1}. Micro-Raman scattering measurements were performed at room temperature with a 532 nm excitation light source (Photon Design Company). A Shimadzu FTIR-4200 was used to measure FTIR spectra. A Hitachi SU-8230 microscope operating at 10.0 kV was used to observe field emission scanning electron microscopy (FE-SEM) pictures. A JEOL JEM-2100F transmission electron microscope was used to obtain TEM pictures at a voltage of 200 kV. A PHI Quantera SXM equipment was used to perform X-ray photoelectron spectroscopy (XPS) using Al K radiation at 20 kV and 5 mA. The C1s level at 285.0 eV was used to calibrate the binding energy shift. Using a JEOL FA-200, an electron paramagnetic resonance (EPR) investigation was performed at room temperature with a microwave power of 0.05 mW. A Hitachi TG/DTA6200 was used to record thermogravimetric curves. A JASCO V-570 spectrophotometer was used to record UV-vis diffusion reflectance spectra (UV-DRS). On a Varian 600PS solid NMR spectrometer, ^{1}H and ^{13}C magic angle spinning (MAS) nuclear magnetic resonance (NMR) spectra were collected. The ^{1}H and ^{13}C resonance frequencies were tuned to 600 and 151 MHz, respectively. For ^{1}H NMR, a 3.2 mm diameter zirconia rotor with a rotation speed of 20 kHz was utilized, while for ^{13}C NMR, a 6 mm diameter zirconia rotor with a rotation speed of 7 kHz was used. The sample was heated to 150 °C under N_2 flow before the ^{1}H NMR test to eliminate water molecules. After the samples had been evacuated at 100°C for 12 hours, N_2 adsorption/desorption was performed at 196°C using a MicrotracBel BELMAX.

2.3.5 Hydrogen evolution experiment

In a Pyrex glass test tube (34 mL), 2 mg of the photocatalyst was dispersed in 5 ml aqueous methanol solution (1/1 in V/V), with no noble metal co-catalyst (such as Pt) added. The solution was deaerated

for 30 minutes with Ar bubbling, then sealed with a silicone rubber septum before being irradiated with a solar simulator (San-Ei Electric Co., Ltd.). A Shimadzu GC-2010 plus gas chromatograph with a BID detector was used to measure the evolved H_2 in headspace. A Pyrex glass tube was irradiated with monochromated light using a Ushio 500 W Xe lamp equipped with a Bunkoukeiki SM-25 monochromator for AQY percent determination. A Bunkoukeiki S1337-1010BQ silicon photodiode was used to determine the number of incident photons.

Apparent quantum yield (AQY %) for the hydrogen evolution reaction was calculated using the following equation:

$$AQY \% = \frac{\text{number of evolved hydrogen molecules x 2}}{\text{number of incident photons}} \; x \; 100$$

2.4   Results and discussion

2.4.1   *Structural and morpholical characterizations*

The layered protonated titanate (LPT) nanosheets were prepared solvothermally from titanium n-butoxide (TBOT) in N, N-dimethylformamide (DMF) and isopropyl alcohol (IPA) at 200 °C for 24h. TiO_2 hierarchical mesoporous spheres were obtained by calcining the prepared LPT in the air at 450 °C. The powder X-ray diffraction (XRD) pattern of LPT is presented in **Figure 2.2a**. The layered structure of LPT is confirmed by the presence of a strong peak at $2\theta = 9.1°$. Moreover, the XRD pattern revealed that the LPT structure is indexed to the typical layered crystal structure of $H_2Ti_2O_5 \cdot nH_2O$ [42]. The interlayer spacing of the layered LPT is calculated to be about 0.96 nm. By calcination of LPT at 450 °C in air, the LPT is transformed into an anatase TiO_2 structure (labeled as LPT-450), as shown in **Figure 2.2a**.

Likewise, the phase purity of prepared samples is further confirmed by Raman spectroscopy, a more surface-sensitive tool that is well-proper to distinguish nanocrystalline impurities. As shown in **Figure 2.2b**, the prepared LPT exhibited significant peaks at 275, 385, 449, and 705 cm^{-1}, which is ascribable to $H_2Ti_2O_5 \cdot nH_2O$ [43,44]. Additionally, Raman spectra confirmed the structure of the obtained anatase TiO_2 by the calcination of LPT at 450 °C, consistent with XRD data (**Figure 2.2a**).

Figure 2.2. *a) XRD patterns and b) Raman spectra of LPT and LPT-450. Reprinted with permission from {Applied Catalysis B: Environmental 285 (2021): 119755} Copyright {2020} Elsevier B.V.*

The morphology was then observed by SEM and TEM analyses. As presented in SEM and TEM images (**Figure 2.3a and inset**), LPT is shown to be comprised of spherically assembled nanosheets of $H_2Ti_2O_5 \cdot nH_2O$. The BET surface area of the LPT hierarchical spheres was 150 m^2 g^{-1}, which was higher than that of a conventional nanoparticulate P25 TiO_2 (**Figure 2.4a**). The layered structure of LPT was converted to anatase TiO_2 after calcination at 450°C in air, whereas the initial hierarchical spherical morphology and high BET surface area were preserved (**Figure 2.4a and 2.3c**).
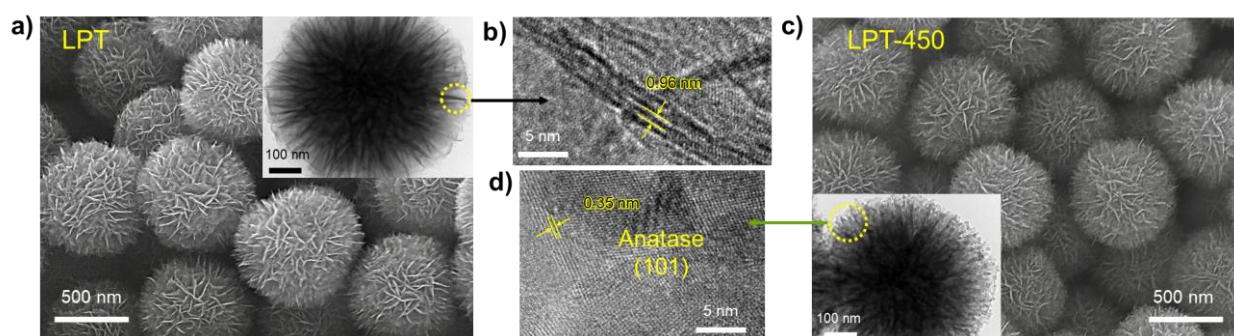
Figure 2.3. *a-d) SEM, TEM, and HRTEM images of LPT and LPT-450. Reprinted with permission from {Applied Catalysis B: Environmental 285 (2021): 119755} Copyright {2020} Elsevier B.V.*

The calcined product (LPT-450) was also proven by high-resolution TEM imaging to be made up of assemblies of nanosheets of anatase nanoparticles (**Figure 2.3d**). Moreover, the hysteresis loop, shown in **Figure 2.4a**, proved the mesoporous nature of LPT and LPT-450 hierarchical spheres. The pore size distribution curve (**Figure 2.4b**) revealed the formation of a uniform mesoporous structure.
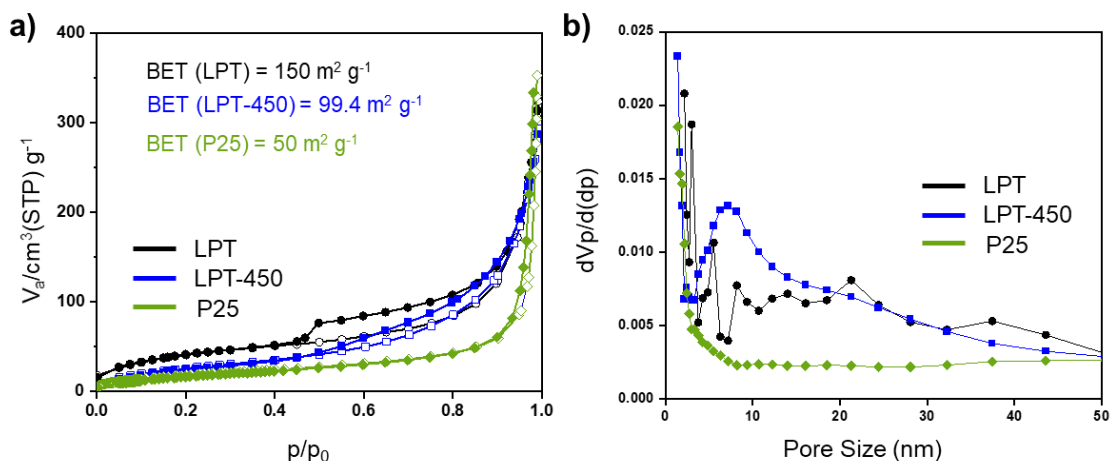
Figure 2.4. *a) N₂ adsorption–desorption isotherms, b) pore-size distribution curves of different samples. Reprinted with permission from {Applied Catalysis B: Environmental 285 (2021): 119755} Copyright {2020} Elsevier B.V.*

Therefore, the original LPT was topochemically converted into hierarchical mesoporous anatase TiO₂. Assembling this unique mesoporous structure with the hierarchical structure and the high surface area is expected to be useful in the migration of photogenerated electron-hole pairs and improving the photocatalytic activity of LPT-450 [45].

2.4.2   *Organic content detection (N content) for possible N doping*

The as-prepared LPT was further characterized by FTIR, TG-DTA, and solid-state ¹³C cross-polarization (CP) MAS NMR analyses to detect the existence of organic species for possible nitrogen doping in LPT-450 during the topochemical conversion process. FTIR spectra (**Figure 2.5a**) confirm the presence of organic species (e.g., C-H, N-H, and C-N) in LPT composition, which can be adsorbed or intercalated during the hydrothermal reaction. The weight loss observed in the TG curve (**Figure 2.5b**) coincides with the decomposition behavior in the DTA curve. The 12.8% weight loss is assigned to evaporating adsorbed water molecules and decomposing the intercalated and/or adsorbed organic components. DTA data further confirm that organic species can be completely decomposed and vaporized at 450 °C.
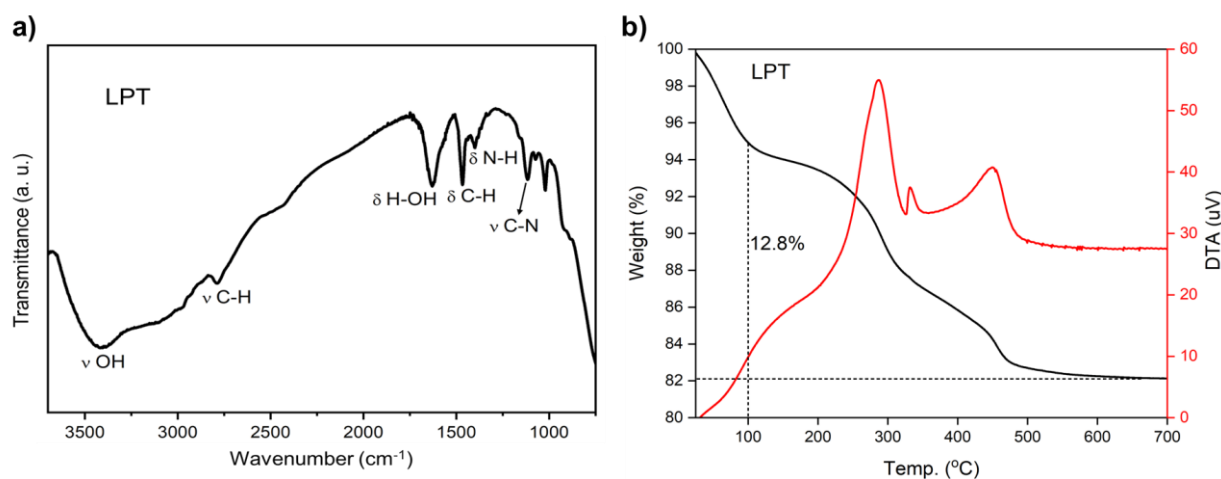
Figure 2.5. a) FTIR spectra, b) TG-DTA curves of LPT. Reprinted with permission from {Applied Catalysis B: Environmental 285 (2021): 119755} Copyright {2020} Elsevier B.V.

Solid-state ^{13}C CP MAS NMR data (**Figure 2.6**) proved that DMF and dimethylamine (DMA, decomposed product of DMF), can be intercalated in LPT during the solvothermal reaction. In the case of LPT-450, it was anticipated that the calcination will result in entire condensation of the layered structure (i.e., shrinkage of interlayer space) as well as the complete decomposition and vaporization of organic components, hardly showing any such peaks. To get more insights into the intercalation of organic species, we treated P25 (commercial TiO_2) with the same hydrothermal conditions used to synthesize LPT, then calcined in air at 450 °C and checked out the possibility of the incorporation of organic species to P25 lattice. **Figure 2.6** revealed that DMF and/or its decomposition products (DMA) cannot be incorporated into P25 crystal spaces, showing the advantages of layered LPT structure for accepting organic impurities to their structure and becoming doped in the calcined sample (LPT-450). Because LPT has only a small amount of water molecules in the interlayer space ($H_2Ti_2O_5.xH_2O$, **Figure 2.2a**) and its gallery height is estimated as 0.42 - 0.69 nm by deducting the single-layer thickness (0.27 - 0.54 nm) from the basal spacing (0.96 nm, **Figure 2.3b**), DMF and DMA were probably positioned in the interlayer space of nanosheets, as well as between nanosheet, and decomposed before introducing them as an N dopant in the anatase structure of the calcined product (LPT-450).
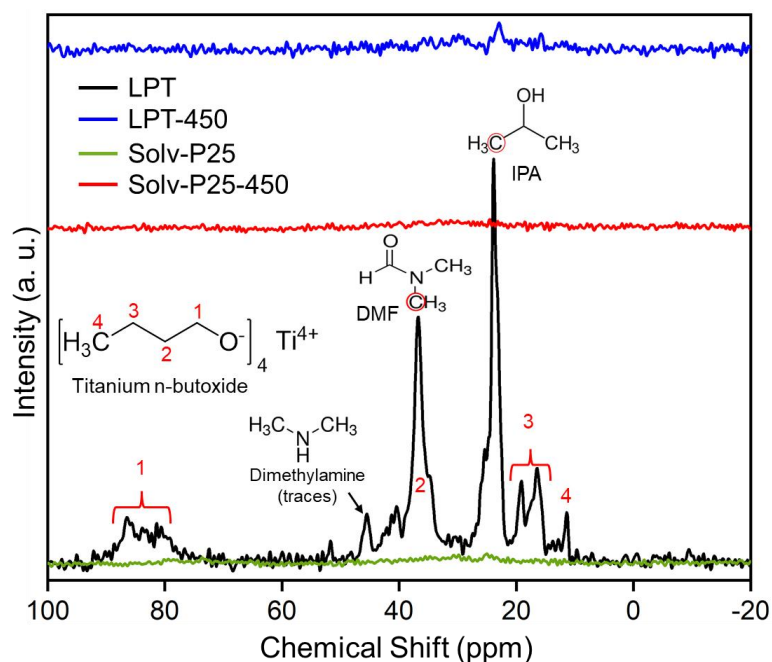
Figure 2.6. *¹³C NMR spectra of LPT, LPT-450, Solv-P25, and Solv-P25-450. Reprinted with permission from {Applied Catalysis B: Environmental 285 (2021): 119755} Copyright {2020} Elsevier B.V.*

2.4.3 *Chemical state and oxygen vacancy (Vo) determination*

XPS analysis was checked out for studying the chemical states of surface elements in LPT and LPT-450 and to determine a probable creation of Vo in LPT-450. The N 1s core-level XPS spectra obtained from LPT (**Figure 2.7a**) exihibited an N 1s peak at 402.2 eV, which corresponds to chemisorbed N or surface N-H of amine moieties in DMF decomposition product (DMA) [46,47], supporting the successful incorporation of organic species in layered titanate structure and consistent with 13C NMR results (**Figure 2.6**). In the case of LPT-450, the N 1s XPS peak at 400.1 eV (**Figure 2.7a**) was typically ascribed to the interstitial nitrogen dopant, suggesting the existence of the Ti−O−N bond and the associated production of Vo [30,31]. The absence of N 1*s* peak at 402.2 eV in LPT-450 further confirms the N doping since it probably disappears during the doping process, just after calcination of LPT. Thus, N 1*s* XPS spectra confirmed the origin of nitrogen as intercalated or chemisorbed N species (comes from DMF and DMA) and proved the successful doping of N into TiO_2 lattice with concomitant Vo. The amount of N in LPT-450 was calculated to be 0.4 atomic%.

As depicted in **Figure 2.7 (b, c)**, LPT showed a Ti $2p3/2$ peak at 459.1 eV, a Ti $2p1/2$ peak at 464.7 eV, and an O $1s$ peak at 530.7 eV. In the case of LPT-450, the Ti $2p3/2$, Ti $2p1/2$, and the O 1s peaks appeared at 458.8, 464.5 eV, and 530.1 eV, respectively. It is noticed that the binding energies of Ti and O in LPT-450 are shifted toward negative direction compared with LPT, which is explained by the fact that $H_2Ti_2O_5 \cdot nH_2O$ ($K_2Ti_2O_5$) is made up of uniquely five-coordinated Ti atoms, different from almost all phases of titania, including anatase, which is made up of six-coordinated Ti atoms [48,49]. Additionally, Ti $2p$ XPS spectra (**Figure 2.7b**) prove the existence of the only Ti^{4+} in LPT and LPT-450 and there are no characteristic peaks was observed for Ti^{3+} (around 457.1 eV) [50]. The O $1s$ peaks (**Figure 2.7c**) also suggest the presence of both lattice O (530.7 eV and 530.1 eV) and surface OH groups (shoulder peaks at 532.4 eV and 532.2 eV) in LPT and LPT-450, respectively. From XPS analysis, it is concluded that the N doping is accompanied by Vo formation (will be confirmed later). Importantly, it was also reported that nitrogen doping is important in stabilizing the oxygen-deficient sites by blocking its re-oxidation [51,52]. Furthermore, this kind of N doping accompanied by Vo is expected to greatly influence the photocatalytic properties of TiO_2.

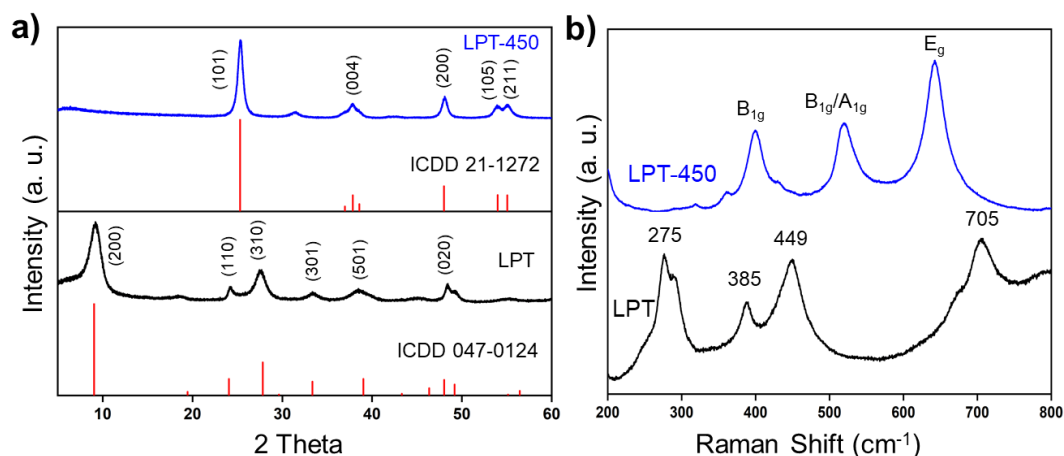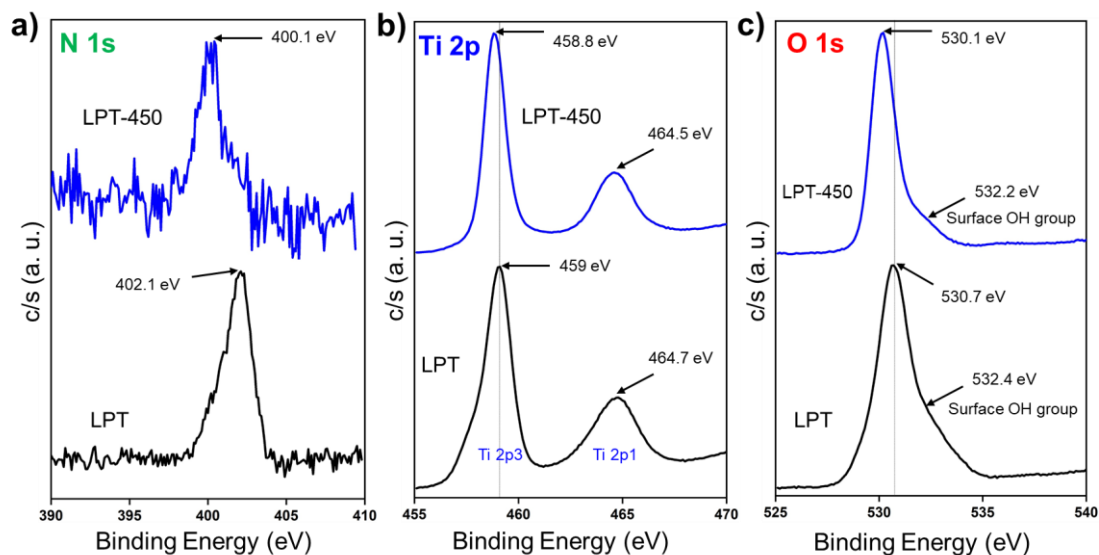***Figure 2.7***. *a) N 1s, b) Ti 2p, and c) O 1s high resolution XPS spectra of LPT and LPT-450. Reprinted with permission from {Applied Catalysis B: Environmental 285 (2021): 119755} Copyright {2020} Elsevier B.V.*

The creation of Vo in LPT-450 was further confirmed by electron paramagnetic resonance (EPR) analysis. **Figure 2.8a** shows that a significant EPR signal was obtained in LPT-450 at g = 2.001, which

is a characteristic feature of Vo, and no obvious EPR signal is observed for commercial TiO_2 (P25) which is made up of anatase and rutile mixture with a moderately high crystallinity [53,54]. Furthermore, the Ti^{3+} signal at g = 1.97 did not exist, which is consistent with the XPS data. In most cases, the formation of Vo is linked to trapped electrons in Vo sites, resulting in color centers (called F-centers). F-centers (electron pair trapped in Vo, equation 1), F+-centers (a single electron trapped in Vo, equation 2), and F++-centers (electron pair deficient Vo or anion vacancy, equation 3) are the three types of color centers in TiO_2 [55].

$$Vo + 2e^- \rightarrow F \qquad (1)$$

$$Vo + e^- \rightarrow F^+ \qquad (2)$$

$$Vo + 0e^- \rightarrow F^{++} \qquad (3)$$
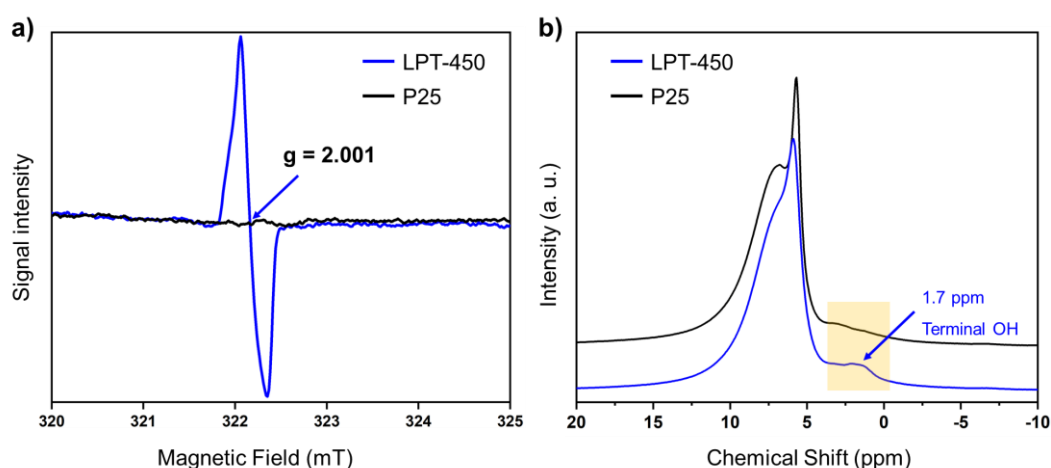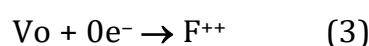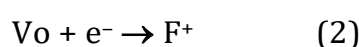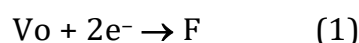
Figure 2.8. a) Electron paramagnetic resonance (EPR) spectra and b) ^1H MAS NMR spectra of LPT-450 and P25. Reprinted with permission from {Applied Catalysis B: Environmental 285 (2021): 119755} Copyright {2020} Elsevier B.V.

The shape and sharp EPR signal (**Figure 2.8a**) prove that the material possesses F+-centers (an electron trapped in Vo) [5,56]. Interestingly, the trapped electron in Vo has been shown to deliver photocatalytic activity with better performance [56]. Therefore, the EPR results further proved that our sample is expected to have improved photocatalytic hydrogen production activity.

A solid-state ^{1}H MAS NMR study was performed to validate the existence of Vo in LPT-450. As seen in **Figure 2.8b**, LPT-450 has a substantially stronger peak at 1.7 ppm, which is ascribed to terminal hydroxyl groups [57,58]. The existence of such groups in anatase has been associated with the introduction of Vo in the lattice [59].

2.4.4 *Optical characteristics of LPT-450*

The electronic properties of TiO2 are usually altered by doping with non-metal elements, such as N, and the introduction of Vo. Using diffuse-reflectance UV-vis spectroscopy and valence band (VB) XPS studies, we were able to determine the electronic band structure of LPT-450. LPT-450 exhibits substantial visible light absorption up to 500 nm, as described in **Figure 2.9a**, due to the existence of the N dopant and Vo. The Tauc plot (**Figure 2.9b**) generated from the UV-vis results showed the bandgap energy of LPT-450 to be 3.08 eV, which is agreeing with the average known bandgap value of anatase (3.1 - 3.2 eV). The VB peak was determined at 2.69 eV in the VB XPS spectra of LPT-450 (**Figure 2.9c**). Thus, the energy diagram of LPT-450 could be drawn as described in **Figure 2.9d** by combining the existing data. LPT-450's bandgap (3.08 eV) is too wide to make it visible light active (> 400 nm). Nevertheless, the created Vo, which has been demonstrated to donate electrons in TiO2 [60], can enhance charge transport in LPT-450 and push the Fermi level toward the CB, hence improving charge separation efficiency [33,61,62]. Moreover, we thought that the produced Vo may prefer to be on the surface rather than in the bulk since LPT-450 is two-dimensional, trapping photogenerated electrons and preventing charge recombination [34,36].
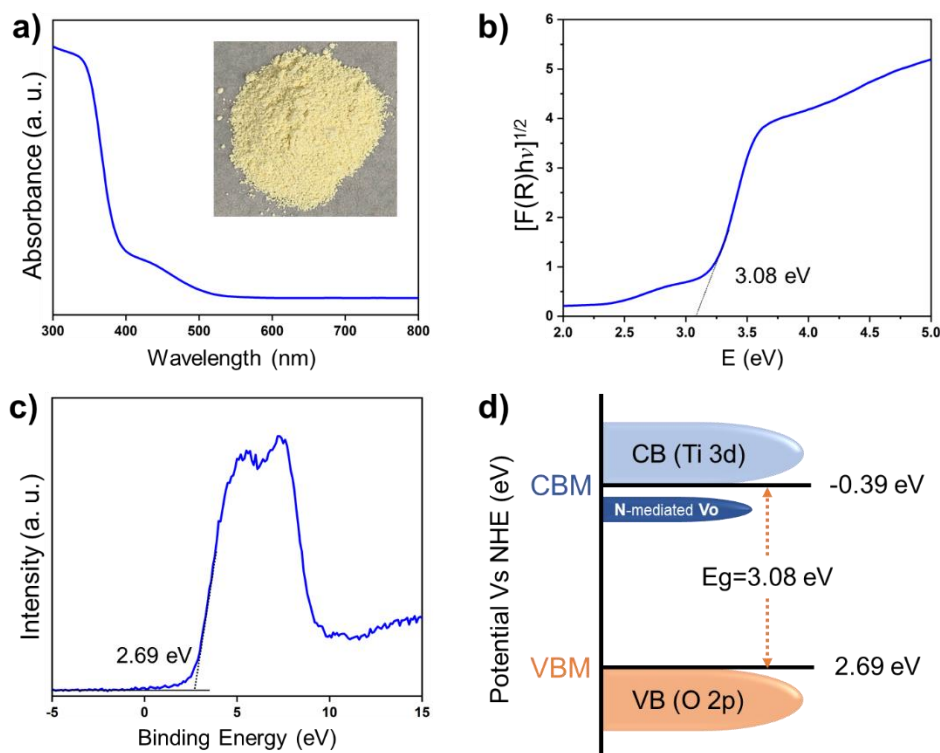
Figure 2.9*. a) UV-Vis spectra and optical image (inset), b) Tauc plot, c) Valence band (VB) XPS, and d) energy band diagram of LPT-450. Reprinted with permission from {Applied Catalysis B: Environmental 285 (2021): 119755} Copyright {2020} Elsevier B.V.*

2.4.5 *Photocatalytic hydrogen production*

The photocatalytic H_2 production activity from water containing methanol as a sacrificial agent was examined under the solar irradiation ($\lambda > 300$ nm, 1 SUN) without utilizing any cocatalyst. **Figure 2.10 (a, b)** shows continuous H_2 evolution profiles and the rate of H_2 generation under solar light irradiation, respectively. As expected, the highest photocatalytic H_2 production is correlated to LPT-450 with a maximum rate of 1035 µmole h^{-1} g^{-1}, which was 33 times greater than that of P25, a benchmark TiO_2 photocatalyst. The hydrogen production activity of LPT-450 was also much greater than that of other co-catalyst-free defective TiO_2 photocatalysts ($\sim$300 µmole h^{-1} g^{-1}) [5]. The stability of the LPT-450 was further investigated for hydrogen evolution under solar light (**Figure 2.10c**). LPT-450 showed high durability toward hydrogen evolution reaction since it provided stable solar hydrogen generation without losing the initial activity (**Figure 2.10c**).

Figure 2.10a showed that LPT possesses no activity toward the current photocatalytic process. The activity of a control sample (Solv-P25-450) produced by solvothermal treatment of P25 with DMF (and IPA) followed by calcination at 450 °C was nearly identical to that of P25. The fact that P25 was unable to adsorb N precursors to be doped in the lattice (**Figure 2.6**) supports these results. The advantages of the present material design for LPT-450 are revealed by our findings.
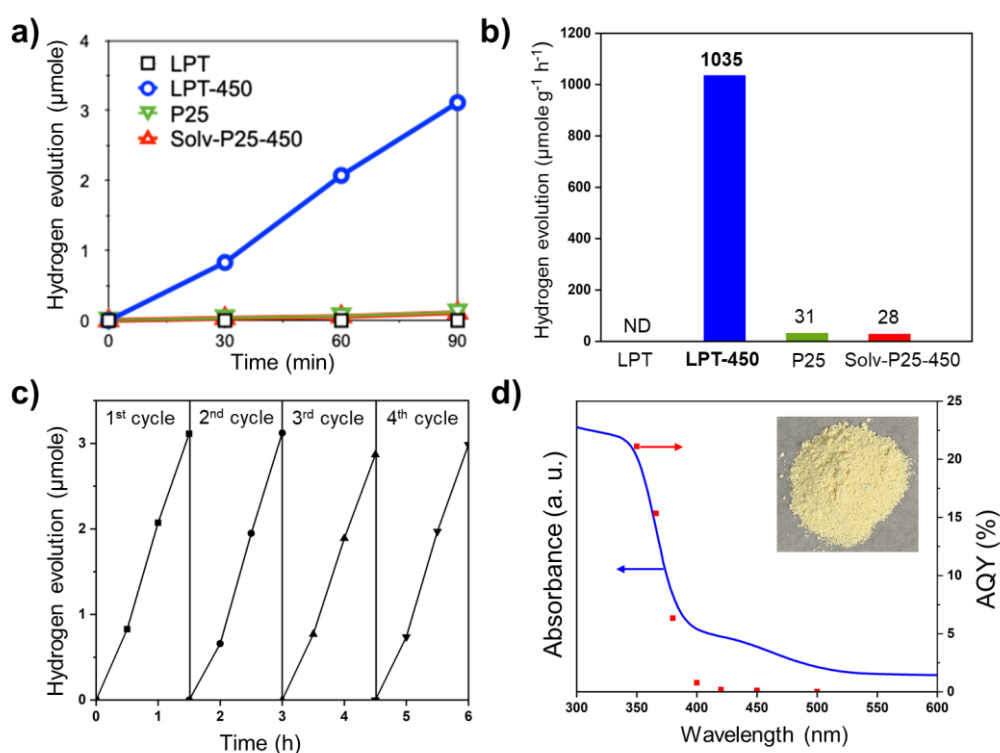
Figure 2.10. a) H₂ evolution profile, b) rate of hydrogen evolution of LPT, LPT-450, P25, and Solv-P25-450, c) stability test for 6 h of LPT-450, and d) AQY% and optical image (inset) of LPT-450. Reprinted with permission from {Applied Catalysis B: Environmental 285 (2021): 119755} Copyright {2020} Elsevier B.V.

Moreover, AQY% was estimated under various wavelengths to additionally evaluate the hydrogen generation efficiency of LPT-450 (**Figure 2.10d**). Under identical reaction conditions, the AQY of 16% was attained at 365 nm, which is close to that of Pt-modified P25 (28% at 365 nm) and a co-catalyst-free defective TiO_2 with remarkably high activity (44% at 365 nm) [16]. On the other hand, the AQY in the visible light range (> 400 nm) did not correspond to its photoabsorption. This data shows the insignificant response of the material to visible light and delivers proof of the abovementioned photocatalytic mechanism where the generated Vo largely improved charge separation and

50

photocatalytic performance. Accordingly, it is worth noting that LPT-450 can be available utilizing a more convenient way than for traditional reduced TiO_2, delivering more economically convenient state-of-the-art-level co-catalyst-free solar hydrogen production activity.

Moreover, even when the irradiation period was increased, LPT-450 exhibited identical activity and stability (**Figure 2.11**). These results confirm again the durability of the LPT-450 toward solar hydrogen generation from water.
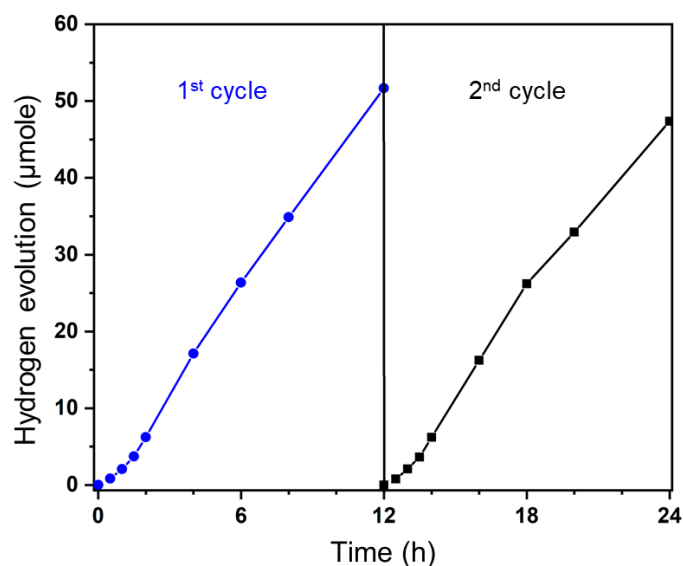
Figure 2.11*. Hydrogen evolution profiles and recycled hydrogen evolution on LPT-450 for a longer irradiation period. Reprinted with permission from {Applied Catalysis B: Environmental 285 (2021): 119755} Copyright {2020} Elsevier B.V.*

LPT-450, as illustrated in **Figure 2.4a**, has a greater surface area (99.4 $m^2 g^{-1}$) and considerably higher mesoporosity than commercial TiO_2 such as P25 (50 $m^2 g^{-1}$). Therefore, the high activity toward the present photocatalytic reaction may be attributed to both morphological character (hierarchical mesoporous sphere) and suitable band structure of the photocatalyst.

Eventually, we examined the dependence of the structure and photocatalytic efficiency of the samples on the calcination temperature of LPT. XRD patterns and Raman spectra (**Figure 2.12a, b**) showed the phase transformation of LPT into TiO_2 after the calcination of LPT from 450 °C to 750 °C. LPT was converted to anatase (at 450 °C and 550 °C), anatase/rutile mixture (at 650 °C), and pure rutile (at 750 °C).
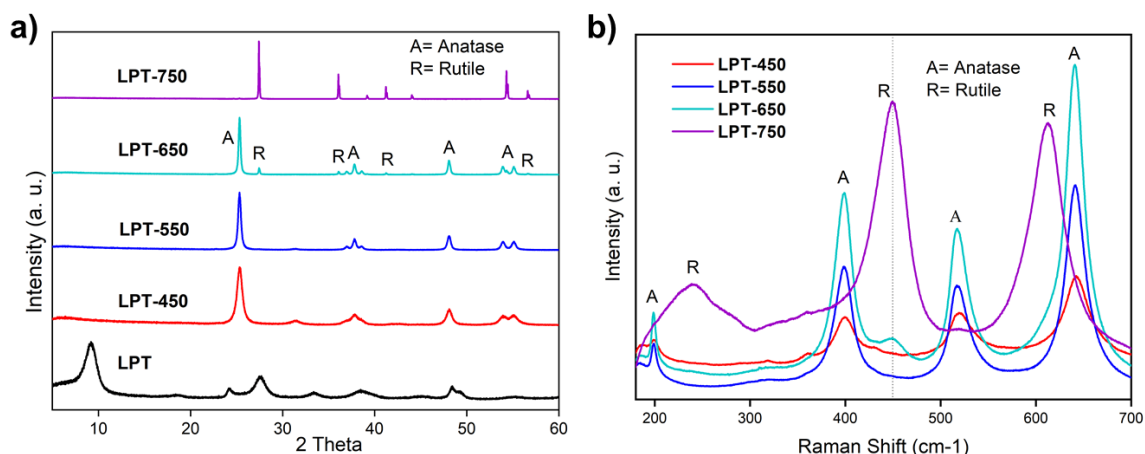
Figure 2.12. a) XRD patterns, b) Raman spectra of calcined LPT products at different temperatures. Reprinted with permission from {Applied Catalysis B: Environmental 285 (2021): 119755} Copyright {2020} Elsevier B.V.

SEM micrographs (**Figure 2.13**) additionally confirmed that LPT-550 and LPT-650 were made up of hierarchical anatase assemblies, like LPT-450, but LPT-750 was made up of rutile particles. However, LPT-450 had a higher photocatalytic H_2 evolution efficiency than the others (**Figure 2.14a**). Lowering the calcination temperature of LPT may restrain the entire elimination of intercalated and/or adsorbed organic impurities (**Figure 2.5b**), resulting in successful N doping with concurrent Vo creation in the calcined product, enhancing the photocatalytic performance.
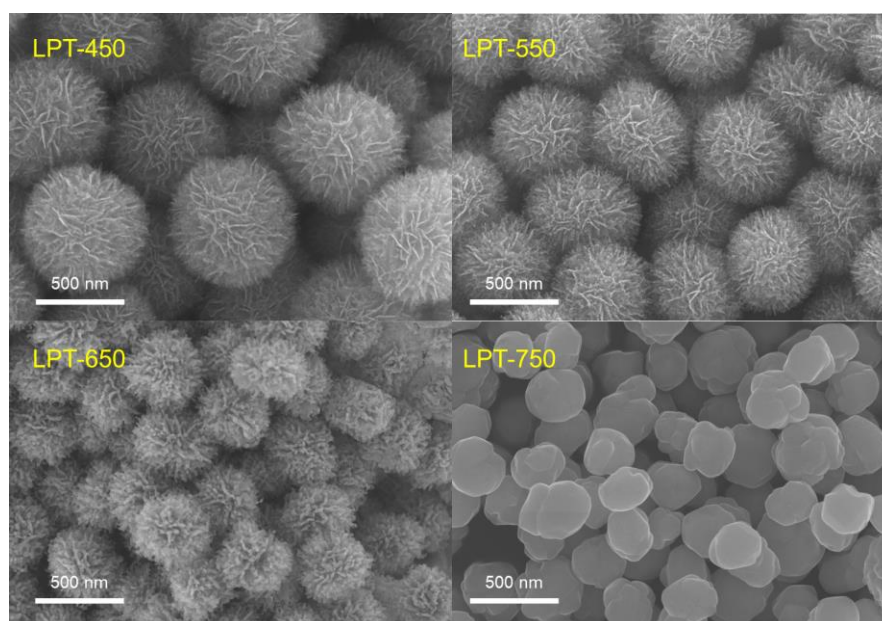
Figure 2.13. SEM micrographs of calcined LPT products at different temperatures. Reprinted with permission from {Applied Catalysis B: Environmental 285 (2021): 119755} Copyright {2020} Elsevier B.V.
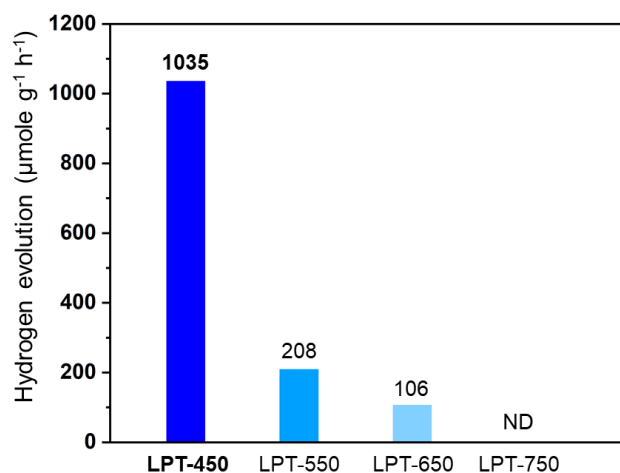
Figure 2.14*. Dependence of the photocatalytic hydrogen evolution activity on the LPT calcination temperature. Reprinted with permission from {Applied Catalysis B: Environmental 285 (2021): 119755} Copyright {2020} Elsevier B.V.*

2.5   Summary

This work describes a novel, simple, and safe method for producing oxygen-defective TiO_2 which provides effective co-catalyst-free solar photocatalytic hydrogen generation activity from water. The synthetic procedure includes the topochemical transformation of a layered titanate ($H_2Ti_2O_5 \cdot nH_2O$) nanosheet mesoporous assembly, containing nitrogen source in the structure, into mesoporous nanosheets assemblies of anatase nanoparticles with both N dopant and concurrently introduced oxygen vacancies. Under solar light irradiation, the obtained material exhibited superb photocatalytic activity that is significantly greater than that of many common kinds of co-catalyst-free defective TiO_2. Enhancing the photocatalytic activity is attributed to nitrogen doping-induced oxygen vacancies, which can promote charge separation. The morphological nature of the material may also partake in raising the photocatalytic activity through providing a high surface area and improving the light absorption properties. TiO_2 and titanates are available with various structures and morphologies, and therefore, the synthetic approach described here is expected to be expanded for introducing additional TiO_2 and titanate-based co-catalyst free materials with better activity toward many energy and environmental applications.

2.6 References

[1]   Z. Wang, C. Li, K. Domen, Recent developments in heterogeneous photocatalysts for solar-driven overall water splitting, Chem. Soc. Rev. 48 (2019) 2109–2125.

[2]   S.J.A. Moniz, S.A. Shevlin, D.J. Martin, Z.X. Guo, J. Tang, Visible-light driven heterojunction photocatalysts for water splitting-a critical review, Energy and Environmental Science. 8 (2015) 731–759.

[3]   Q. Lu, G.S. Hutchings, W. Yu, Y. Zhou, R. V. Forest, R. Tao, J. Rosen, B.T. Yonemoto, Z. Cao, H. Zheng, J.Q. Xiao, F. Jiao, J.G. Chen, Highly porous non-precious bimetallic electrocatalysts for efficient hydrogen evolution, Nature Communications. 6 (2015) 1–8.

[4]   Y.P. Zhu, J. Yin, E. Abou-Hamad, X. Liu, W. Chen, T. Yao, O.F. Mohammed, H.N. Alshareef, Highly Stable Phosphonate-Based MOFs with Engineered Bandgaps for Efficient Photocatalytic Hydrogen Production, Advanced Materials. 32 (2020) 1906368.

[5]   A. Naldoni, M. Altomare, G. Zoppellaro, N. Liu, Š. Kment, R. Zbořil, P. Schmuki, Photocatalysis with reduced TiO_2 : From Black TiO_2 to cocatalyst-free hydrogen production, ACS Catalysis. 9 (2019) 345–364.

[6]   M. Altomare, N.T. Nguyen, S. Hejazi, P. Schmuki, A Cocatalytic Electron-Transfer Cascade Site-Selectively Placed on TiO_2 Nanotubes Yields Enhanced Photocatalytic H_2 Evolution, Advanced Functional Materials. 28 (2018) 1704259.

[7]   A.H. Zaki, A. El-Shafey, S.M. Moatmed, R.A. Abdelhay, E.F. Rashdan, R.M. Saleh, M. Abd-El Fatah, M.M. Tawfik, M. Esmat, S.I. El-dek, Morphology transformation from titanate nanotubes to TiO_2 microspheres, Materials Science in Semiconductor Processing. 75 (2018) 10–17.

[8]   S. Wang, S. Lin, D. Zhang, G. Li, M.K.H. Leung, Controlling charge transfer in quantum-size titania for photocatalytic applications, Applied Catalysis B: Environmental. 215 (2017) 85–92.

[9]   J. Chu, Y. Sun, X. Han, B. Zhang, Y. Du, B. Song, P. Xu, Mixed Titanium Oxide Strategy for Enhanced Photocatalytic Hydrogen Evolution, ACS Applied Materials and Interfaces. 11 (2019) 18475–18482.

[10]   X. Liu, G. Zhu, X. Wang, X. Yuan, T. Lin, F. Huang, Progress in Black Titania: A New Material for Advanced Photocatalysis, Advanced Energy Materials. 6 (2016).

[11]   A. Sinhamahapatra, J.P. Jeon, J.S. Yu, A new approach to prepare highly active and stable black titania for visible light-assisted hydrogen production, Energy and Environmental Science. 8 (2015) 3539–3544.

[12]   X. Chen, S.S. Mao, Titanium dioxide nanomaterials: Synthesis, properties, modifications and applications, Chemical Reviews. 107 (2007) 2891–2959.

[13]   J. Prakash, S. Sun, H.C. Swart, R.K. Gupta, Noble metals-TiO_2 nanocomposites: From fundamental mechanisms to photocatalysis, surface enhanced Raman scattering and antibacterial applications, Applied Materials Today. 11 (2018) 82–135.

[14]   Z.H.N. Al-Azri, W.T. Chen, A. Chan, V. Jovic, T. Ina, H. Idriss, G.I.N. Waterhouse, The roles of metal co-catalysts and reaction media in photocatalytic hydrogen production: Performance evaluation of M/TiO_2 photocatalysts (M = Pd, Pt, Au) in different alcohol-water mixtures, Journal of Catalysis. 329 (2015) 355–367.

[15]   M. Ye, J. Gong, Y. Lai, C. Lin, Z. Lin, High-efficiency photoelectrocatalytic hydrogen generation enabled by palladium quantum dots-sensitized TiO_2 nanotube arrays, Journal of the American Chemical Society. 134 (2012) 15720–15723.

[16]   K. Zhang, L. Wang, J.K. Kim, M. Ma, G. Veerappan, C.L. Lee, K.J. Kong, H. Lee, J.H. Park, An order/disorder/water junction system for highly efficient co-catalyst-free photocatalytic hydrogen generation, Energy and Environmental Science. 9 (2016) 499–503.

[17]   Y. AlSalka, A. Hakki, J. Schneider, D.W. Bahnemann, Co-catalyst-free photocatalytic hydrogen evolution on TiO_2: Synthesis of optimized photocatalyst through statistical material science, Applied Catalysis B: Environmental. 238 (2018) 422–433.

[18]   X. Zhou, V. Häublein, N. Liu, N.T. Nguyen, E.M. Zolnhofer, H. Tsuchiya, M.S. Killian, K. Meyer, L. Frey, P. Schmuki, TiO_2 Nanotubes: Nitrogen-Ion Implantation at Low Dose Provides Noble-Metal-Free Photocatalytic H_2-Evolution Activity, Angewandte Chemie - International Edition. 55 (2016) 3763–3767.

[19]   S. Mohajernia, P. Andryskova, G. Zoppellaro, S. Hejazi, S. Kment, R. Zboril, J. Schmidt, P. Schmuki, Influence of Ti^{3+} defect-type on heterogeneous photocatalytic H_2 evolution activity of TiO_2, Journal of Materials Chemistry A. 8 (2020) 1432–1442.

[20]   N. Liu, H.G. Steinrück, A. Osvet, Y. Yang, P. Schmuki, Noble metal free photocatalytic H_2 generation on black TiO_2: On the influence of crystal facets vs. crystal damage, Applied Physics Letters. 110 (2017) 072102.

[21]   N. Liu, X. Zhou, N.T. Nguyen, K. Peters, F. Zoller, I. Hwang, C. Schneider, M.E. Miehlich, D. Freitag, K. Meyer, D. Fattakhova-Rohlfing, P. Schmuki, Black Magic in Gray Titania: Noble-Metal-Free Photocatalytic H_2 Evolution from Hydrogenated Anatase, ChemSusChem. 10 (2017) 62–67.

[22]   N. Liu, C. Schneider, D. Freitag, E.M. Zolnhofer, K. Meyer, P. Schmuki, Noble-Metal-Free Photocatalytic H2Generation: Active and Inactive 'Black' TiO2Nanotubes and Synergistic Effects, Chemistry - A European Journal. 22 (2016) 13810–13814.

[23]   N. Liu, C. Schneider, D. Freitag, U. Venkatesan, V.R.R. Marthala, M. Hartmann, B. Winter, E. Spiecker, A. Osvet, E.M. Zolnhofer, K. Meyer, T. Nakajima, X. Zhou, P. Schmuki, Hydrogenated Anatase: Strong Photocatalytic Dihydrogen Evolution without the Use of a Co-Catalyst, Angewandte Chemie. 126 (2014) 14425–14429.

[24]   N. Liu, C. Schneider, D. Freitag, M. Hartmann, U. Venkatesan, J. Müller, E. Spiecker, P. Schmuki, Black TiO_2 nanotubes: Cocatalyst-free open-circuit hydrogen generation, Nano Letters. 14 (2014) 3309–3313.

[25]   W. Fang, L. Khrouz, Y. Zhou, B. Shen, C. Dong, M. Xing, S. Mishra, S. Daniele, J. Zhang, Reduced {001}-TiO_{2-x} photocatalysts: Noble-metal-free CO_2 photoreduction for selective CH_4 evolution, Physical Chemistry Chemical Physics. 19 (2017) 13875–13881.

[26]   L. Liu, Y. Jiang, H. Zhao, J. Chen, J. Cheng, K. Yang, Y. Li, Engineering Coexposed {001} and {101} Facets in Oxygen-Deficient TiO2 Nanocrystals for Enhanced CO2 Photoreduction under Visible Light, ACS Catalysis. 6 (2016) 1097–1108.

[27]   D. Zhang, X. Ma, H. Zhang, Y. Liao, Q. Xiang, Enhanced photocatalytic hydrogen evolution activity of carbon and nitrogen self-doped TiO_2 hollow sphere with the creation of oxygen vacancy and Ti^{3+}, Materials Today Energy. 10 (2018) 132–140.

[28]   L. Gomathi Devi, R. Kavitha, Review on modified N-TiO2 for green energy applications under UV/visible light: Selected results and reaction mechanisms, RSC Advances. 4 (2014) 28265–28299.

[29]   R. Asahi, T. Morikawa, H. Irie, T. Ohwaki, Nitrogen-doped titanium dioxide as visible-light-sensitive photocatalyst: Designs, developments, and prospects, Chemical Reviews. 114 (2014) 9824–9852.

[30]   C.W. Dunnill, I.P. Parkin, Nitrogen-doped TiO2 thin films: Photocatalytic applications for healthcare environments, Dalton Transactions. 40 (2011) 1635–1640.

[31]   J. Wang, D.N. Tafen, J.P. Lewis, Z. Hong, A. Manivannan, M. Zhi, M. Li, N. Wu, Origin of photocatalytic activity of Nitrogen-doped TiO_2 nanobelts, Journal of the American Chemical Society. 131 (2009) 12290–12297.

[32]   C. Di Valentin, G. Pacchioni, A. Selloni, S. Livraghi, E. Giamello, Characterization of paramagnetic species in N-doped TiO_2 powders by EPR spectroscopy and DFT calculations, Journal of Physical Chemistry B. 109 (2005) 11414–11419.

[33]   X. Pan, M.Q. Yang, X. Fu, N. Zhang, Y.J. Xu, Defective TiO_2 with oxygen vacancies: Synthesis, properties and photocatalytic applications, Nanoscale. 5 (2013) 3601–3614.

[34]   M. Kong, Y. Li, X. Chen, T. Tian, P. Fang, F. Zheng, X. Zhao, Tuning the relative concentration ratio of bulk defects to surface defects in TiO_2 nanocrystals leads to high photocatalytic efficiency, Journal of the American Chemical Society. 133 (2011) 16414–16417.

[35]   G. Wang, H. Wang, Y. Ling, Y. Tang, X. Yang, R.C. Fitzmorris, C. Wang, J.Z. Zhang, Y. Li, Hydrogen-treated TiO_2 nanowire arrays for photoelectrochemical water splitting, Nano Letters. 11 (2011) 3026–3033.

[36]   J. Zhuang, W. Dai, Q. Tian, Z. Li, L. Xie, J. Wang, P. Liu, X. Shi, D. Wang, Photocatalytic degradation of RhB over TiO_2 bilayer films: Effect of defects and their location, Langmuir. 26 (2010) 9686–9694.

[37]   Z. Haider, Y.S. Kang, Facile preparation of hierarchical TiO_2 nano structures: Growth mechanism and enhanced photocatalytic H_2 production from water splitting using methanol as a sacrificial reagent, ACS Applied Materials and Interfaces. 6 (2014) 10342–10352.

[38]   B. Liu, L.M. Liu, X.F. Lang, H.Y. Wang, X.W. Lou, E.S. Aydil, Doping high-surface-area mesoporous TiO_2 microspheres with carbonate for visible light hydrogen production, Energy and Environmental Science. 7 (2014) 2592–2597.

[39]   Z. Sun, J.H. Kim, Y. Zhao, D. Attard, S.X. Dou, Morphology-controllable 1D-3D nanostructured TiO_2 bilayer photoanodes for dye-sensitized solar cells, Chemical Communications. 49 (2013) 966–968.

[40]   Z. Gao, Z. Wu, X. Li, J. Chang, D. Wu, P. Ma, F. Xu, S. Gao, K. Jiang, Application of hierarchical TiO_2 spheres as scattering layer for enhanced photovoltaic performance in dye sensitized solar cell, CrystEngComm. 15 (2013) 3351–3358.

[41]   H. Bin Wu, X.W. Lou, H.H. Hng, Synthesis of uniform layered protonated titanate hierarchical spheres and their transformation to anatase TiO_2 for lithium-ion batteries, Chemistry - A European Journal. 18 (2012) 2094–2099.

[42]   N. Sutradhar, A. Sinhamahapatra, S. Kumar Pahari, H.C. Bajaj, A. Baran Panda, Room temperature synthesis of protonated layered titanate sheets using peroxo titanium carbonate complex solution, Chemical Communications. 47 (2011) 7731–7733.

[43]   C. Liu, M. He, X. Lu, Q. Zhang, Z. Xu, Reaction and crystallization mechanism of potassium dititanate fibers synthesized by low-temperature calcination, Crystal Growth and Design. 5 (2005) 1399–1404.

[44]   A. Kudo, T. Kondo, Photoluminescent and photocatalytic properties of layered caesium titanates, $Cs_2Ti_nO_{2n+1}$ (n = 2, 5, 6), Journal of Materials Chemistry. 7 (1997) 777–780.

[45]   Y. Zhao, Q. Chen, F. Pan, H. Li, G.Q. Xu, W. Chen, Uniform Mesoporous Anatase Hollow Spheres: An Unexpectedly Efficient Fabrication Process and Enhanced Performance in Photocatalytic Hydrogen Evolution, Chemistry - A European Journal. 25 (2019) 10965–10970.

[46]   K. Batalović, N. Bundaleski, J. Radaković, N. Abazović, M. Mitrić, R.A. Silva, M. Savić, J. Belošević-Čavor, Z. Rakočević, C.M. Rangel, Modification of N-doped TiO_2 photocatalysts using noble metals (Pt, Pd) - A combined XPS and DFT study, Physical Chemistry Chemical Physics. 19 (2017) 7062–7071.

[47]   J. Wang, C. Fan, Z. Ren, X. Fu, G. Qian, Z. Wang, N-doped TiO_2/C nanocomposites and N-doped TiO_2 synthesised at different thermal treatment temperatures with the same hydrothermal precursor, Dalton Transactions. 43 (2014) 13783–13791.

[48]   H. Hattori, Y. Ide, T. Sano, Microporous titanate nanofibers for highly efficient UV-protective transparent coating, Journal of Materials Chemistry A. 2 (2014) 16381–16388.

[49]   S. Andersson, A.D. Wadsley, Five co-ordinated Titanium in $K_2Ti_2O_5$, Nature. 187 (1960) 499–500.

[50]   M.C. Biesinger, L.W.M. Lau, A.R. Gerson, R.S.C. Smart, Resolving surface chemical states in XPS analysis of first row transition metals, oxides and hydroxides: Sc, Ti, V, Cu and Zn, Applied Surface Science. 257 (2010) 887–898.

[51]   G. Liu, F. Li, D.W. Wang, D.M. Tang, C. Liu, X. Ma, G.Q. Lu, H.M. Cheng, Electron field emission of a nitrogen-doped TiO_2 nanotube array, Nanotechnology. 19 (2008).

[52]   T. Ihara, M. Miyoshi, Y. Iriyama, O. Matsumoto, S. Sugihara, Visible-light-active titanium oxide photocatalyst realized by an oxygen-deficient structure and by nitrogen doping, Applied Catalysis B: Environmental. 42 (2003) 403–409.

[53]   Y. Ide, N. Inami, H. Hattori, K. Saito, M. Sohmiya, N. Tsunoji, K. Komaguchi, T. Sano, Y. Bando, D. Golberg, Y. Sugahara, Remarkable Charge Separation and Photocatalytic Efficiency Enhancement through Interconnection of TiO_2 Nanoparticles by Hydrothermal Treatment, Angewandte Chemie - International Edition. 55 (2016) 3600–3605.

[54]   O.O. Prieto-Mahaney, N. Murakami, R. Abe, B. Ohtani, Correlation between photoeatalytic activities and structural and physical properties of titanium(IV) oxide powders, Chemistry Letters. 38 (2009) 238–239.

[55]   N. Serpone, Is the band gap of pristine TiO_2 narrowed by anion- and cation-doping of titanium dioxide in second-generation photocatalysts?, Journal of Physical Chemistry B. 110 (2006) 24287–24293.

[56]   S. Chen, Y. Xiao, Y. Wang, Z. Hu, H. Zhao, W. Xie, A facile approach to prepare black TiO_2 with oxygen vacancy for enhancing photocatalytic activity, Nanomaterials. 8 (2018) 1–16.

[57]   Y. Zhao, T. Shi, J. Shang, L. Ding, X. Cao, C. Chen, J. Zhao, Rapid proton exchange between surface bridging hydroxyls and adsorbed molecules on TiO_2, Applied Catalysis B: Environmental. 277 (2020) 119234.

[58]   M. Crocker, R.H.M. Herold, A.E. Wilson, M. Mackay, C.A. Emeis, A.M. Hoogendoorn, ^{1}H NMR spectroscopy of titania. Chemical shift assignments for hydroxy groups in crystalline and amorphous forms of TiO_2, Journal of the Chemical Society, Faraday Transactions. 92 (1996) 2791–2798.

[59]   A. Tilocca, A. Selloni, Reaction pathway and free energy barrier for defect-induced water dissociation on the (101) surface of TiO_2-anatase, Journal of Chemical Physics. 119 (2003) 7445–7450.

[60]   A. Janotti, J.B. Varley, P. Rinke, N. Umezawa, G. Kresse, C.G. Van De Walle, Hybrid functional studies of the oxygen vacancy in TiO_2, Physical Review B - Condensed Matter and Materials Physics. 81 (2010) 085212.

[61]   Y.H. Hu, A highly efficient photocatalyst-hydrogenated black TiO_2 for the photocatalytic splitting of water, Angewandte Chemie - International Edition. 51 (2012) 12410–12412.

[62]   D.C. Cronemeyer, Infrared absorption of reduced rutile TiO_2 single crystals, Physical Review. 113 (1959) 1222–1226.

Chapter 3:

Facile synthesis of layered titanate nanowires for photocatalytic removal of toxic metal cations

3.1   Introduction

Water pollution has become more prevalent because of the rapid population and industrial growth. In addition to other demands, water consumption has expanded dramatically in the agricultural, industrial, and home sectors, consuming large amounts of the available freshwater, allowing various pollutants to get into the water. Among various pollutants, heavy metal cations are one of the most pressing pollution problems due to their nonbiodegradability and bioaccumulation in living tissues and therefore have been studied by many researchers worldwide. Different methods have been introduced for addressing the heavy metal ions pollution problem including adsorption, precipitation, ion exchange, biological processes, and reverse osmosis [1]. Among them, ion exchange is considered a promising technology in a wide range of practical applications, including the removal of toxic compounds and the collection of noble elements from water.

Due to their great surface area (considerable ion exchange capacity) and chemical and thermal stabilities, layered inorganic solids, which are made up of inorganic nanosheets and interlayer exchangeable ions, have been widely investigated as ion exchangers [2–4]. Back exchange processes easily liberate collected ions from layered inorganic materials, which restricts their practical applicability. Various layered inorganic materials, such as synthetic micas, on the other hand, undergo structural collapse during ion exchange, resulting in tight immobilization of collected ions in the interlayer region (so-called irreversible ion exchange) [5,6]. Consequently, the complete collection and the safe disposal of collected hazardous ions from water can be achieved. Nevertheless, since the ion diffusion in layered materials is notoriously slow, new layered solid-based ion exchangers with both rapid adsorption and immobilization capabilities for metal cations are required. Therefore, effective collection and safe disposal of harmful metal cations from aqueous solutions are crucial for the

application of such materials in environmental remediation [5].

A photocatalytic process, in which the light energy is used to generate electron-hole pairs in the semiconducting material, can spontaneously reduce the adsorbed metal cations and fix metals on surfaces. Thus, it is considered a safer disposal process than adsorption and ion exchange processes. However, the development of photocatalysts for this reaction is yet challenging [7,8].

In recent decades, one-dimensional (1D) TiO_2 nanostructures have drawn big attention due to their interesting physicochemical properties. TiO_2 nanowires (NWs) are a particularly important family of 1D nanostructures because they provide a high specific surface area, excellent accessibility, and unique charge transport (separation) capabilities [9–11]. TiO_2 NWs are being applied in a variety of environmental and energy-related applications, including photocatalysis, solar cells, and supercapacitors [12–18]. 2D layered titanates, on the other hand, have been widely studied for a variety of environmental and energy applications [19–23]. Lepidocrocite-type layered titanates have considerable merits over other layered titanates, including rich intercalation chemistry, high exfoliation ability, and composition-tunable characteristics [24–26]. Owing to these interesting properties, they have been used in such applications as cation exchange, adsorption, photocatalysis [27–32]. The dimensional control of the 2D layered structure to the 1D NW structure of lepidocrocite-type layered titanates has the potential to improve properties and open new applications [33–36]. Nevertheless, the synthesis of its NW structure was reported in a few studies, and the traditional synthetic processes are comparatively difficult without utilizing lepidocrocite-type layered titanates as starting materials [33–36]. Moreover, the improved photocatalytic activity of lepidocrocite-type layered titanates, which is critical for practical applications, has been barely reported.

3.2   Chapter scope

Considering the above explanations and the fact that TiO_2 NWs have shown dramatically enhanced photocatalytic activity when compared to bulk TiO_2, layered titanate NWs might show excellent adsorption/immobilization ability for metal ions under irradiation of light. From this point of view, we report here on a simple synthesis of NWs of a layered titanate with a lepidocrocite structure, $K_xTi_{2-x/3}Li_{x/3}O_4$ (named KTLO), one of the most studied layered titanates. KTLO NW structure is successfully

synthesized by a simple one-pot solvothermal reaction (**Scheme 1**). The obtained KTLO NWs exhibit efficient and rapid adsorption/immobilization of Cd^{2+} from water with the assistance of photoirradiation, which cannot be achieved by even state-of-the-art cation exchangers and a benchmark TiO_2. A combination of 1D and 2D structural characteristics, outstanding cation exchange ability, and high photo-induced charge separation/photocatalytic efficiency gave rise to these traits.
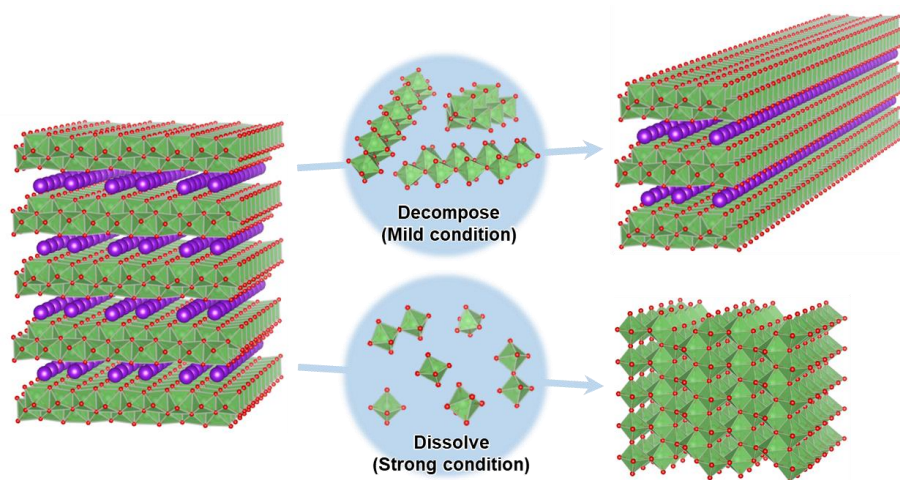
Scheme 3.1. *Graphical representation for the synthesis of KTLO NWs through decomposition/recrystallization of KTLO under solvothermal conditions (upper). That of anatase TiO_2 through dissolution/deposition of KTLO is also shown (lower). Color coding: red = O, purple = K, green = Ti. Reprinted with permission from {Inorganic chemistry 58.12 (2019): 7989-7996} Copyright {2019} by American Chemical Society.*

3.3   Experimental details

3.3.1   Materials

All chemicals were utilized as received. K_2CO_3 (99.5%) was purchased from Nacalai Tesque, Li_2CO_3 (>98%), and tetrapropylammonium hydroxide (TPAOH, 40 wt% aqueous solution) was purchased from Tokyo Chemical Industry, ammonium fluoride (NH_4F) was purchased from Sigma Aldrich, and TiO_2 P25 was purchased from Nippon Aerosil. Anatase (JRC-TIO-1) was supplied by the Catalysis Society of Japan. $CdCl_2$ (99.9%) and $NiCl_2$ (99.9%) were purchased from STREM chemicals and Sigma Aldrich, respectively. Formic acid (98%) and $H_2PtCl_6 \cdot 6H_2O$ (99.9%) were purchased from Wako Pure Chemical Industry.

3.3.2 Preparation of KTLO

KTLO was prepared by the solid-state reaction using K_2CO_3, Li_2CO_3, and TiO_2 P25 with a molar ratio of 2.4: 0.8: 10.4 according to the previous report [37]. The starting materials were mixed in agitating mortar for 2 h. The mixture was then calcined in air for 20 hours at 600°C. After cooling to room temperature, the powder was re-mixed before being calcined in air at 600°C for another 20 hours.

3.3.3 Synthesis of KTLO NWs

A Teflon-lined stainless-steel autoclave containing the mixture of 0.78 g of TPAOH, 0.014 g of NH_4F, and 0.2 g of KTLO, was kept at 170 °C for 7 days. The product was washed after the solvothermal reaction with ethanol and dried at 60 °C. Under the same conditions, anatase nanoparticles (with a primary particle size of around 20 nm) were solvothermally treated. For mechanistic objectives, the solvothermal reaction of KTLO was carried out at 170°C under various conditions (TPAOH quantity, reaction duration).

3.3.4 Characterization

3.3.4.1 Structural characterization

A Rigaku SmartLab diffractometer was used to collect powder X-ray diffraction (XRD) data, with Cu K radiation at 40 kV and 30 mA at a scan rate of 1 min^{-1}. Micro-Raman scattering measurements were performed at room temperature with a 532 nm excitation light source (Photon Design Company). A PHI Quantera SXM equipment was used to perform X-ray photoelectron spectroscopy (XPS) using Al K radiation at 20 kV and 5 mA. The C1s level at 285.0 eV was used to calibrate the binding energy shift.

3.3.4.2 Morphological characterization

A Hitachi SU-8230 microscope operating at 10.0 kV was used to observe field emission scanning electron microscopy (FE-SEM) pictures. A JEOL JEM-2100F transmission electron microscope was used to obtain TEM pictures at a voltage of 200 kV.

3.3.4.3 Thermal and Optical measurements

A Hitachi TG/DTA6200 was used to record thermogravimetric curves. UV–Vis spectra were obtained with a JASCO V-570 spectrophotometer.

An Agilent 710-ES spectrometer was used to perform inductively coupled plasma atomic emission spectroscopy (ICP-AES).

3.3.5   *Photoreduction and cation exchange of metal cations*

In the photoreduction experiment, the catalyst (15 mg) was placed in a Pyrex glass tube (34 mL) filled with an aqueous solution of $CdCl_2$ (20 mL, ca. 50 for Cd^{2+}) or $NiCl_2$ (20 mL, 95 ppm for Ni^{2+}) and deaerated by Ar bubbling. Methanol was used during the reaction as a sacrificial agent. Under stirring, a solar simulator (San-Ei Electric, > 300 nm, 1000 Wm^2) was used to irradiate the glass tube, which was sealed with a rubber septum. The concentration of Cd^{2+} or Ni^{2+} in the supernatant was determined by ICP-AES after the mixture had been separated. To validate the deposition of Cd and Ni, XRD and XPS were used to examine the recovered catalyst. Cd^{2+} or Ni^{2+} cation exchange was performed in the absence of light irradiation.

3.3.6   *Photocatalytic Formic acid oxidation*

In a Pyrex glass tube (34 mL), the catalyst (15 mg) was dispersed in an aqueous solution (5 mL) containing 5 vol percent formic acid and then aerated by O_2 bubbling. Under stirring, a solar simulator (San-Ei Electric, > 300 nm, 1000 W m^2) was used to irradiate the glass tube, which was sealed with a rubber septum. A Shimadzu GC-2010 plus gas chromatograph with a BID detector was used to measure CO_2 in the headspace.

3.3.7   *Photocatalytic Hydrogen production*

In a Pyrex glass test tube (34 mL), 15 mg of the photocatalyst was dispersed in 5 ml aqueous methanol solution (1/1 in V/V). Pt (0.5 wt%) was used as a co-catalyst. The solution was deaerated for 30 minutes with Ar bubbling, then sealed with a silicone rubber septum before being irradiated with a solar simulator (San-Ei Electric Co., Ltd.). A Shimadzu GC-2010 plus gas chromatograph with a BID detector was used to measure the evolved H_2 in the headspace.

3.4   Results and Discussion

3.4.1   Formation and properties of KTLO NWs

Under alkali solvothermal conditions, TiO_2 materials are transformed to their 1D nanostructure (e.g., nanotubes), as is well known. Interzeolite conversion, on the other hand, inspired the current established solvothermal process for synthesizing KTLO NWs, which is now acknowledged as a viable approach for strategically designing zeolites [38,39]. In this process, it is suggested that the original zeolite decomposes into smallish segments (so-named nanoparts) and the nanoparts recrystallize into another zeolite under solvothermal conditions via the help of structure-directing agents and mineralizers. Therefore, the above conversion strategy drove us to develop a new solvothermal reaction to transform 2D KTLO into 1D KTLO NWs.

The starting material (KTLO) was synthesized by solid-state reaction at 600 ℃, followed by the solvothermal reaction in the existence of TPAOH and NH_4F at 170 ℃ to synthesize KTLO NWs, as described in the experimental section. As depicted in the SEM micrograph (**Figure 3.1a**), the original KTLO was found to be composed of platelike particles with a thickness of 5-10 nm and a lateral size of 100-200 nm. The solvothermal product was formed of nanowire-shape particles with a length of several hundreds of nanometres and a diameter of approximately 10 nm (named KTLO NWs), as depicted in **Figure 3.1b**.
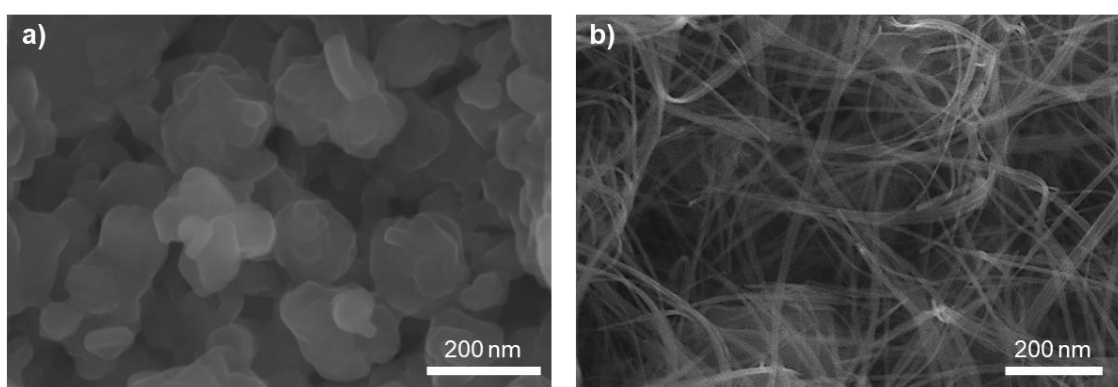
Figure 3.1. *SEM micrographs of a) KTLO and b) KTLO NWs. Reprinted with permission from {Inorganic chemistry 58.12 (2019): 7989-7996} Copyright {2019} by American Chemical Society.*

Additionally, XRD and Raman analyses (**Figure 3.2a, b**) proved that the KTLO NWs product possesses the same diffraction patterns and Raman peaks of the original KTLO (just a little portion of anatase was included in the NW yield), revealing that the KTLO NWs product is maintaining the layered structure of the original layered KTLO. In combination with the XRD findings, HRTEM and ED (**Figure 3.2d**) confirmed the layered structure of KTLO NWs with an interplanar spacing of 0.79 nm.
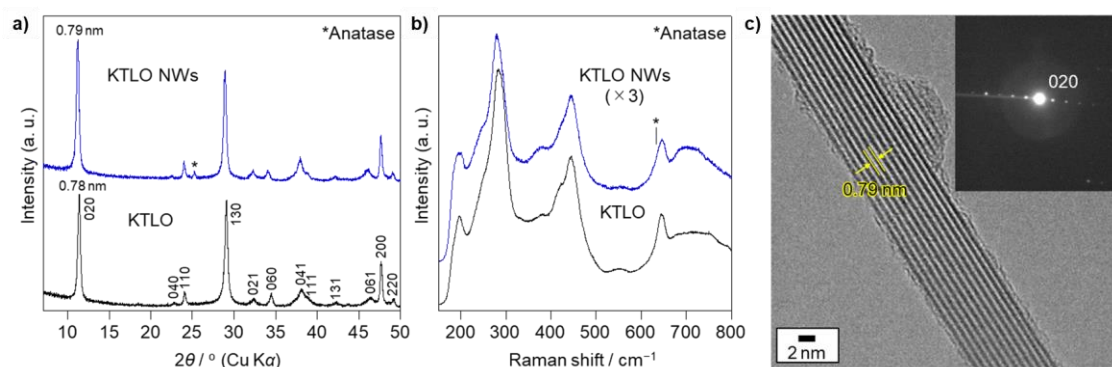
Figure 3.2. a) XRD patterns, b) Raman spectra of KTLO and KTLO NWs, and c) HRTEM image and ED pattern of KTLO NWs. Reprinted with permission from {Inorganic chemistry 58.12 (2019): 7989-7996} Copyright {2019} by American Chemical Society.

We investigated the composition of the produced KTLO NWs since the hydration/swelling ability of layered materials is dependent on the composition (layer charge density), and KTLO has the empirical formula $K_xTi_{2-x/3}Li_{x/3}O_4$ (the range of x studied was 0.6 ~ 0.8). The composition of KTLO and KTLO NWs was estimated to be $K_{0.80}Ti_{1.73}Li_{0.27}O_4$ and $K_{0.63}H_{0.21}Ti_{1.72}Li_{0.28}O_4$, respectively, based on ICP analysis presented in **Table 3.1**.

Table 3.1. Composition of KTLO and KTLO NWs. Reprinted with permission from {Inorganic chemistry 58.12 (2019): 7989-7996} Copyright {2019} by American Chemical Society

	Composition (mass%)[a]		
	K	Ti	Li
KTLO	16.1	43.0	0.92
KTLO NWs	12.8	44.5[b]	0.94

[a] Determined by ICP of the dissolved samples with HF.

[b] Including the Ti content of anatase as impurity.

KTLO and KTLO NWs have nearly identical layer charge densities (($[Ti_{1.73}Li_{0.27}O_4]^{0.80-}$ *vs* $[Ti_{1.72}Li_{0.28}O_4]^{0.84-}$), whilst KTLO NWs have a lower quantity of the interlayer K^+ (H^+ should exist to neutralize the negative charge of the layers). Consequently, more interlayer H_2O (or H_3O^+) molecules can be hosted on KTLO NWs (as depicted in **Figure 3.3**), resulting in a somewhat wider basal spacing than KTLO NWs (**Figure 3.2a**).
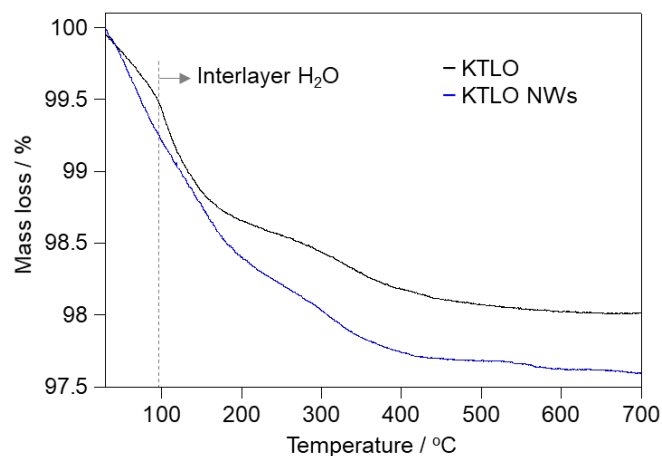
Figure 3.3. *TGA curves of KTLO and KTLO NWs. Reprinted with permission from {Inorganic chemistry 58.12 (2019): 7989-7996} Copyright {2019} by American Chemical Society.*

The formation mechanism of KTLO NWs was discussed by performing the solvothermal reaction of KTLO under different conditions. The solvothermal reaction of KTLO under different conditions was used to discuss the formation mechanism of KTLO NWs. As depicted in SEM micrographs (**Figure 3.4a-c**), the NWs quantity dropped as the quantity of TPAOH increased whereas the quantity and size of spindle-shaped particles rose. Additionally, XRD analysis (**Figure 3.4d**) revealed the weakening of diffraction peaks corresponding to KTLO and the intensifying of those due to TiO_2 anatase, consistent with SEM results.
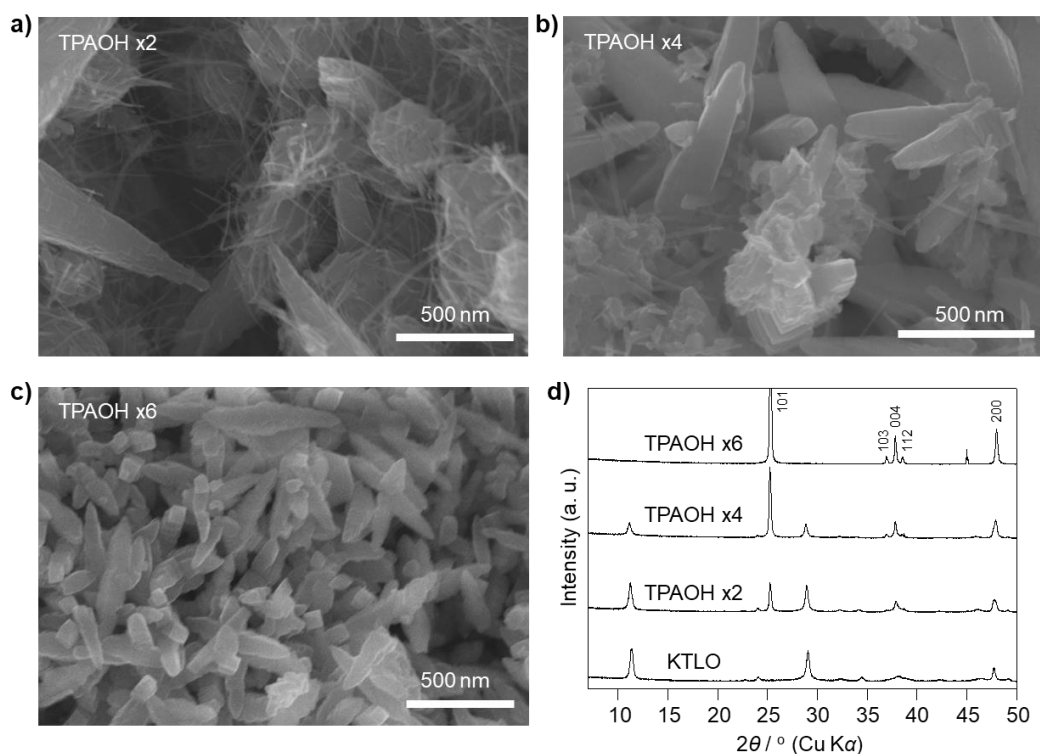
Figure 3.4. *SEM micrographs of solvothermal products of KTLO produced at different TPAOH concentrations. (d) XRD patterns of KTLO and solvothermal products at different TPAOH concentrations. Reprinted with permission from {Inorganic chemistry 58.12 (2019): 7989-7996} Copyright {2019} by American Chemical Society.*

According to our earlier findings [8,40–43], the decomposition/dissolution of initial layered titanates should be enhanced by using TPAOH and the recrystallization of the decomposed/dissolved species should be achieved with the help of NH_4F, which works as a mineralizer. Hence a probable pathway for the creation of KTLO NWs from KTLO can be explained in **Scheme 1**. Under typical conditions (milder TPAOH concentration), KTLO decomposes into tiny segments (i.e., 1D chains of edge- and corner-shared TiO_6 octahedra), and these segments assemble into 1D KTLO NWs. While, under harsh conditions (higher TPAOH concentration), KTLO dissolves into Ti^{4+} to deposit anatase TiO_2. It was also reported that when treated with strong HCl [44] and swollen/exfoliated in water containing organic ammoniums [45], KTLO, and similar layered titanates were found to disintegrate into such tiny 1D segments.

Moreover, we solvothermally treated KTLO under identical conditions for a shorter duration to attain a deeper understanding of the formation mechanism. The solvothermal product, collected after

69

3 days using a typical amount of TPAOH at 170 °C, still contains a significant amount of KTLO, as depicted in **Figure 3.5a,b**. Therefore, 3 days were not enough for converting the original KTLO into KTLO NWs. That is why we adjusted the solvothermal reaction duration to be 7 days for obtaining better ad uniform nanowires morphology (**Figure 3.1b**).
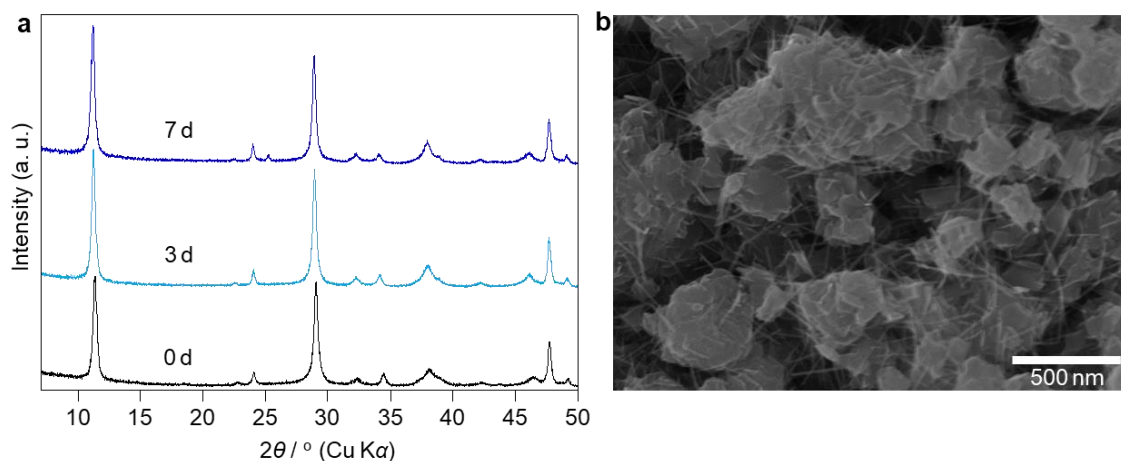
Figure 3.5. (a) XRD patterns of KTLO and its solvothermal products obtained at different reaction times. 0 d and 7 d labels are corresponding to KTLO and KTLO NWs, respectively. (b) SEM micrograph of the solvothermal product obtained after 3 days. Reprinted with permission from {Inorganic chemistry 58.12 (2019): 7989-7996} Copyright {2019} by American Chemical Society.

Furthermore, we applied the typical solvothermal reaction on anatase TiO_2 nanoparticles. In comparison to the starting anatase nanoparticles, after the solvothermal reaction, the structure and morphology were hardly modified; only the particle size and crystallinity lightly changed. This result proved that anatase is tough adequate to neither decompose nor dissolve beneath the existing basic conditions, but KTLO, a metastable phase, is unstable.
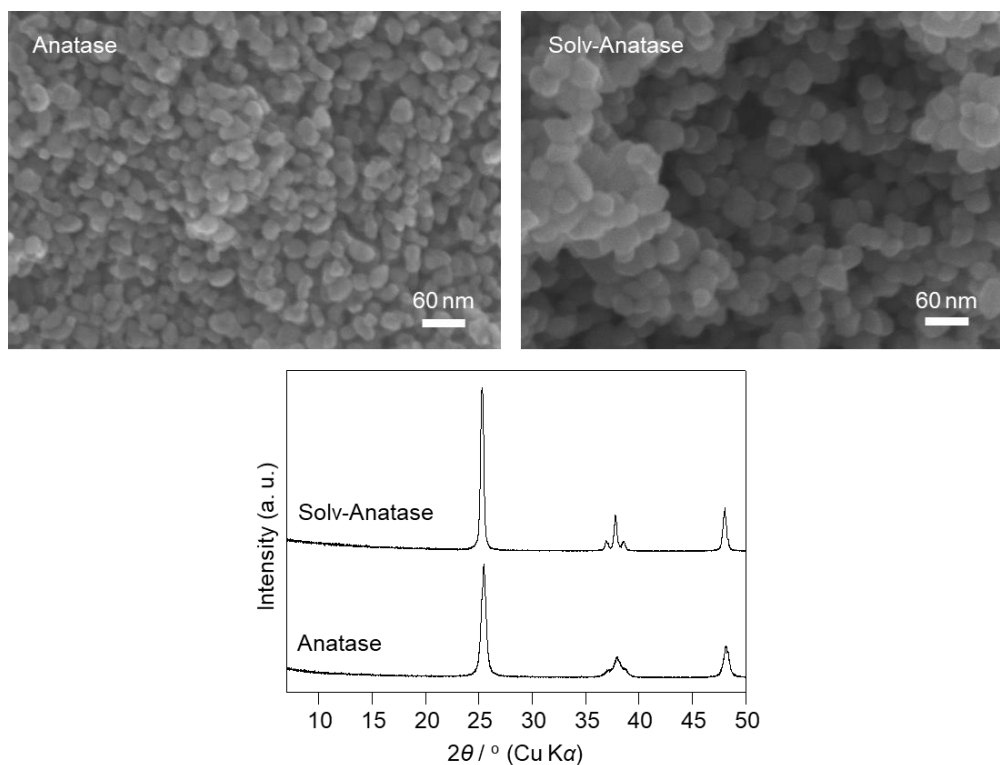
Figure 3.6*. SEM micrographs and XRD patterns of anatase and its solvothermal product. Reprinted with permission from {Inorganic chemistry 58.12 (2019): 7989-7996} Copyright {2019} by American Chemical Society.*

3.4.2　Ion exchange ability & photoactivity of KTLO NWs

We expected that the obtained KTLO NWs showed better cation–exchange properties than KTLO because KTLO NWs had much smaller dimensions for accessibility of cations (cation diffusion) inside the particles. We first examined the adsorption of Cd^{2+} from aqueous $CdCl_2$ solution (pH = 4.8). We chose Cd^{2+} (ca. 50 ppm) as an adsorbate since it is one of the most noxious ions being in the environment and hard to be adsorbed using conventional ion exchangeable layered inorganic solids and TiO_2 [46,47]. As depicted in **Figure 3.7a**, Cd^{2+} was adsorbed more quickly when the KTLO NW was used as an adsorbent. Within 20 minutes, the Cd^{2+} adsorption was done. While it took more than 60 minutes when KTLO was used. The maximum adsorption capacity was calculated to be 0.7 mmol/g, which was approximately equal to the cation exchange capacity (1.5 mequiv/g) [48].

These findings suggest that interlayer K^+ cation exchange and replacement with Cd^{2+} are done. The Cd^{2+} adsorption on the commercial TiO_2 (P25) was additionally evaluated and found to be insignificant,

71

compatible with prior results [7]. This makes sense because P25 has a positively charged surface below its isoelectric point (ca. 6.4) [49] that repels cations.

The photoactivity of KTLO NWs was then investigated to decide if it could photoreduce metal ions faster than KTLO. It was estimated by performing two well-known photocatalytic processes; formic acid oxidation and H_2 evolution from water [50]. As demonstrated in **Figure 3.7b**, KTLO NWs had much-increased photocatalytic activity toward formic acid oxidation. Given that the UV-vis spectra of KTLO and KTLO NWs are nearly similar (**Figure 3.7c**), the increased photoactivity of KTLO NWs is owing to the improved charge separation efficiency of their 1D nanostructure [51]. The same result was concluded when performing the H_2 evolution reaction (**Figure 3.7d**). It is also worth mentioning that the H_2 production is difficult to catalyze using low-active TiO_2-based photocatalysts such as layered titanates [52], but KTLO did. This result confirms again the improved charge separation efficiency of the obtained KTLO nanowires.

As illustrated in the XRD analysis depicted in **Figure 3.2a**, KTLO NWs have a very smallish portion of anatase (0.1 wt%) as a secondary phase. As a result, one may argue that KTLO NWs and this small portion of anatase form a composite, improving the photoactivity of KTLO NWs by interparticle electron transfer. Therefore, we examined the photocatalytic activity of a physically mixed anatase (0.1 wt%)/KTLO. The results showed that the photoactivity of this mixture was insignificant and almost identical to that of the original KTLO. These findings confirm that there was no contribution from that small portion of anatase in enhancing the photocatalytic activity of KTLO NWs and it was due to the 1D nanostructure-related charge separation performance.
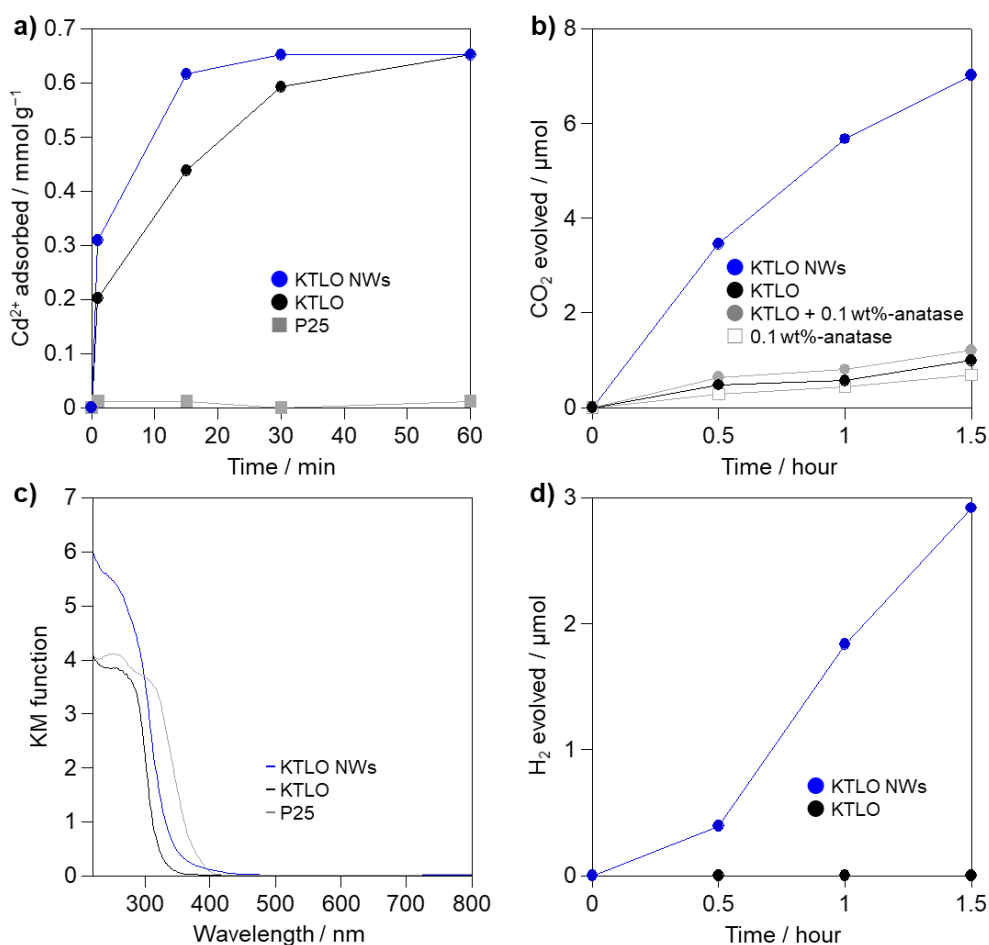
Figure 3.7. (a) The adsorbed amount of Cd^{2+} using KTLO, KTLO NWs, and commercial TiO_2 (P25). (b) CO_2 evolved during photocatalytic formic acid oxidation reaction using KTLO and KTLO NWs under solar light. Those of the anatase/KTLO mixture and pure anatase are also shown. (c) UV-Vis spectra of KTLO, KTLO NWs, and P25. (d) H_2 evolved from water using KTLO and KTLO NWs under solar light. Reprinted with permission from {Inorganic chemistry 58.12 (2019): 7989-7996} Copyright {2019} by American Chemical Society.

3.4.3 *Photo-fixation of metal cations on KTLO NWs*

Eventually, the photocatalytic reduction of metal cations like Cd^{2+} and Ni^{2+} was examined utilizing KTLO NWs. As expected, KTLO NWs exhibited a significantly high activity toward the photocatalytic reduction of metal cations. As depicted in **Figure 3.8a**, the photocatalytic reduction of Cd^{2+} to Cd happened very quickly using KTLO NWs, where about 1.3 mequiv g^{-1} of Cd was deposited on KTLO NWs in a minute. While it was not successful using P25, a benchmark TiO_2 photocatalyst, and KTLO. Even cutting-edge inorganic cation exchangers require more time (more than several minutes) [53] to only adsorb

equivalent quantities of metal ions, thus this finding is remarkable. The combination of the improved cation exchange and photoactivity must account for the high activity of KTLO NWs towards this reaction. Similarly, Ni^{2+} photoreduction activity was considerably high in KTLO NWs. The reaction was not successful too in the case of P25 and KTLO (**Figure 3.8b**). Even after easy decantation, the KTLO NWs employed in the photoreduction experiments were readily recovered from water. This is a benefit of the material for realistically practical applications.
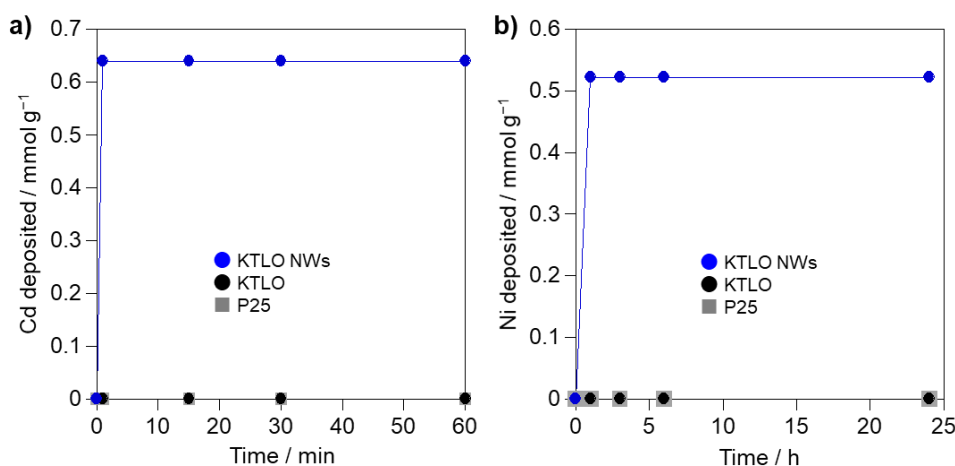
Figure 3.8. Photocatalytic reduction of a) Cd^{2+} and b) Ni^{2+} in water using KTLO, KTLO NWs, and P25 under solar light. Reprinted with permission from {Inorganic chemistry 58.12 (2019): 7989-7996} Copyright {2019} by American Chemical Society.

The immobilization of Cd in the interlayer distance of KTLO NWs was confirmed using XRD, XPS, and HRTEM analyses. After the photoreduction of Cd^{2+}, the peak assigned to the basal spacing was shifted to the lower 2θ and considerably broadened whereas a small and broad peak due to Cd was observed (**Figure 3.9a**). The 0+ state of Cd was also proved by XPS, as depicted in **Figure 3.9b**. This infers to the existence of Cd metal inside the particle or within the interlayer distance of KTLO NWs. Moreover, Cd nanoparticles of about 0.5-1 nm were noticed as depicted in **Figure 3.9 (c, d)**, revealing that Cd nanoparticles were most likely present inside KTLO NWs. As a result of the higher charge separation efficiency, that is, the efficient migration of photogenerated electrons to the surface of KTLO layers, we may deduce that KTLO NWs quickly photoreduce the accumulated Cd^{2+} in the interlayer space, suppressing electron-hole recombination in the layers.
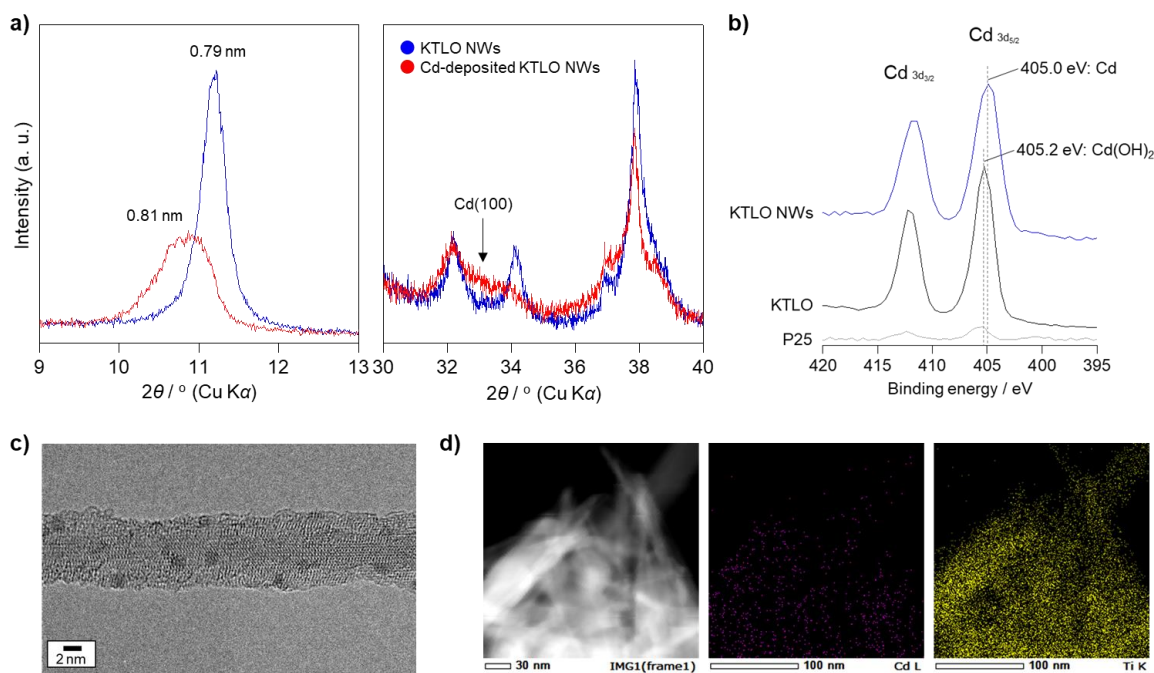
Figure 3.9. *a) Low- and high angle XRD patterns before and after Cd photoreduction, b) XPS spectra of P25, KTLO, and KTLO NWs after Cd^{2+} photoreduction, c) HRTEM of the recovered KTLO NWs, and d) HAADF-STEM images and the corresponding EDX elemental maps of KTLO NWs after Cd^{2+} photo-deposition. Reprinted with permission from {Inorganic chemistry 58.12 (2019): 7989-7996} Copyright {2019} by American Chemical Society.*

3.5   Summary

In this chapter, a simple solvothermal strategy for converting a 2D lepidocrocite-type layered titanate ($K_xTi_{2-x/3}Li_{x/3}O_4$ termed KTLO) into its corresponding 1D nanowires (NWs) was reported. Compared to KTLO, the newly developed KTLO NWs exhibited largely enhanced cation exchange and photo-induced charge separation efficiency, which was attributed to the combination of 1D and 2D structural properties. As a result, the KTLO NWs showed ultrafast and effective photoreduction of toxic metal cations in water, such as Cd^{2+}, into the corresponding metals immobilized within the NWs, whereas a benchmark TiO_2 photocatalyst (P25) and KTLO could not photocatalyze this reaction. Moreover, the photoimmobilizing rates obtained from KTLO NWs were much greater than that of state-of-the-art cation exchangers. Based on these findings, we confirm that the KTLO NWs can be used for the safe capture and disposal of toxic metal cations and recovery of valuable metals from the environment. The present solvothermal method can be applied to numerous 2D layered materials like layered perovskites.

Therefore, a variety of nanowire structures can be designed to attain better functions and new applications for solving energy and environmental problems.

3.6   Reference:

[1]   V.N.H. Nguyen, R. Amal, D. Beydoun, Effect of formate and methanol on photoreduction/removal of toxic cadmium ions using TiO_2 semiconductor as photocatalyst, Chemical Engineering Science. 58 (2003).

[2]   A. Clearfield, Role of ion exchange in solid-state chemistry, Chemical Reviews. 88 (1988) 125–148.

[3]   S.M. Auerbach, K.A. Carrado, P.K. Dutta, Handbook of layered materials, CRC Press, 2004.

[4]   Y. Ide, N. Ochi, M. Ogawa, Effective and selective adsorption of Zn^{2+} from seawater on a layered silicate, Angewandte Chemie. 123 (2011) 680–682.

[5]   S. Komarneni, R. Roy, A Cesium-Selective Ion Sieve Made by Topotactic Leaching of Phlogopite Mica, Science. 239 (1988) 1286–1288.

[6]   N. Li, L. Zhang, Y. Chen, M. Fang, J. Zhang, H. Wang, Highly efficient, irreversible and selective ion exchange property of layered titanate nanostructures, Advanced Functional Materials. 22 (2012) 835–841.

[7]   M.R. Prairie, L.R. Evans, B.M. Stange, S.L. Martinez, An investigation of titanium dioxide photocatalysis for the treatment of water contaminated with metals and organic chemicals, Environmental Science & Technology. 27 (1993) 1776–1782.

[8]   Y. Ide, W. Shirae, T. Takei, D. Mani, J. Henzie, Merging Cation Exchange and Photocatalytic Charge Separation Efficiency in an Anatase/$K_2Ti_4O_9$ Nanobelt Heterostructure for Metal Ions Fixation, Inorganic Chemistry. 57 (2018) 6045–6050.

[9]   F.X. Xiao, J. Miao, H.B. Tao, S.F. Hung, H.Y. Wang, H. Bin Yang, J. Chen, R. Chen, B. Liu, One-dimensional hybrid nanostructures for heterogeneous photocatalysis and photoelectrocatalysis, Small. 11 (2015) 2115–2131.

[10]   M. Ge, C. Cao, J. Huang, S. Li, Z. Chen, K.Q. Zhang, S.S. Al-Deyab, Y. Lai, A review of one-dimensional TiO$_2$ nanostructured materials for environmental and energy applications, Journal of Materials Chemistry A. 4 (2016) 6772–6801.

[11]   X. Wang, Z. Li, J. Shi, Y. Yu, One-dimensional titanium dioxide nanomaterials: Nanowires, nanorods, and nanobelts, Chemical Reviews. 114 (2014) 9346–9384.

[12]   D. V Bavykin, J.M. Friedrich, F.C. Walsh, Protonated titanates and TiO$_2$ nanostructured materials: synthesis, properties, and applications, Advanced Materials. 18 (2006) 2807–2824.

[13]   A.R. Armstrong, G. Armstrong, J. Canales, R. García, P.G. Bruce, Lithium-ion intercalation into TiO$_2$-B nanowires, Advanced Materials. 17 (2005) 862–865.

[14]   Z.J. Zhou, J.Q. Fan, X. Wang, W.H. Zhou, Z.L. Du, S.X. Wu, Effect of highly ordered single-crystalline TiO$_2$ nanowire length on the photovoltaic performance of dye-sensitized solar cells, ACS Applied Materials and Interfaces. 3 (2011) 4349–4353.

[15]   H. Bin Wu, H.H. Hng, X.W.D. Lou, Direct synthesis of anatase TiO$_2$ nanowires with enhanced photocatalytic activity, Advanced Materials. 24 (2012) 2567–2571.

[16]   X. Lu, M. Yu, G. Wang, T. Zhai, S. Xie, Y. Ling, Y. Tong, Y. Li, H-TiO$_2$@MnO$_2$//H-TiO$_2$@C core-shell nanowires for high performance and flexible asymmetric supercapacitors, Advanced Materials. 25 (2013) 267–272.

[17]   J. Tang, J. Li, P. Da, Y. Wang, G. Zheng, Solar-Energy-Driven Photoelectrochemical Biosensing Using TiO$_2$ Nanowires, Chemistry - A European Journal. 21 (2015) 11288–11299.

[18]   L. Chen, X. Sheng, D. Wang, J. Liu, R. Sun, L. Jiang, X. Feng, High-Performance Triphase Bio-Photoelectrochemical Assay System Based on Superhydrophobic Substrate-Supported TiO$_2$ Nanowire Arrays, Advanced Functional Materials. (2018) 1801483.

[19]   T. Okada, Y. Ide, M. Ogawa, Organic-inorganic hybrids based on ultrathin oxide layers: designed nanostructures for molecular recognition, Chemistry-An Asian Journal. 7 (2012) 1980–1992.

[20]   Y. Ide, M. Sadakane, T. Sano, M. Ogawa, Functionalization of layered titanates, Journal of Nanoscience and Nanotechnology. 14 (2014) 2135–2147.

[21]   B. Luo, G. Liu, L. Wang, Recent advances in 2D materials for photocatalysis, Nanoscale. 8 (2016) 6904–6920.

[22]   C. Tan, X. Cao, X.-J. Wu, Q. He, J. Yang, X. Zhang, J. Chen, W. Zhao, S. Han, G.-H. Nam, Recent advances in ultrathin two-dimensional nanomaterials, Chemical Reviews. 117 (2017) 6225–6331.

[23]   D. Sangian, Y. Ide, Y. Bando, A.E. Rowan, Y. Yamauchi, Materials Nanoarchitectonics Using 2D Layered Materials: Recent Developments in the Intercalation Process, Small. 14 (2018) 1800551.

[24]   T. Sasaki, F. Izumi, M. Watanabe, Intercalation of pyridine in layered titanates, Chemistry of Materials. 8 (1996) 777–782.

[25]   T. Sasaki, M. Watanabe, Osmotic swelling to exfoliation. Exceptionally high degrees of hydration of a layered titanate, Journal of the American Chemical Society. 120 (1998) 4682–4689.

[26]   F. Geng, R. Ma, A. Nakamura, K. Akatsuka, Y. Ebina, Y. Yamauchi, N. Miyamoto, Y. Tateyama, T. Sasaki, Unusually stable ~100-fold reversible and instantaneous swelling of inorganic layered materials, Nature Communications. 4 (2013).

[27]   R. Ma, T. Sasaki, Nanosheets of oxides and hydroxides: Ultimate 2D charge-bearing functional crystallites, Advanced Materials. 22 (2010) 5082–5104.

[28]   Y. Ide, M. Ogawa, Interlayer Modification of a Layered Titanate with Two Kinds of Organic Functional Units for Molecule Specific Adsorption, Angewandte Chemie International Edition. 46 (2007) 8449–8451.

[29]   Y. Ide, M. Matsuoka, M. Ogawa, Efficient visible-light-induced photocatalytic activity on gold-nanoparticle-supported layered titanate, Journal of the American Chemical Society. 132 (2010) 16762–16764.

[30]   Y. Ide, Y. Nakasato, M. Ogawa, Molecular recognitive photocatalysis driven by the selective adsorption on layered titanates, Journal of the American Chemical Society. 132 (2010) 3601–3604.

[31]   J.L. Gunjakar, I.Y. Kim, J.M. Lee, Y.K. Jo, S. J. Hwang, Exploration of nanostructured functional materials based on hybridization of inorganic 2D nanosheets, The Journal of Physical Chemistry C. 118 (2014) 3847–3863.

[32]   L. F. Hu, R. Li, J. He, L. Da, W. Lv, J. Hu, Structure and photocatalytic performance of layered $HNbWO_6$ nanosheet aggregation, Journal of Nanophotonics. 9 (2015) 93041.

[33]   J. Li, Z. Tang, Z. Zhang, Layered hydrogen titanate nanowires with novel lithium intercalation properties, Chemistry of Materials. 17 (2005) 5848–5855.

[34]   F. Wu, Z. Wang, X. Li, H. Guo, Hydrogen titanate and TiO_2 nanowires as anode materials for lithium-ion batteries, Journal of Materials Chemistry. 21 (2011) 12675–12681.

[35]   Y. Ishikawa, S. Tsukimoto, K.S. Nakayama, N. Asao, Ultrafine sodium titanate nanowires with extraordinary Sr ion-exchange properties, Nano Letters. 15 (2015) 2980–2984.

[36]   T. Saito, M. Zhang, R.D. Kavthe, K. Akagi, K.S. Nakayama, T. Adschiri, N. Asao, Dealloying-oxidation technique as a powerful synthetic tool for sodium titanate nanowires with high ion-exchange ability, Chemistry Letters. 46 (2017) 1825–1827.

[37]   M. Ogawa, M. Morita, S. Igarashi, S. Sato, A green synthesis of a layered titanate, potassium lithium titanate; lower temperature solid-state reaction and improved materials performance, Journal of Solid State Chemistry. 206 (2013) 9–13.

[38]   M. Dusselier, M.E. Davis, Small-pore zeolites: Synthesis and catalysis, Chemical Reviews. 118 (2018) 5265–5329.

[39]   T. Sano, M. Itakura, M. Sadakane, High Potential of Interzeolite Conversion Method for Zeolite Synthesis, Journal of the Japan Petroleum Institute. 56 (2013) 183–197.

[40]   H. Hattori, Y. Ide, T. Sano, Microporous titanate nanofibers for highly efficient UV-protective transparent coating, Journal of Materials Chemistry A. 2 (2014) 16381–16388.

[41]   Y. Ide, K. Komaguchi, A photocatalytically inactive microporous titanate nanofiber as an excellent and versatile additive to enhance the TiO_2 photocatalytic activity, Journal of Materials Chemistry A. 3 (2015) 2541–2546.

[42]   Y. Ide, N. Inami, H. Hattori, K. Saito, M. Sohmiya, N. Tsunoji, K. Komaguchi, T. Sano, Y. Bando, D. Golberg, Y. Sugahara, Remarkable Charge Separation and Photocatalytic Efficiency Enhancement through Interconnection of TiO_2 Nanoparticles by Hydrothermal Treatment, Angewandte Chemie - International Edition. 55 (2016) 3600–3605.

[43]   Y. Ide, W. Shirae, Hydrothermal Conversion of Layered Niobate $K_4Nb_6O_{17}$. $3H_2O$ to Rare Microporous Niobate $K_6Nb_{10.8}O_{30}$, Inorganic Chemistry. 56 (2017) 10848–10851.

[44]   K. Saito, S. Tominaka, S. Yoshihara, K. Ohara, Y. Sugahara, Y. Ide, Room-temperature rutile TiO_2 nanoparticle formation on protonated layered titanate for high-performance heterojunction creation, ACS Applied Materials & Interfaces. 9 (2017) 24538–24544.

[45]	F. Geng, R. Ma, Y. Ebina, Y. Yamauchi, N. Miyamoto, T. Sasaki, Gigantic swelling of inorganic layered materials: a bridge to molecularly thin two-dimensional nanosheets, Journal of the American Chemical Society. 136 (2014) 5491–5500.

[46]	Y. Ide, N. Ochi, M. Ogawa, Effective and Selective Adsorption of Zn^{2+} from Seawater on a Layered Silicate, Angewandte Chemie. 123 (2011) 680–682.

[47]	M.R. Prairie, L.R. Evans, B.M. Stange, S.L. Martinez, An investigation of titanium dioxide photocatalysis for the treatment of water contaminated with metals and organic chemicals, Environmental Science & Technology. 27 (1993) 1776–1782.

[48]	T. Sasaki, M. Watanabe, Y. Michiue, Y. Komatsu, F. Izumi, S. Takenouchi, Preparation and Acid-Base properties of a protonated titanate with the lepidocrocite-like layer structure, Chemistry of Materials. 7 (1995) 1001–1007.

[49]	B. Ohtani, Y. Okugawa, S. Nishimoto, T. Kagiya, Photocatalytic activity of titania powders suspended in aqueous silver nitrate solution: correlation with pH-dependent surface structures, Journal of Physical Chemistry. 91 (1987) 3550–3555.

[50]	O. O. Prieto-Mahaney, N. Murakami, R. Abe, B. Ohtani, Correlation between photocatalytic activities and structural and physical properties of titanium (IV) oxide powders, Chemistry Letters. 38 (2009) 238–239.

[51]	X. Wang, Z. Li, J. Shi, Y. Yu, One-dimensional titanium dioxide nanomaterials: Nanowires, nanorods, and nanobelts, Chemical Reviews. 114 (2014) 9346–9384.

[52]	K. Saito, M. Kozeni, M. Sohmiya, K. Komaguchi, M. Ogawa, Y. Sugahara, Y. Ide, Unprecedentedly enhanced solar photocatalytic activity of a layered titanate simply integrated with TiO_2 nanoparticles, Physical Chemistry Chemical Physics. 18 (2016) 30920–30925.

[53]	Y. Ishikawa, S. Tsukimoto, K.S. Nakayama, N. Asao, Ultrafine sodium titanate nanowires with extraordinary Sr ion-exchange properties, Nano Letters. 15 (2015) 2980–2984.

Chapter 4:

Structural conversion of Cu-titanate into photoactive plasmonic Cu-TiO$_2$ for H$_2$ generation in visible light

4.1 Introduction

Hydrogen (H$_2$) has long been considered the ideal energy carrier, and it holds promise as a next-generation energy vector for addressing a wide range of environmental and energy issues. Nevertheless, the entire usage of H$_2$ has not been realized yet, owing to hardships in reaching safe delivery and controllable storage [1]. Therefore, developing effective and suitable H$_2$ storage solutions remains a critical problem for the future of the hydrogen economy. The search for appropriate H$_2$ storage materials that can release H$_2$ in situ under mild reaction conditions for direct application in fuel cells has become more popular [2–5]. On the other hand, the current demand around green H$_2$ generation is a crucial challenge to produce green alternative fuels to hold down the greenhouse gases released from fossil fuels [6–10]. There are several approaches to produce H$_2$ safely through a green approach [11,12]. Ammonia borane (AB; NH$_3$BH$_3$) has appeared as a prospective hydrogen storage material [13,14], thanks to its nontoxicity, low molecular weight (30.87 g mol^{-1}), high theoretical hydrogen gravimetric capacity (19.6 wt%), and excellent stability in solid form under ambient conditions. Pyrolysis [15] or hydrolytic dehydrogenation [3] can be employed to release the hydrogen stored in AB. Since the pyrolysis requires extremely high temperatures and only produces 6.5 wt% (1 equiv based on AB) of hydrogen, hydrolytic dehydrogenation is thought to be the more promising process since up to 3 equiv of hydrogen based on AB can be obtained under mild reaction conditions with suitable catalysts. Therefore, dehydrogenation of ammonia borane—an excellent reservoir of H$_2$, is one bright strategy that can release three equimolar H$_2$ from each molecule of ammonia borane in the existence of a photocatalyst without any gaseous side products [16,17].

Precious noble metal nanoparticles (NPs) are one of the most widely studied catalytic materials in H$_2$ production from AB owing to their outstanding catalytic characteristics [18,19]. The synthesis of

catalysts based on earth-abundant and less expensive first-row transition metals, such as Cu, has received a lot of interest to boost catalytic activity while reducing the usage of pricey noble metal NPs [18,20]. Metal NPs require a catalyst support to enhance their stability and catalytic activity. Unique catalytic activities may be achieved by using appropriate supports, such as metal oxides (e.g., TiO_2), mesostructured materials, polymers, and carbon materials, which retain site isolation of active NPs from aggregation and synergistic effects owing to robust metal-support interaction.

Layered titanates are unique in the structure and reactivity to reach a set of new nanoarchitectures and sometimes to a specific type of heterostructure that can be a promising photocatalyst for energy carrier generation [21–23]. These versatile layered titanates in interconversion to a new structure can sometimes lead to serendipity in finding a new structure of titania which usually has either a rutile or anatase structure [24–26]. In such cases, the obtained new structure can adopt defect, vacancy, doped species, and a heterostructure or a pure crystal phase (e.g., anatase or rutile) but a new nanoshape [23,25,27–29]. The interconversion can simply occur by changing the media's pH by adding an acid or an alkaline species (*e.g.*, quaternary alkylammonium hydroxide solutions) at room temperature or under solvothermal conditions [30,31]. Furthermore, the layered titanates have a high potential for cation exchange, and this can lead to an opportunity to create hybrid heterostructures with new and tunable structures which may have better interface [32–35].

So far, some metal oxides structures have been proposed as (photo)catalysts for H_2 production from ammonia borane [36–41]. Since this ammonia borane can act as a reducing agent, exposing the metal oxide to the solution of ammonia borane may cause considerable structural changes until the structure reaches a stable form under the reaction conditions. However, despite this altering feature of the ammonia borane, there is no report to study the structural evolution of the (photo)catalyst once the photocatalyst is being treated with the ammonia borane.

4.2   Chapter scope

In this chapter, we have used the interconversion strategy to interconvert the Cu-loaded layered titanates to CuO-loaded titania (CuO-TiO_2) with anatase crystal structure as visible-range photocatalyst (**Scheme 4.1**) for H_2 generation from ammonia borane. We carefully studied the structural evolution of

the photocatalyst by UV-vis spectroscopy, transmission electron microscopy (TEM) once the photocatalyst photocatalyzed the reaction. We found that the CuO nanostructures are unstable in the solution media of ammonia borane and convert to metallic Cu and photocatalyzes the reaction through its in situ-obtained plasmonic features, leading to the enhancement in the photocatalytic activity in the visible range. However, the titania structure was stable throughout the reaction.
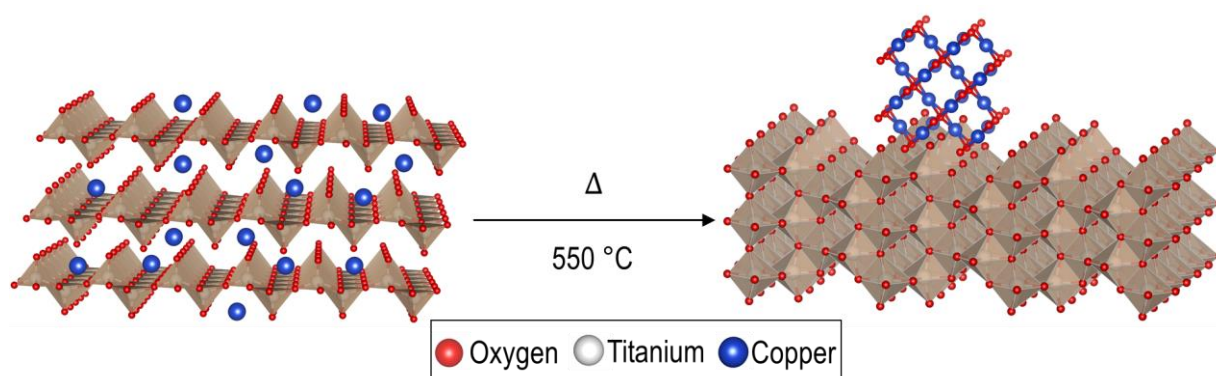
Scheme 4.1. *Graphical representation for the interconversion of Cu-loaded layered titanate to CuO-loaded anatase TiO$_2$.*

4.3   Experimental details

4.3.1   Materials

All reagents and solvents were purchased commercially and used as received. *N,N*-dimethylformamide (DMF, 99.8%), titanium (IV) butoxide (TBOT, 97%), and P25 were purchased from Sigma-Aldrich. Isopropyl alcohol (IPA, 99.8%) was purchased from Chameleon. Copper (II) nitrate trihydrate (99.9%) was purchased from Wako.

4.3.2   Preparation of layered protonated titanate (LPT) precursor

LPT precursor was prepared by the solvothermal reaction reported in our previous work [42]. 25 ml of IPA was mixed with 8.3 ml of DMF. TBOT (0.83 ml) was then added to this mixture. The solution was then transferred to a stainless-steel autoclave lined with Teflon and held at 200°C for 24 hours. The precipitate was recovered by centrifugation at 3500 rpm for 10 minutes after the autoclave had cooled, washed with ethanol multiple times, and dried at 60°C to obtain LPT.

4.3.3 Synthesis of photocatalyst

For the synthesis of a pure TiO_2, the precursor (LPT) was calcined in air at 550 ℃ in an alumina crucible for 2 h at a heating rate of 2 ℃ min^{-1}. To obtain Cu-loaded TiO_2 samples, LPT was first stirred at 800 rpm with different weight ratios of $Cu(NO_3)_2.3H_2O$ for 4 hours to enable cation-exchange reaction. LPT containing Cu^{2+} in the structure was then separated and dried at 60 ℃ overnight. Finally, the obtained Cu^{2+}/LPT was calcined in air at 550℃ in an alumina crucible for 2 h at a heating rate of 2 ℃ min^{-1}. Likewise, a control sample, Cu-loaded P25, was prepared by mixing P25 nanopowder with $Cu(NO_3)_2.3H_2O$ solution.

4.3.4 Characterization

A Rigaku SmartLab diffractometer was used to collect powder X-ray diffraction (XRD) data, with Cu K radiation at 40 kV and 30 mA at a scan rate of 1 min^{-1}. An Agilent 5800 was used to perform inductively coupled plasma optical emission spectroscopy (ICP-OES). A PHI Quantera SXM equipment was used to perform X-ray photoelectron spectroscopy (XPS) using Al K radiation at 20 kV and 5 mA. The C1s level at 285.0 eV was used to calibrate the binding energy shift. A Hitachi SU-8230 microscope operating at 10.0 kV was used to observe field emission scanning electron microscopy (FE-SEM) pictures. A JEOL JEM-2100F was used to obtain transmission electron microscope (TEM) pictures at a voltage of 200 kV. A JASCO V-570 spectrophotometer was used to record UV-vis diffusion reflectance spectra (UV-DRS).

4.3.5 Hydrogen production from ammonia borane (AB)

Separately, an AB solution (20 μmole) was deaerated for 30 minutes using Ar bubbling. In a Pyrex glass test tube (34 mL), 5 mg of the powder was dispersed in 4.9 ml water, and the solution was also deaerated by Ar bubbling for 30 minutes before being sealed with a silicone rubber septum. After that, a glass syringe was used to add 0.1 ml of the AB to the dispersion, which was then irradiated with a UV cut-off filter (> 420nm, AM1.5 Solar simulator, San-Ei Electric Co., Ltd.) while stirring. A Shimadzu GC-2010 plus gas chromatograph with a BID detector was used to measure the evolved H_2 in the headspace.

4.4   Results and Discussion

4.4.1   Structural characterizations

TiO_2 nanosheets containing various amounts of Cu^{2+} ions (denoted here as X%-TiO_2, where X = wt% Cu) were successfully synthesized using a simple cation-exchange reaction followed by calcination at 550 °C in air. ICP-OES analysis confirmed that the Cu loading in the X%-TiO_2 nanosheets was almost the same as the loaded amount in the cation-exchange step (**Table 4.1**).

Table 4.1. *The loaded Cu content on different samples as measured by ICP-OES.*

Sample	Measured element	Cu content (wt %)
TiO_2	Cu	0
1.2%Cu-TiO_2	Cu	1.2
3.4%Cu-TiO_2	Cu	3.4
5.4%Cu-TiO_2	Cu	5.4

XRD patterns of pure TiO_2 nanosheets and X%-TiO_2 nanosheets are presented in **Figure 4.1a**. The XRD pattern of pure TiO_2 matches that of the tetragonal anatase phase (JCPDS 21-1272). The crystal structure of TiO_2 was not changed by modification with low weight ratios of Cu (e.g., X = 1.2% or 3.4%), showing only the characteristic peaks of the anatase TiO_2 phase (**Figure 4.1a**). The results revealed these samples to maintain a pure anatase structure but with Cu doped in the anatase TiO_2 lattice [43]. Other authors have concluded that signals related to Cu species might not have been possible to detect due to their small size or the lower loading of Cu in the samples in question [44]. For 5.4%Cu-TiO_2, the XRD pattern shows an extra peak around 2θ = 35.5° ((002) plane, JCPDS 80-1917), indicating the coexistence of the CuO phase with TiO_2 (**Figure 4.1a**).
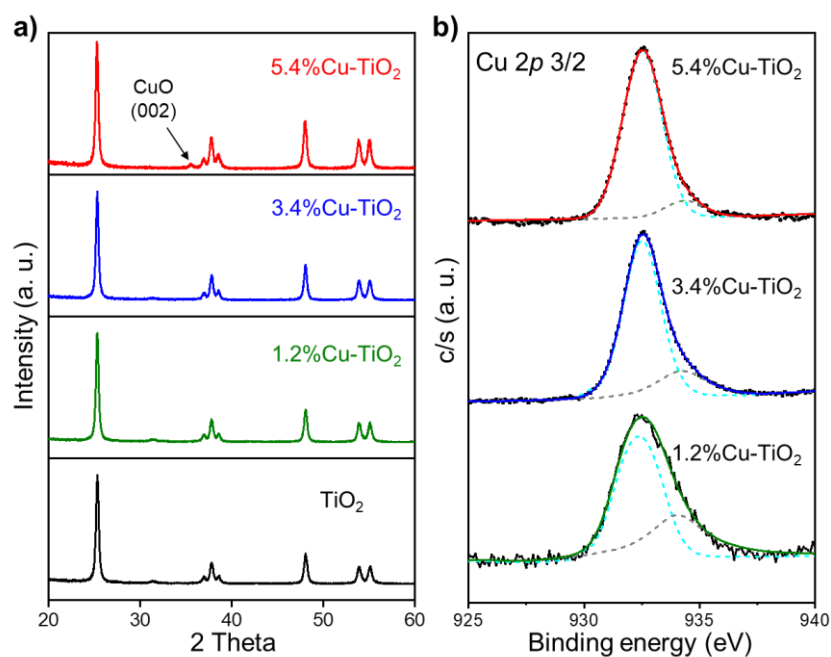
Figure 4.1. a) XRD patterns and b) Cu 2p XPS core-level spectra of pure TiO_2 and X%Cu-TiO_2 (X = 1.2, 3.4, and 5.4) nanosheets.

The chemical bonding of the Cu, Ti, and O elements in pure TiO_2 and X%-TiO_2 nanosheets was examined using XPS. **Figure 4.1b** shows the high-resolution Cu $2p3/2$ core-level photoelectron spectra of Cu-TiO_2 samples. The Cu $2p$ 3/2 core-level XPS peak observed at ca. 932.5 eV exists in all Cu/TiO_2 samples as the major peak—more likely Cu^+. However, XRD results (**Figure 4.1a**) and UV-Vis spectra (**Figure 4.5a**) exhibit Cu^{2+} as the major species. The fact that a large portion of surface Cu^{2+} can be reduced to Cu^+ under high-vacuum conditions and photoelectron beam during XPS measurement can be the main reasons for finding Cu^+ as the major fraction in XPS observation [45,46]. As shown in **Figure 4.2a**, high-resolution XPS core-level spectra of Ti $2p3/2$ and Ti $2p1/2$ of pristine TiO_2 are observed at 458.96 and 464.70 eV, respectively, assigned to the presence of typical Ti^{4+}. In contrast, Cu-loaded TiO_2 samples showed slightly lower binding energy after Cu^{2+} loading, agreeing with previous studies [47,48]. The O $1s$ peak of pure TiO_2 and Cu-loaded samples was deconvoluted into two peaks (**Figure 4.2c**). The lower binding energy peak around 530.23 eV is assigned to the lattice oxygen of the anatase structure of TiO_2, while the other peak at 531.52 eV is attributed to surface OH groups [47–49].
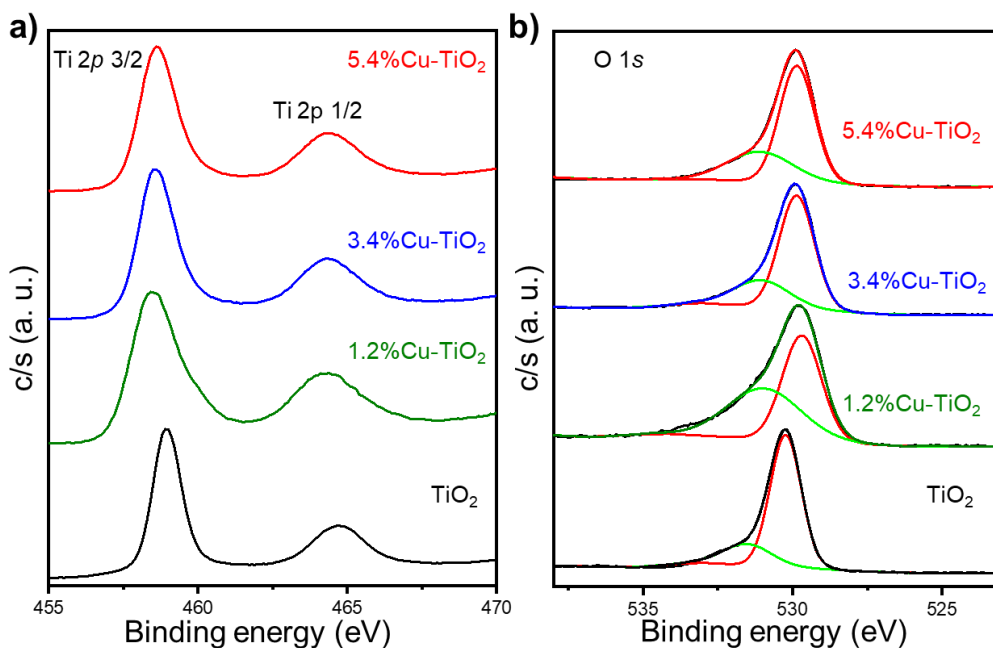
Figure 4.2. a) Ti 2p and b) O 1s XPS core-level spectra of TiO$_2$ and X%Cu-TiO$_2$ (X=1.2, 3.4, and 5.4).

4.4.2 Morphological characterizations

The morphology of pure TiO$_2$ and 5.4%-TiO$_2$ was observed by SEM and TEM. The pure TiO$_2$ is shown to take the form of a spherical nanosheet assembly composed of anatase nanoparticles (**Figure 4.3a**). The SEM and TEM micrographs shown in **Figure 4.3b** additionally confirm that the 5.4%-TiO$_2$ sample, which is shown below to have the highest hydrogen production activity from ammonia–borane (AB), retains its original TiO$_2$ morphology after the Cu loading process.
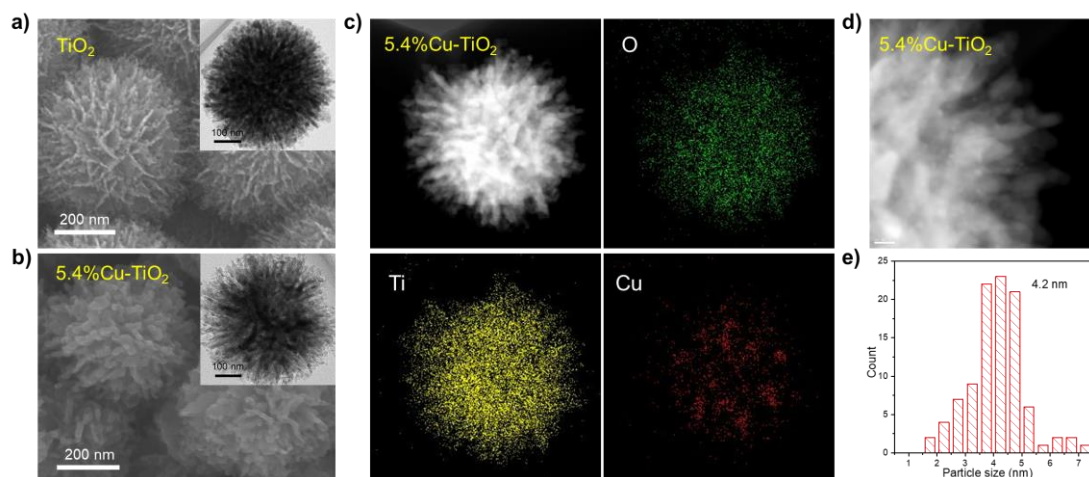
Figure 4.3. *a) SEM and TEM (inset) micrographs of pure TiO₂ nanosheets and b) SEM and TEM (inset) images, c) STEM image and corresponding EDX mapping and d) high-magnification STEM image, and e) particle size distribution of 5.4%Cu-TiO₂ nanosheets.*

The presence and distribution of Cu species within TiO$_2$ nanosheets in the 5.4%Cu-TiO$_2$ sample is difficult to characterize using SEM and TEM imaging due to their small size. We therefore performed STEM and corresponding EDX mapping analyses, presented in **Figure 4.3c**, demonstrating the uniform distribution of CuO nanoparticles inside the TiO$_2$ nanosheets. Furthermore, the average particle size of CuO NPs was estimated to be 4.2 nm (**Figure 4.3d, e**). EDX elemental analysis results that confirm the presence of Cu species in TiO$_2$ nanosheets are shown in **Figure 4.4**.
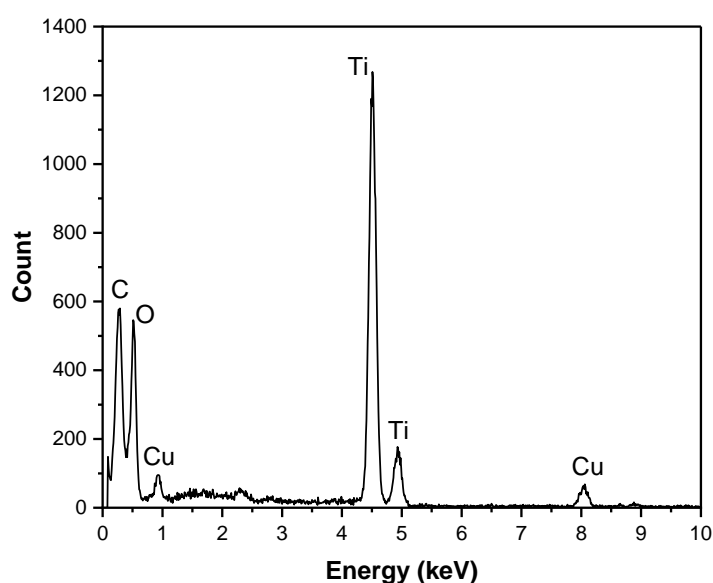
Figure 4.4. *EDX elemental analysis of 5.4%Cu-TiO₂.*

4.4.3 Optical properties

Doping with transition metal ions, including Cu, normally modifies the optical absorption of TiO_2 materials. **Figure 4.5a** shows UV–Vis diffuse reflectance spectra of pure TiO_2 and the X%Cu-TiO_2 nanosheets. Pure TiO_2 nanosheets exhibited absorption only in the UV region ($\lambda < 400$ nm) due to the typical bandgap transition of TiO_2. From the Tauc plot (**Figure 4.5b**) plotted using the UV–Vis data, the bandgap energy of pure TiO_2 nanosheets was calculated to be 3.14 eV, consistent with the typical bandgap value of TiO_2.

Furthermore, the UV–Vis spectra of all the modified samples reveal, in addition to the bandgap transition in the UV region, increased absorption in the visible region. The 1.2% and 3.4%Cu-TiO_2 samples exhibited two additional absorption features. That in the 650 - 850 nm range indicates d–d transitions of Cu^{2+} ions [50,51], and the other in the 400 - 550 nm range partly overlaps the main bandgap transition and is ascribed to charge transfer from the valence band (O 2p) of TiO_2 to Cu^{2+} levels [52,53]. The powerful light absorption in both the UV and visible regions that appears for the 5.4%Cu-TiO_2 sample, with bandgap narrowing (**Figure 4.5b**), clearly indicates the coupling of TiO_2 with CuO [54], consistent with the XRD results (**Figure 4.1a**). The superior light absorption ability of the X%Cu-TiO_2 nanosheets, particularly the 5.4%Cu-TiO_2 sample, is expected to enhance catalytic activity under visible light (to be detailed below).
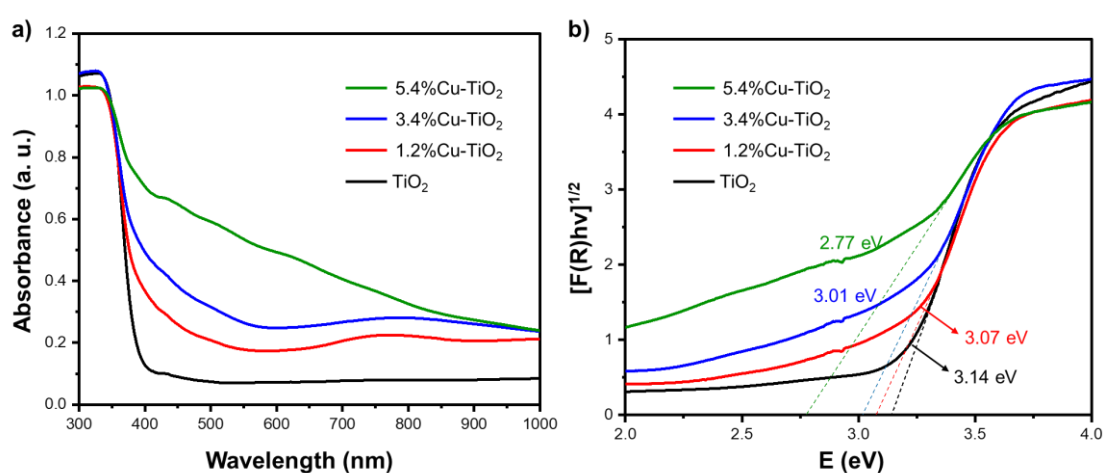
***Figure 4.5**. a) UV–Vis spectra and b) the corresponding Tauc plot of pure TiO_2 and X%Cu-TiO_2 (X = 1.2, 3.4, and 5.4)*

4.4.4 *Photocatalytic hydrolysis of ammonia–borane (AB)*

The photocatalytic activity of H_2 production from AB is shown in **Figure 4.6a**. The stored H_2 in AB can be released via hydrolysis pathways, in which H_2 is generated stoichiometrically in a 3:1 (H_2/AB) molar ratio, as shown in **Equation (4.1)**.

$$NH_3-BH_3 + 2H_2O \rightarrow 3H_2 + NH_4^+ + BO_2^- \qquad\qquad (\mathbf{4.1})$$
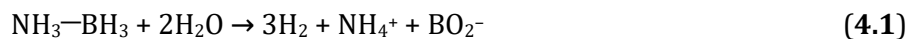
As shown in **Figure 4.6a**, pure TiO_2 photocatalyst showed no activity towards AB hydrolysis under visible light irradiation owing to its wide bandgap energy (3.14 eV, **Figure 4.5b**). However, all the Cu-loaded TiO_2 samples exhibited a considerable improvement under visible light irradiation ($\lambda >$ 420 nm), demonstrating the essential role that Cu species play in catalyzing the hydrolytic dehydrogenation of AB. As expected, the 5.4%Cu-TiO_2 photocatalyst appears to be the best in the Cu-loaded TiO_2 series, producing the exact equivalent amount of H_2 to AB (3 mol of H_2/mol of AB) within only 15 min of reaction. The hydrolysis of AB using the 5.4%Cu-TiO_2 sample, which is shown to have the best photocatalytic activity, was also examined under dark conditions. In contrast to its H_2 production under visible light (3 mol H_2/mol AB, 15 min), the same amount of H_2/mole AB could be produced under dark conditions after 35 min (**Figure 4.6b**), which indicates the accelerating influence of visible light irradiation on the catalytic hydrolysis of AB.
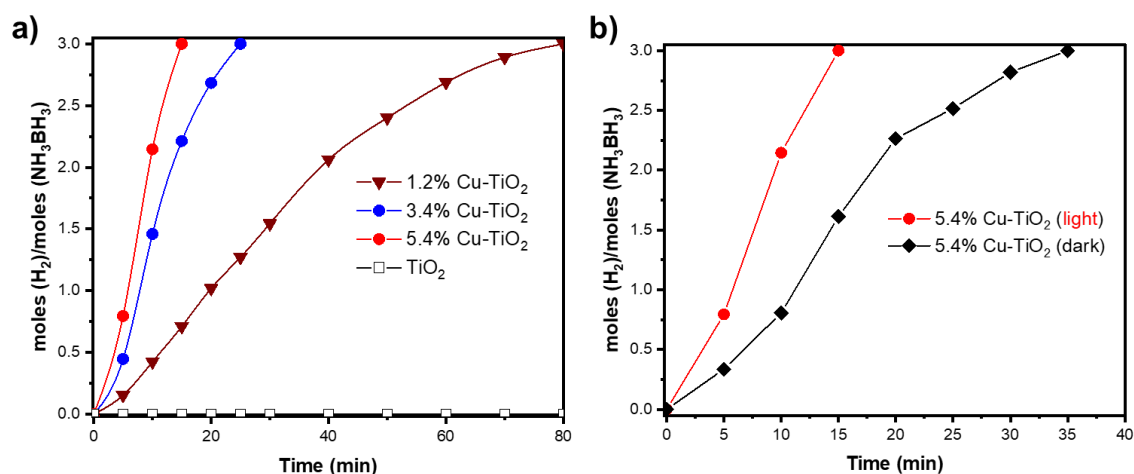
Figure 4.6. *a) Hydrogen evolution profile of TiO₂, 1.2%Cu-TiO₂, 3.4%Cu-TiO₂, and 5.4%Cu-TiO₂ under visible light (λ > 420 nm), b) hydrogen evolution profile of 5.4%Cu-TiO₂ under visible light (red line) and dark (black line) conditions.*

We further studied the reaction mechanism by characterizing the recovered catalyst (Re5.4%Cu-TiO$_2$) using XRD and UV-Vis analyses. As shown in **Figure 4.7a**, the XRD peak related to CuO (002) has disappeared in the Re5.4%Cu-TiO$_2$ product, and a new peak related to metallic Cu (111) is observed. The UV–Vis spectra (**Figure 4.7b**) of Re5.4%Cu-TiO$_2$ exhibited a surface plasmon resonance (SPR) absorption band around 630 nm, which is a significant feature of metallic Cu nanoparticles (NPs) [55]. These results confirmed the formation of Cu NPs during the photocatalytic dehydrogenation of AB. The recovered catalyst maintains the original morphology of TiO$_2$ nanosheets (**Figure 4.7c**), confirming its stability after the photocatalytic reaction.
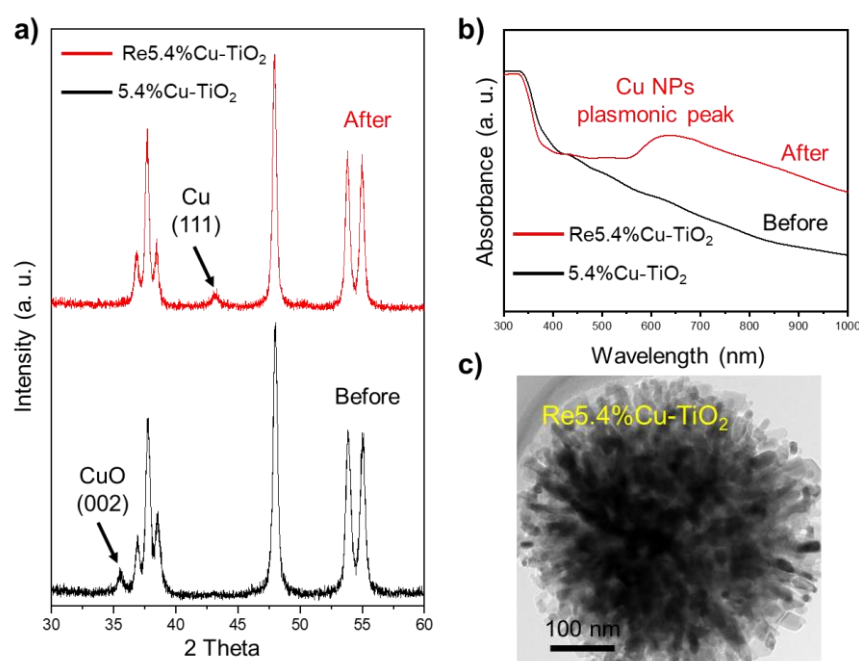
***Figure 4.7**. a) XRD patterns, b) UV–Vis spectra of 5.4%Cu-TiO$_2$ before and after photocatalytic decomposition of AB, and c) TEM micrograph of the recovered sample after the photocatalytic reaction.*

It is therefore of note that the CuO species in the 5.4%Cu-TiO$_2$ sample transform to metallic Cu NPs while located in the TiO$_2$ nanosheets matrix (**Scheme 4.2**). This phenomenon occurs in the presence of AB, since aside from its H$_2$ storage property, AB can also act as a strong reducing agent [56].
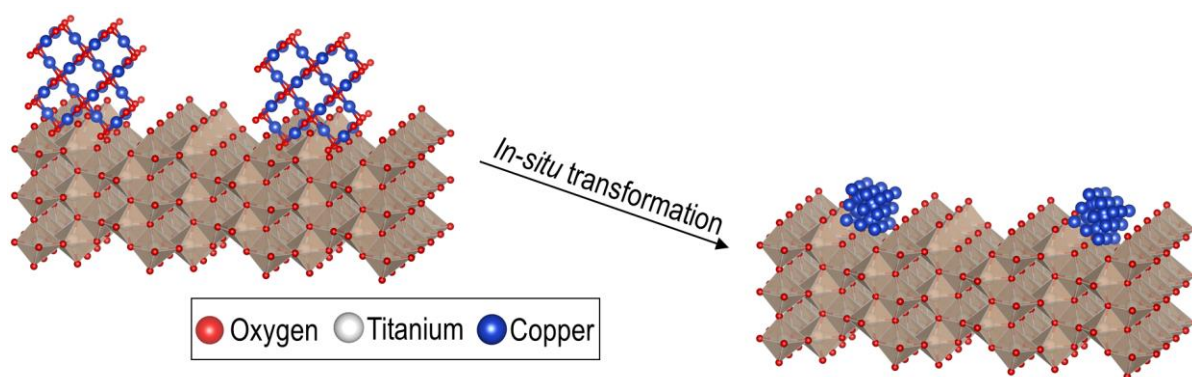
Scheme 4.2. *Schematic illustration for the in-situ transformation of CuO species into metallic Cu NPs while located in the TiO$_2$ nanosheets matrix.*

Previous reports have suggested the mechanism for the dehydrogenation of AB under dark conditions to include the adsorption of AB on the metallic NPs to form an activated complex species, followed by the dissociation of the B−N bond under attack by H$_2$O molecules; the hydrolysis of the resulting BH$_3^-$ gives an intermediate that generates H$_2$ [57,58]. We concluded that the formation of plasmonic Cu NPs is the critical component in the improved photocatalytic activity seen under light. As shown in **Scheme 4.3**, When the catalytic system is induced by visible light, electron-hole pairs are generated in Cu NPs by the effect of SPR. Photogenerated electrons of metallic Cu NPs can be easily injected into the CB of TiO$_2$ (hot electron injection) [59–62] to form a highly nucleophilic surface. On the other side, photogenerated holes are kept on the Cu NPs' side, forming a highly electrophilic surface. An unbalanced charged surface is created by this sensitized structure and significantly accelerates the dehydrogenation of AB. As for the mechanism of the dehydrogenation of AB (mentioned above), we note that when the attack by an H$_2$O molecule dissociates the B−N bond, the NH$_3^+$ might react with electrons (e$^-$) located on the CB of TiO$_2$, as described in **Equation 4.2.** In contrast, the hydrolysis of the BH$_3^-$ may occur spontaneously on the hole (h$^+$) site of Cu NPs, as described in **Equation 4.3.**

$$NH_3^+ + H_2O + e^- \rightarrow NH_4OH \qquad\qquad\qquad (\textbf{4.2})$$

$$BH_3^- + 2H_2O + h^+ \rightarrow 3H_2 + HBO_2 \qquad\qquad\qquad (\textbf{4.3})$$
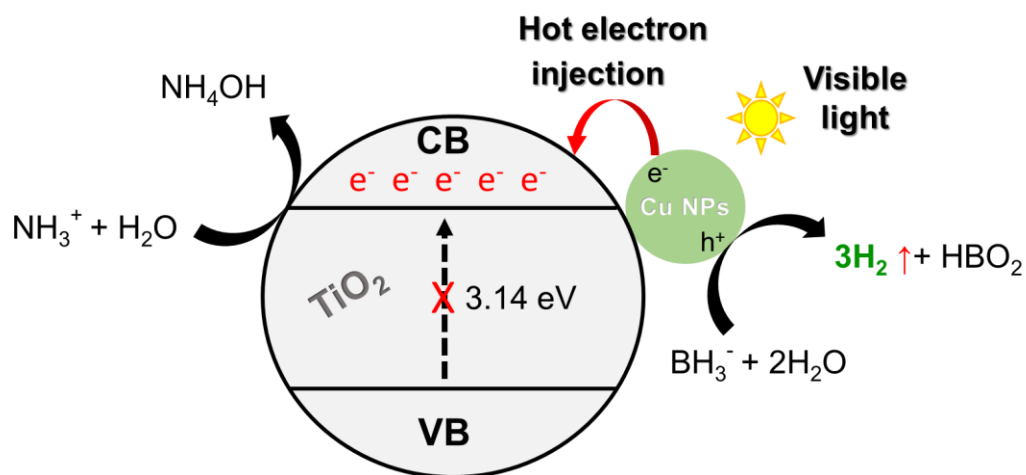
Scheme 4.3. *Proposed mechanism of H$_2$ production from ammonia–borane using 5.4%Cu–TiO$_2$ under visible light irradiation.*

The stability of the 5.4%Cu-TiO$_2$ photocatalyst was also examined for hydrogen generation from AB under visible light irradiation (**Figure 4.8**). After five cycles, it continued to show stable photocatalytic hydrogen evolution activity, with no significant degradation of the initial activity. These results demonstrate the durability of the material for visible light-driven photocatalytic hydrogen generation from AB. The prolonged durability of the catalyst might be credited to the fact that the ultrafine Cu species have been efficiently distributed and trapped between the TiO$_2$ nanosheet layers, reducing the tendency of Cu nanoparticles to aggregate.
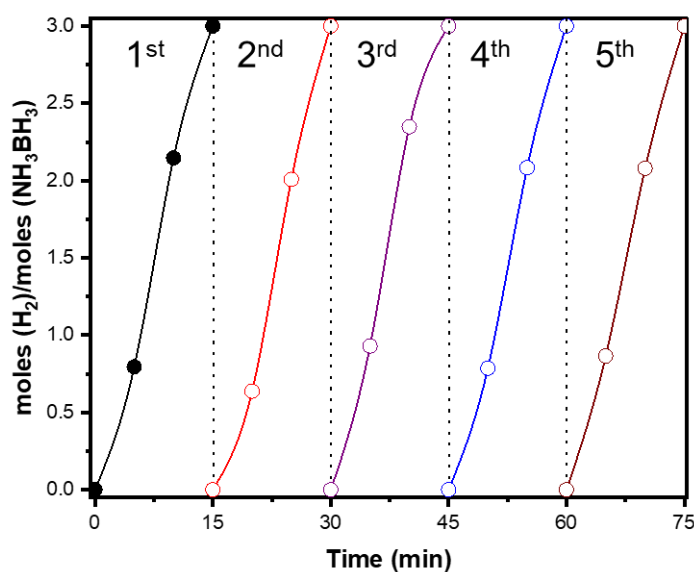
Figure 4.8. *Recycled hydrogen evolution for 75 h of 5.4%Cu-TiO$_2$.*

We further investigated the influence of the excitation wavelength on the hydrogen production activity to emphasize the contribution of the plasmonic Cu NPs to the reaction. As depicted in **Figure 4.9**, the hydrogen production activity depends upon the absorption band of the catalyst in the visible light region (> 420 nm), and the higher activity occurs at 650 nm (compared to the other studied wavelengths) where the λ_{max} of the Cu(0) locates. This photocatalytic dependence on the Cu(0)'s absorption band provides evidence of the abovementioned photocatalytic mechanism in which Cu(0) species play a dominant role in the enhanced photocatalytic efficiency.
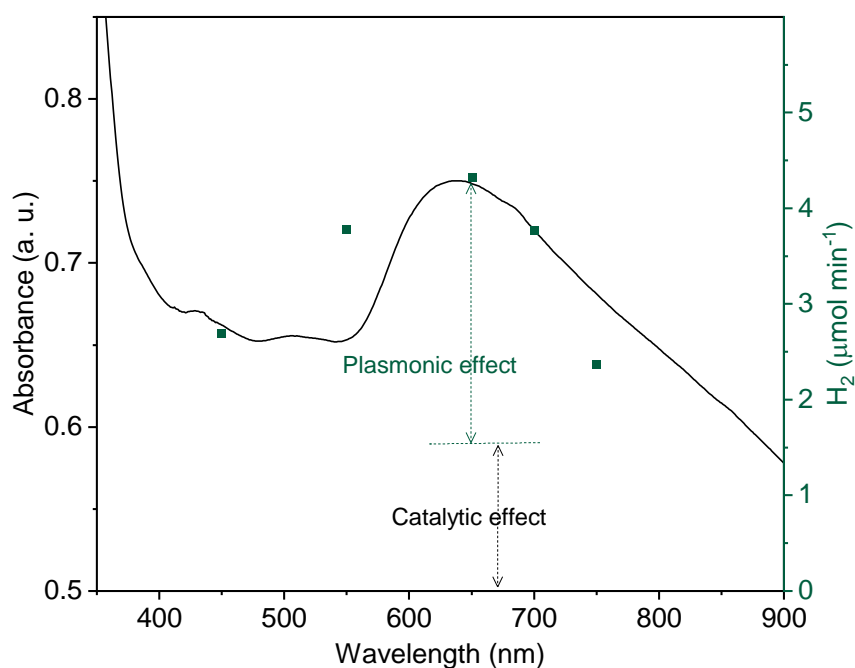
Figure 4.9. *Dependence of the hydrogen production from ammonia borane on the excitation wavelength.*

Finally, we prepared CuO-P25 as a reference sample by the present synthetic method using P25, a benchmark TiO_2 photocatalyst, with $Cu(NO_3)_2$. P25 was not capable to adsorb Cu^{2+} ions effectively like LPT. We found out that under identical conditions, P25 can only adsorb 1 wt% Cu ions from an equal solution of 10 wt% of Cu^{2+} ions, showing its low cation exchange ability compared with the starting layered titanate (**Figure 4.10a**). In addition to the excellent cation exchange ability of layered titanates, the nanosheets can also contribute to enhancing the light absorption properties, improving the photocatalytic activity. Therefore, the hydrogen evolution from AB using Cu-P25-550 was insignificant compared to that of Cu-LPT-550. After 80 minutes, it is even unable to produce the exact equivalent amount of H_2 to AB (3 mol of H_2/mol of AB) (**Figure 4.10b**). These results show the advantages of the present material design for providing both ion exchange and photocatalytic features, which can be

beneficial for solving environmental and energy problems, including water purification and green hydrogen production.
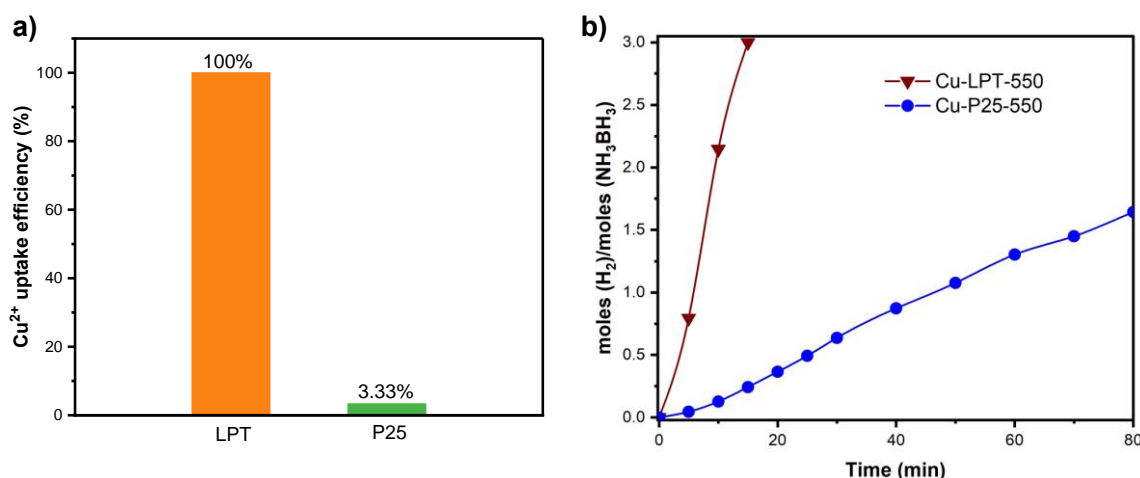
Figure 4.10*. a) Cu^{2+} ion uptake efficiency using LPT and P25, b) hydrogen evolution profile of their calcined products at 550 °C.*

4.5   Summary

In this chapter, we have reported an effective strategy for the interconversion of Cu-loaded layered titanate into CuO-loaded TiO_2 that shows high photocatalytic H_2 production activity from ammonia–borane (AB) under visible light. In the presence of AB, the CuO species readily converted to metallic Cu nanoparticles, since, aside from being an H_2 carrier compound, AB can act as a robust reducing agent. The introduced Cu nanoparticles photocatalyze the reaction through their in-situ-obtained plasmonic features, leading to accelerated photocatalytic hydrogen production under visible light irradiation. We believe that this synthetic method using copper oxide suggests the potential use of other metal oxides from transition metal titanate-based layered materials to give enhanced performance in energy and environmental applications.

4.6   References

[1]   J. Yang, A. Sudik, C. Wolverton, D.J. Siegel, High capacity hydrogen storage materials: attributes for automotive applications and techniques for materials discovery, Chemical Society Reviews. 39 (2010) 656–675.

[2]   H.-L. Jiang, K. Singh, J.-M. Yan, X.-B. Zhang, Q. Xu, Liquid-Phase Chemical Hydrogen Storage: Catalytic Hydrogen Generation under Ambient Conditions, ChemSusChem. 3 (2010) 541–549.

[3]   M. Yadav, Q. Xu, Liquid-phase chemical hydrogen storage materials, Energy & Environmental Science. 5 (2012) 9698–9725.

[4]   K. Mori, M. Dojo, H. Yamashita, Pd and Pd-Ag nanoparticles within a macroreticular basic resin: An efficient catalyst for hydrogen production from formic acid decomposition, ACS Catalysis. 3 (2013) 1114–1119.

[5]   K. Mori, P. Verma, R. Hayashi, K. Fuku, H. Yamashita, Color-Controlled Ag Nanoparticles and Nanorods within Confined Mesopores: Microwave-Assisted Rapid Synthesis and Application in Plasmonic Catalysis under Visible-Light Irradiation, Chemistry – A European Journal. 21 (2015) 11885–11893.

[6]   J.K. Stolarczyk, S. Bhattacharyya, L. Polavarapu, J. Feldmann, Challenges and Prospects in Solar Water Splitting and CO_2 Reduction with Inorganic and Hybrid Nanostructures, ACS Catalysis. 8 (2018) 3602–3635.

[7]   Y. Peng, K. Jiang, W. Hill, Z. Lu, H. Yao, H. Wang, Large-Scale, Low-Cost, and High-Efficiency Water-Splitting System for Clean H_2 Generation, ACS Applied Materials & Interfaces. 11 (2019) 3971–3977.

[8]   E. Doustkhah, M. Hasani, Y. Ide, M.H.N. Assadi, Pd Nanoalloys for H_2 Generation from Formic Acid, ACS Applied Nano Materials. 3 (2019) 22–43.

[9]   Q. Wang, K. Domen, Particulate Photocatalysts for Light-Driven Water Splitting: Mechanisms, Challenges, and Design Strategies, Chemical Reviews. 120 (2019) 919–985.

[10] H. El-Hosainy, R. Tahawy, M. Esmat, M. El-Kemary, Y. Ide, Immobilization of Iron Minerals on a Layered Silicate for Enhancing its Solar Photocatalytic Activity toward H_2 Production, Frontiers in Energy Research. 9 (2021) 83.

[11] S.Z. Tóth, I. Yacoby, Paradigm Shift in Algal H_2 Production: Bypassing Competitive Processes, Trends in Biotechnology. 37 (2019) 1159–1163.

[12] Y. Ma, X. Wang, Y. Jia, X. Chen, H. Han, C. Li, Titanium Dioxide-Based Nanomaterials for Photocatalytic Fuel Generations, Chemical Reviews. 114 (2014) 9987–10043.

[13] A. Staubitz, A.P.M. Robertson, I. Manners, Ammonia-Borane and Related Compounds as Dihydrogen Sources, Chemical Reviews. 110 (2010) 4079–4124.

[14] E.K. Abo-Hamed, T. Pennycook, Y. Vaynzof, C. Toprakcioglu, A. Koutsioubas, O.A. Scherman, Highly Active Metastable Ruthenium Nanoparticles for Hydrogen Production through the Catalytic Hydrolysis of Ammonia Borane, Small. 10 (2014) 3145–3152.

[15] A. Gutowska, L. Li, Y. Shin, C.M. Wang, X.S. Li, J.C. Linehan, R.S. Smith, B.D. Kay, B. Schmid, W. Shaw, M. Gutowski, T. Autrey, Nanoscaffold Mediates Hydrogen Release and the Reactivity of Ammonia Borane, Angewandte Chemie. 117 (2005) 3644–3648.

[16] E. Doustkhah, S. Rostamnia, N. Tsunoji, J. Henzie, T. Takei, Y. Yamauchi, Y. Ide, Templated synthesis of atomically-thin Ag nanocrystal catalysts in the interstitial space of a layered silicate, Chemical Communications. 54 (2018) 4402–4405.

[17] C. Yüksel Alpaydın, S.K. Gülbay, C. Ozgur Colpan, A review on the catalysts used for hydrogen production from ammonia borane, International Journal of Hydrogen Energy. 45 (2020) 3414–3434.

[18] C.D. Mboyi, J. Roger, K. Fajerwerg, M.L. Kahn, J.-C. Hierso, C.D. Mboyi, D. Poinsot, J. Roger, J.-C. Hierso, K. Fajerwerg, M.L. Kahn, The Hydrogen-Storage Challenge: Nanoparticles for Metal-Catalyzed Ammonia Borane Dehydrogenation, Small. 17 (2021) 2102759.

[19] M. Liu, L. Zhou, X. Luo, C. Wan, L. Xu, Recent Advances in Noble Metal Catalysts for Hydrogen Production from Ammonia Borane, Catalysts 10 (2020 788.

[20] C. Wang, J. Zhao, X. Du, S. Sun, X. Yu, X. Zhang, Z. Lu, L. Li, X. Yang, Hydrogen production from ammonia borane hydrolysis catalyzed by non-noble metal-based materials: a review, Journal of Materials Science. 56 (2021) 2856–2878.

[21] T. (Tip) Sirinakorn, S. Bureekaew, M. Ogawa, Layered Titanates ($Na_2Ti_3O_7$ and $Cs_2Ti_5O_{11}$) as Very High Capacity Adsorbents of Cadmium(II), Bulletin of the Chemical Society of Japan. 92 (2018) 1–6.

[22] T. (Ko) Saothayanun, T. (Tip) Sirinakorn, M. Ogawa, Layered alkali titanates ($A_2Ti_nO_{2n+1}$): possible uses for energy/environment issues, Frontiers in Energy. (2021) 1–25.

[23] E. Doustkhah, M.H.N. Assadi, K. Komaguchi, N. Tsunoji, M. Esmat, N. Fukata, O. Tomita, R. Abe, B. Ohtani, Y. Ide, In situ Blue titania via band shape engineering for exceptional solar H_2 production in rutile TiO_2, Applied Catalysis B: Environmental. 297 (2021) 120380.

[24] H. Yuan, R. Besselink, Z. Liao, J.E. ten Elshof, The swelling transition of lepidocrocite-type protonated layered titanates into anatase under hydrothermal treatment, Scientific Reports 2014 4:1. 4 (2014) 1–6.

[25] D. Mani, R. Tahawy, E. Doustkhah, M. Shanmugam, M. Arivanandhan, R. Jayavel, Y. Ide, A rutile TiO_2 nanobundle as a precursor of an efficient visible-light photocatalyst embedded with Fe_2O_3, Inorganic Chemistry Frontiers. 8 (2021) 4423–4430.

[26] A.H. Zaki, A. El-Shafey, S.M. Moatmed, R.A. Abdelhay, E.F. Rashdan, R.M. Saleh, M. Abd-El Fatah, M.M. Tawfik, M. Esmat, S.I. El-dek, Morphology transformation from titanate nanotubes to TiO_2 microspheres, Materials Science in Semiconductor Processing. 75 (2018) 10–17.

[27] K. Saito, S. Tominaka, S. Yoshihara, K. Ohara, Y. Sugahara, Y. Ide, Room-Temperature Rutile TiO_2 Nanoparticle Formation on Protonated Layered Titanate for High-Performance Heterojunction Creation, ACS Applied Materials and Interfaces. 9 (2017) 24538–24544.

[28] M. Esmat, A.A. Farghali, Samaa.I. El-Dek, M.H. Khedr, Y. Yamauchi, Y. Bando, N. Fukata, Y. Ide, Conversion of a 2D Lepidocrocite-Type Layered Titanate into Its 1D Nanowire Form with Enhancement of Cation Exchange and Photocatalytic Performance, Inorganic Chemistry. 58 (2019) 7989–7996.

[29] Y. Ide, W. Shirae, Hydrothermal Conversion of Layered Niobate $K_4Nb_6O_{17}\cdot 3H_2O$ to Rare Microporous Niobate $K_6Nb_{10.8}O_{30}$, Inorganic Chemistry. 56 (2017) 10848–10851.

[30] M. Ogawa, T. Yoshinao, Intercalation of Alkylammonium Cations into a Layered Titanate in the Presence of Macrocyclic Compounds, Chemistry of Materials. 11 (1998) 30–32.

[31] F. Kishimoto, Y. Takamura, S. Nakagawa, Y. Wada, Manipulation of the Magnetic Properties of Co- and Fe-Doped Layered Titanates by Alkyl Ammonium Intercalation, Advanced Materials Interfaces. 3 (2016) 1600509.

[32] N. Li, L. Zhang, Y. Chen, M. Fang, J. Zhang, H. Wang, Highly Efficient, Irreversible and Selective Ion Exchange Property of Layered Titanate Nanostructures, Advanced Functional Materials. 22 (2012) 835–841.

[33] X. Gu, F. Chen, B. Zhao, J. Zhang, Photocatalytic reactivity of Ce-intercalated layered titanate prepared with a hybrid method based on ion-exchange and thermal treatment, Superlattices and Microstructures. 50 (2011) 107–118.

[34] Z. Hong, M. Wei, Layered titanate nanostructures and their derivatives as negative electrode materials for lithium-ion batteries, Journal of Materials Chemistry A. 1 (2013) 4403–4414.

[35] X. Gu, F. Chen, B. Zhao, J. Zhang, Photocatalytic reactivity of Ce-intercalated layered titanate prepared with a hybrid method based on ion-exchange and thermal treatment, Superlattices and Microstructures. 50 (2011) 107–118.

[36] H. Ma, C. Na, Isokinetic Temperature and Size-Controlled Activation of Ruthenium-Catalyzed Ammonia Borane Hydrolysis, ACS Catalysis. 5 (2015) 1726–1735.

[37] H. Liang, B. Zhang, H. Ge, X. Gu, S. Zhang, Y. Qin, Porous TiO_2/Pt/TiO_2 Sandwich Catalyst for Highly Selective Semihydrogenation of Alkyne to Olefin, ACS Catalysis. 7 (2017) 6567–6572.

[38] J. Hu, Z. Chen, M. Li, X. Zhou, H. Lu, Amine-Capped Co Nanoparticles for Highly Efficient Dehydrogenation of Ammonia Borane, ACS Applied Materials and Interfaces. 6 (2014) 13191–13200.

[39] S. Akbayrak, S. Özkar, Magnetically Isolable Pt^0/Co_3O_4 Nanocatalysts: Outstanding Catalytic Activity and High Reusability in Hydrolytic Dehydrogenation of Ammonia Borane, ACS Applied Materials & Interfaces. 13 (2021) 34341–34348.

[40] R. Tahawy, E. Doustkhah, E.S.A. Abdel-Aal, M. Esmat, F.E. Farghaly, H. El-Hosainy, N. Tsunoji, F.I. El-Hosiny, Y. Yamauchi, M.H.N. Assadi, Y. Ide, Exceptionally stable green rust, a mixed-valent iron-layered double hydroxide, as an efficient solar photocatalyst for H_2 production from ammonia borane, Applied Catalysis B: Environmental. 286 (2021) 119854.

[41] E. Doustkhah, S. Rostamnia, B. Zeynizadeh, J. Kim, Y. Yamauchi, Y. Ide, Efficient H_2 Generation Using Thiourea-based Periodic Mesoporous Organosilica with Pd Nanoparticles, Chemistry Letters. 47 (2018) 1243–1245.

[42] M. Esmat, H. El-Hosainy, R. Tahawy, W. Jevasuwan, N. Tsunoji, N. Fukata, Y. Ide, Nitrogen doping-mediated oxygen vacancies enhancing co-catalyst-free solar photocatalytic H_2 production activity in anatase TiO_2 nanosheet assembly, Applied Catalysis B: Environmental. 285 (2021).

[43] K. Bhattacharyya, G.P. Mane, V. Rane, A.K. Tripathi, A.K. Tyagi, Selective CO_2 Photoreduction with Cu-Doped TiO_2 Photocatalyst: Delineating the Crucial Role of Cu-Oxidation State and Oxygen Vacancies, Journal of Physical Chemistry C. (2021).

[44] J. Fernández-Catalá, M. Navlani-García, P. Verma, Á. Berenguer-Murcia, K. Mori, Y. Kuwahara, H. Yamashita, D. Cazorla-Amorós, Photocatalytically-driven H_2 production over Cu/TiO_2 catalysts decorated with multi-walled carbon nanotubes, Catalysis Today. 364 (2021) 182–189.

[45] H. Irie, K. Kamiya, T. Shibanuma, S. Miura, D.A. Tryk, T. Yokoyama, K. Hashimoto, Visible light-sensitive Cu(II)-grafted TiO_2 photocatalysts: Activities and X-ray absorption fine structure analyses, Journal of Physical Chemistry C. 113 (2009) 10761–10766.

[46] Y. te Liao, Y.Y. Huang, H.M. Chen, K. Komaguchi, C.H. Hou, J. Henzie, Y. Yamauchi, Y. Ide, K.C.W. Wu, Mesoporous TiO_2 Embedded with a Uniform Distribution of CuO Exhibit Enhanced Charge Separation and Photocatalytic Efficiency, ACS Applied Materials and Interfaces. 9 (2017) 42425–42429.

[47] X. Zhu, G. Wen, H. Liu, S. Han, S. Chen, Q. Kong, W. Feng, One-step hydrothermal synthesis and characterization of Cu-doped TiO_2 nanoparticles/nanobucks/nanorods with enhanced photocatalytic performance under simulated solar light, Journal of Materials Science: Materials in Electronics 2019 30:14. 30 (2019) 13826–13834.

[48] H.J. Choi, M. Kang, Hydrogen production from methanol/water decomposition in a liquid photosystem using the anatase structure of Cu loaded TiO_2, International Journal of Hydrogen Energy. 32 (2007) 3841–3848.

[49] K. Bhattacharyya, G.P. Mane, V. Rane, A.K. Tripathi, A.K. Tyagi, Selective CO_2 Photoreduction with Cu-Doped TiO_2 Photocatalyst: Delineating the Crucial Role of Cu-Oxidation State and Oxygen Vacancies, The Journal of Physical Chemistry C. 125 (2021).

[50] N.L. Dias Filho, Adsorption of Cu(II) and Co(II) complexes on a silica gel surface chemically modified with 2-mercaptoimidazole, Microchimica Acta 1999 130:4. 130 (1999) 233–240.

[51] G. Colón, M. Maicu, M.C. Hidalgo, J.A. Navío, Cu-doped TiO_2 systems with improved photocatalytic activity, Applied Catalysis B: Environmental. 67 (2006) 41–51.

[52] H. Irie, S. Miura, K. Kamiya, K. Hashimoto, Efficient visible light-sensitive photocatalysts: Grafting Cu(II) ions onto TiO_2 and WO_3 photocatalysts, Chemical Physics Letters. 457 (2008) 202–205.

[53] H. Irie, K. Kamiya, T. Shibanuma, S. Miura, D.A. Tryk, T. Yokoyama, K. Hashimoto, Visible Light-Sensitive Cu(II)-Grafted TiO_2 Photocatalysts: Activities and X-ray Absorption Fine Structure Analyses, Journal of Physical Chemistry C. 113 (2009) 10761–10766.

[54] Y. Liao, Y.Y. Huang, H.M. Chen, K. Komaguchi, C.H. Hou, J. Henzie, Y. Yamauchi, Y. Ide, K.C.W. Wu, Mesoporous TiO_2 Embedded with a Uniform Distribution of CuO Exhibit Enhanced Charge Separation and Photocatalytic Efficiency, ACS Applied Materials and Interfaces. 9 (2017) 42425–42429.

[55] P. Liu, H. Wang, X. Li, M. Rui, H. Zeng, Localized surface plasmon resonance of Cu nanoparticles by laser ablation in liquid media, RSC Advances. 5 (2015) 79738–79745.

[56] Chiara Faverio, M. Fiorenza Boselli, Fabrizio Medici, Maurizio Benaglia, Ammonia borane as a reducing agent in organic synthesis, Organic & Biomolecular Chemistry. 18 (2020) 7789–7813.

[57] Q. Xu, M. Chandra, Catalytic activities of non-noble metals for hydrogen generation from aqueous ammonia–borane at room temperature, Journal of Power Sources. 163 (2006) 364–370.

[58] K. Mori, P. Verma, R. Hayashi, K. Fuku, H. Yamashita, Color-Controlled Ag Nanoparticles and Nanorods within Confined Mesopores: Microwave-Assisted Rapid Synthesis and Application in

Plasmonic Catalysis under Visible-Light Irradiation, Chemistry - A European Journal. 21 (2015) 11885–11893.

[59]   Yang Tian, Tetsu Tatsuma, Mechanisms and Applications of Plasmon-Induced Charge Separation at TiO_2 Films Loaded with Gold Nanoparticles, Journal of the American Chemical Society. 127 (2005) 7632–7637.

[60]   T. Yamaguchi, E. Kazuma, N. Sakai, T. Tatsuma, Photoelectrochemical Responses from Polymer-coated Plasmonic Copper Nanoparticles on TiO_2, Chemistry Letters. 41 (2012) 1340–1342.

[61]   Rupinder Kaur, Bonamali Pal, Plasmonic coinage metal–TiO_2 hybrid nanocatalysts for highly efficient photocatalytic oxidation under sunlight irradiation, New Journal of Chemistry. 39 (2015) 5966–5976.

[62]   K.K. M., B. K., N. G., S. B., V. A., Plasmonic resonance nature of Ag-Cu/TiO_2 photocatalyst under solar and artificial light: Synthesis, characterization and evaluation of H_2O splitting activity, Applied Catalysis B: Environmental. 199 (2016) 282–291.

Chapter 5:
Conclusion

Solar energy is a long-term renewable resource that can meet our energy demands. A semiconductor photocatalysis that can use solar energy received a lot of attention in recent years, due to its capability for targeting environmental concerns while also delivering renewable energy. To promote its real-world application potential, a lot of research has gone into the innovation of a highly efficient semiconductor photocatalyst. Therefore, the semiconductor photocatalyst is considered an excellent prospect for solar energy applications, including energy conversion and environmental remediation. The energy conversion aspect primarily involves hydrogen production, CO_2 reduction, and nitrogen fixation. Furthermore, recent research has found that its environmental remediation applications are more likely to deal with water detoxification (i.e., toxic metals removal) and air purification (i.e., NOx conversion).

Of many possible semiconductor photocatalysts, TiO_2 has appealed to considerable interests in the photocatalysis field due to its high reactivity, excellent stability, nontoxicity, low cost, and suitable electronic band structure for many chemical reactions. TiO_2 was the first semiconductor to be reported as a photocatalyst back in 1972, and it has been well investigated and applied for addressing many energy and environmental issues.

In this thesis, layered titanates have been used as a unique and reactive structure to reach out to a set of new nanoarchitectures that provided promising photocatalysts for photocatalytic fuel generation and environmental remediation. This process includes the structural conversion of layered titanates into new structures (e.g., anatase TiO_2) or morphologies (e.g., nanowires) using simple solvothermal reactions.

In such cases, the obtained new structures adopt defect, vacancy, and/or doped species that could be useful for effective photocatalytic hydrogen production activity. In this regard, we have reported, in chapter 2, the topochemical conversion of layered titanates to anatase TiO_2 with both

nitrogen dopant and oxygen vacancy (Vo). The introduction of such Vo in TiO_2 (i.e., defective TiO_2) was found to be an alternate technique for achieving efficient co-catalyst-free photocatalytic hydrogen production activity. The defective TiO_2 photocatalyst was successfully synthesized by the calcination of mesoporous spherical assemblies of layered titanate nanosheets. Under simulated solar light irradiation, this material exhibits remarkable co-catalyst-free solar photocatalytic activity for hydrogen evolution via water splitting (>1.0 mmol g^{-1} h^{-1} and 21% apparent quantum yield at 350 nm), which is significantly higher than that of typical co-catalyst-free defective TiO_2 materials (~0.3 mmol g^{-1} h^{-1}). Enhancing the photocatalytic activity was explained by its Vo-induced high charge separation efficiency. The morphological nature of the material may also partake in raising the photocatalytic activity through providing a high surface area and improving the light absorption properties.

Moreover, converting layered titanates from 2D layered structure to 1D nanowire structure was succeeded in the third chapter using a simple solvothermal reaction. This structural transformation led to accelerated cation exchange ability and enhanced charge separation efficiency of layered titanate. The 1D nanowire structure of layered titanates, therefore, exhibited ultrafast removal/photoreduction of toxic Cd^{2+} cations in water, which cannot be achieved by a benchmark TiO_2 (P25) photocatalyst and even state-of-the-art cation exchangers. Importantly, the nanowires employed in the photoreduction process were readily recovered from the aqueous solution by decantation. Thus, we believe that the 1D nanostructure reported here can be used for the safe capture and disposal of toxic metal cations and recovery of valuable metals from the environment.

Furthermore, the layered titanates have a high potential for cation exchange, and this can lead to an opportunity to create hybrid heterostructures with new and tunable structures which may have a better photocatalytic performance. In the fourth chapter, we succeeded in using the cation exchange strategy to prepare Cu titanates and then the conversion strategy to convert the Cu titanates to CuO-TiO_2 with an anatase crystal structure as visible-range photocatalyst for H_2 generation from ammonia borane ($NH_3 \cdot BH_3$; AB). We examined the *in-situ* structural conversion of the CuO-TiO_2 during photocatalytic hydrogen generation from AB under visible light and studied the impact of the reaction media and of photoirradiation on the catalyst's final structure. The results revealed that the CuO

nanoparticles converted to metallic Cu nanoparticles, photocatalyzing the reaction through their *in-situ*-formed plasmonic features.

Finally, we hope these studies will open doors to discover very reactive nano-architected materials for application in different photocatalytic reactions. We also believe that the structural conversion and engineering strategies reported in this thesis can be expanded to generate additional TiO_2 and titanate-based photocatalysts with better performance for countering energy and environmental problems.

List of publications

2019

(1) **Esmat, M.**; Farghali, A. A.; El-Dek, S. I.; Khedr, M. H.; Yamauchi, Y.; Bando, Y.; Fukata, N.; Ide, Y. Conversion of a 2D Lepidocrocite-Type Layered Titanate into Its 1D Nanowire Form with Enhancement of Cation Exchange and Photocatalytic Performance. *Inorganic Chemistry* 2019, *58* (12), 7989–7996.

(2) Doustkhah, E.; Najafi Zare, R.; Yamauchi, Y.; Taheri-Kafrani, A.; Mohtasham, H.; **Esmat, M.**; Ide, Y.; Fukata, N.; Rostamnia, S.; Sadeghi, M. H.; Assadi, M. H. N. Template-Oriented Synthesis of Hydroxyapatite Nanoplates for 3D Bone Printing. *Journal of Materials Chemistry B* 2019, *7* (45), 7228–7234.

2020

(3) **Esmat, M.**; Mohtasham, H.; Gadelhak, Y.; Mehrebani, R. T.; Tahawy, R.; Rostamnia, S.; Fukata, N.; Khaksar, S.; Doustkhah, E. 2D Mesoporous Channels of PMO; a Platform for Cluster-like Pt Synthesis and Catalytic Activity in Nitrophenol Reduction. *Catalysts* 2020, *10* (2).

(4) Abdelaal, H. M.; Shaikjee, A.; **Esmat, M.** High Performing Photocatalytic ZnO Hollow Sub-Micro-Spheres Fabricated by Microwave Induced Self-Assembly Approach. *Ceramics International* 2020, *46* (12), 19815–19821.

2021

(5) **Esmat, M.**; El-Hosainy, H.; Tahawy, R.; Jevasuwan, W.; Tsunoji, N.; Fukata, N.; Ide, Y. Nitrogen Doping-Mediated Oxygen Vacancies Enhancing Co-Catalyst-Free Solar Photocatalytic H_2 Production Activity in Anatase TiO_2 Nanosheet Assembly. *Applied Catalysis B: Environmental* 2021, *285*, 119755.

(6) Abdelbar, M. F.; Abdelhameed, M.; **Esmat, M.**; El-Kemary, M.; Fukata, N. Energy Management in Hybrid Organic-Silicon Nanostructured Solar Cells by Downshifting Using CdZnS/ZnS and CdZnSe/ZnS Quantum Dots. *Nano Energy* 2021, *89*.

(7) Doustkhah, E.; Assadi, M. H. N.; Komaguchi, K.; Tsunoji, N.; **Esmat, M.**; Fukata, N.; Tomita, O.; Abe, R.; Ohtani, B.; Ide, Y. In Situ Blue Titania via Band Shape Engineering for Exceptional Solar H_2 Production in Rutile TiO_2. *Applied Catalysis B: Environmental* 2021, *297*, 120380.

(8) Tahawy, R.; Doustkhah, E.; Abdel-Aal, E. S. A.; **Esmat, M.**; Farghaly, F. E.; El-Hosainy, H.; Tsunoji, N.; El-Hosiny, F. I.; Yamauchi, Y.; Assadi, M. H. N.; Ide, Y. Exceptionally Stable Green Rust, a Mixed-Valent

Iron-Layered Double Hydroxide, as an Efficient Solar Photocatalyst for H_2 Production from Ammonia Borane. *Applied Catalysis B: Environmental* 2021, *286*, 119854.

(9) El-Hosainy, H.; Tahawy, R.; **Esmat, M.**; El-Kemary, M.; Ide, Y. Immobilization of Iron Minerals on a Layered Silicate for Enhancing Its Solar Photocatalytic Activity toward H_2 Production. *Frontiers in Energy Research* 2021, *9*.

(10) Torad, N.L.; El-Hosainy, H.; **Esmat, M.**; El-Kelany, K.E.; Tahawy, R.; Na, J.; Ide, Y.; Fukata, N.; Chaikittisilp, W.; Hill J.P.; Zhang, X; El-Kemary, M.; Yamauchi. Y. Phenyl-Modified Carbon Nitride Quantum Nanoflakes for Ultra-Highly Selective Sensing of Formic Acid: A Combined Experimental by QCM and Density Functional Theory Study. *ACS Applied Materials & Interfaces* 2021, 13(41), 48595-48610.

2022

(11) **Esmat, M.**; Doustkhah, E.; Abdelbar, M; El-Hosainy, H.; Tahawy, R.; Abdelhameed, M.; Ide, Y; Fukata, N. Structural conversion of Cu-titanate into photoactive plasmonic Cu-TiO_2 for H_2 generation in visible light. *ACS Sustainable Chemistry & Engineering* 2022 (revision submitted).

(12) Hassandoost, R., Kotb, A., Movafagh, Z., **Esmat, M.**, Guegan, R., Endo, S., Jevasuwan, W., Fukata, N., Sugahara, Y., Khataee, A. and Yamauchi, Y. Nanoarchitecturing Bimetallic Manganese Cobaltite Spinels for Sonocatalytic Degradation of Oxytetracycline. *Chemical Engineering Journal* 2022, 431, 133851.

ACKNOWLEDGMENT

First and foremost, I would like to thank my God "*Allah*" for guiding and helping me through this long journey to fulfill my dreams.

Special thanks go to my supervisor, *Prof. Naoki Fukata*, for allowing me to conduct my PhD in his research group. During my PhD, he helped me through his scientific guidelines, discussions, critical questions, and being supportive and motivational.

I also would like to express my deep and sincere thanks to *Prof. Yusuke Ide*, our collaborator, for his undivided attention and continuous support during my PhD.

I would like to thank my thesis committee members - *Prof. Jie Tang, Prof. Satoshi Ishii, and Prof. Kaoru Toko* - for accepting the evaluation of my thesis and giving insightful comments.

I would like to acknowledge all my colleagues in the Nanostructured Semiconducting Materials group at NIMS – **Dr. Wipakorn Jevasuwan, Dr. Ryo Matsumura, Mohamed Abdelhameed, Mostafa Abdelbar, Yonglie Sun,** and **Rahmat Hadi Sarutro** - for the friendly environment provided.

My gratitude also goes to my colleagues in the Mesoscale Materials Chemistry group at NIMS for the friendly environment provided, especially **Dr. Hamza El-Hosainy, Dr. Rafat Tahawy,** and **Dr. Esmail Doustkhah**.
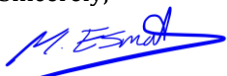
I would also like to thank past mentors at the Faculty of Postgraduate Studies for Advanced Sciences, Beni-Suef University in Egypt - **Prof. Mohamed Khedr, Prof. Ahmed Farghali,** and **Prof. Samaa El-Dek** - for helping me to be where I am today.

I express my very sincere gratitude to my family; **my beloved mother, and my lovely brothers and sisters**, who are providing me with unfailing support and countless encouragement.

Finally, I ask Almighty Allah to have mercy on **my father**.

<div align="center">وَٱلْحَمْدُ لِلَّهِ رَبِّ ٱلْعَٰلَمِين</div>

Sincerely,

Mohamed Esmat
February 2022
Tsukuba, Japan